NAVAL POSTGRADUATE SCHOOL
MONTEREY, CALIFORNIA

THESIS

UNDERWATER ACOUSTIC PULSE PROPAGATION USING THE RECURSIVE RAY ACOUSTICS (RRA) ALGORITHM

by

Ding-chen Chang

June, 1995

Thesis Advisor: Lawrence J. Ziomek

Approved for public release; distribution is unlimited.

REPORT DOCUMENTATION PAGE

Form Approved OMB No. 0704-0188

1. AGENCY USE ONLY *(Leave blank)*	2. REPORT DATE June 1995	3. REPORT TYPE AND DATES COVERED Master's Thesis

4. TITLE AND SUBTITLE
UNDERWATER ACOUSTIC PULSE PROPAGATION USING THE RECURSIVE RAY ACOUSTICS (RRA) ALGORITHM

5. FUNDING NUMBERS

6. AUTHOR(S) Chang, Ding-chen

7. PERFORMING ORGANIZATION NAME(S) AND ADDRESS(ES)
Naval Postgraduate School
Monterey CA 93943-5000

8. PERFORMING ORGANIZATION REPORT NUMBER

9. SPONSORING/MONITORING AGENCY NAME(S) AND ADDRESS(ES)

10. SPONSORING/MONITORING AGENCY REPORT NUMBER

11. SUPPLEMENTARY NOTES The views expressed in this thesis are those of the author and do not reflect the official policy or position of the Department of Defense or the U.S. Government.

12a. DISTRIBUTION/AVAILABILITY STATEMENT
Approved for public release; distribution is unlimited.

12b. DISTRIBUTION CODE

13. ABSTRACT *(maximum 200 words)*

The purpose of this thesis is to demonstrate the ability to predict the pulse shape at the location of a receiver in the ocean for a given transmitted pulse and ocean medium model by using the Recursive Ray Acoustics (RRA) Algorithm together with the Linear Space-Variant Ocean (LSVOCN) computer program. In addition, the effects of different ocean environments on the received pulse shape are examined.

In this thesis, the ocean medium is treated as a linear, time-invariant, space-variant filter. The RRA Algorithm is used as a subroutine to calculate the spatial impulse response or complex frequency response of the ocean-medium filter. The LSVOCN computer program, which incorporates the coupling equations, couples the transmitted electrical signal, and the transmit and receive apertures to the ocean-medium filter to predict the received pulse. Computer simulation test case results show that the LSVOCN computer program is able to predict the received pulse correctly and that the shape of the received pulse is strongly affected by different ocean-medium environments.

14. SUBJECT TERMS Recursive Ray Acoustics (RRA) Algorithm, Linear Space-Variant Ocean (LSVOCN), and the Coupling equations			15. NUMBER OF PAGES 83 16. PRICE CODE
17. SECURITY CLASSIFICATION OF REPORT Unclassified	18. SECURITY CLASSIFICATION OF THIS PAGE Unclassified	19. SECURITY CLASSIFICATION OF ABSTRACT Unclassified	20. LIMITATION OF ABSTRACT UL

NSN 7540-01-280-5500

Standard Form 298 (Rev. 2-89)
Prescribed by ANSI Std. 239-18 298-102

Approved for public release; distribution is unlimited.

UNDERWATER ACOUSTIC PULSE PROPAGATION USING THE RECURSIVE RAY ACOUSTICS (RRA) ALGORITHM

Ding-chen Chang
Lieutenant , Taiwan Navy
B.S., CHUNG CHENG Institute of Technology, Taiwan , 1988

Submitted in partial fulfillment
of the requirements for the degree of

MASTER OF SCIENCE IN ENGINEERING ACOUSTICS

from the

NAVAL POSTGRADUATE SCHOOL
June 1995

Author: Ding-chen Chang

Approved by: Lawrence J. Ziomek, Thesis Advisor

Charles W. Therrien, Second Reader

Anthony A. Atchley, Chairman
Engineering Acoustics Academic Committee

ABSTRACT

The purpose of this thesis is to demonstrate the ability to predict the pulse shape at the location of a receiver in the ocean for a given transmitted pulse and ocean medium model by using the Recursive Ray Acoustics (RRA) Algorithm together with the Linear Space-Variant Ocean (LSVOCN) computer program. In addition, the effects of different ocean environments on the received pulse shape are examined.

In this thesis, the ocean medium is treated as a linear, time-invariant, space-variant filter. The RRA Algorithm is used as a subroutine to calculate the spatial impulse response or complex frequency response of the ocean-medium filter. The LSVOCN computer program, which incorporates the coupling equations, couples the transmitted electrical signal, and the transmit and receive apertures to the ocean-medium filter to predict the received pulse. Computer simulation test case results show that the LSVOCN computer program is able to predict the received pulse correctly and that the shape of the received pulse is strongly affected by different ocean-medium environments.

TABLE OF CONTENTS

I. INTRODUCTION

The purpose of this thesis is to demonstrate the ability to predict the pulse shape at the location of a receiver in the ocean for a given transmitted pulse and ocean medium model by using the Recursive Ray Acoustics (RRA) Algorithm [Refs. 1, 2] together with the Linear Space-Variant Ocean (LSVOCN) computer program [Refs. 3, 4, 5]. In addition, the effects of different ocean environments on the received pulse shape are examined.

The propagation of small-amplitude acoustic signals in an unbounded or bounded inhomogeneous fluid medium can be described by a linear wave equation. Therefore, we can treat an unbounded or bounded inhomogeneous fluid medium as a linear filter. The principles of linear, time-variant, space-variant filter theory, and time-domain and spatial-domain Fourier transform theory provide for a consistent, logical, and straightforward mathematical framework, known as the coupling equations, for the solution of small-amplitude acoustic pulse-propagation problems. A linear, time-variant, space-variant filter is one that satisfies the principle of superposition (i.e., homogeneity and additivity) but whose own properties change with time and space [Ref. 6, pg. 651]. As long as we know the input signal and the impulse response or transfer function of the linear ocean-medium filter, the output signal can be calculated. The impulse response and the transfer function (complex frequency response) of the linear ocean-medium filter, and the coupling equations and pulse propagation are discussed in Chapter II.

In this thesis, the ocean medium is treated as a linear, time-invariant, space-variant filter. A time-invariant ocean-medium filter implies that both the transmit and receive apertures are motionless and that no other motion is being modeled. A space-variant ocean-medium filter implies that the properties of the ocean medium change as a function of space. The coupling equations, that is, the equations that describe the interactions between the transmit signal, the transmit aperture, the ocean medium, and the receive aperture are modeled by the Linear Space-Variant Ocean (LSVOCN) computer program [Refs. 3, 4, 5]. The transmit signals used in this thesis are amplitude and angle modulated carriers. The

transmit aperture and the receive aperture are modeled as an omnidirectional point source and omnidirectional point receiver, respectively. The ocean medium is bounded by the ocean surface and bottom. The speed of sound is an arbitrary function of depth, and includes the special case of a homogeneous medium in which the speed of sound is constant.

The spatial impulse response of the linear ocean-medium filter is calculated by the Recursive Ray Acoustics (RRA) Algorithm [Refs.1, 2]. The RRA Algorithm is able to calculate the three-dimensional spatial coordinates, angles of propagation, travel time, path length, and the magnitude and phase of the acoustic pressure along a ray path when the speed of sound is an arbitrary function of depth. After finding all the eigenrays between a transmitter and a receiver, and calculating the magnitude and phase of the acoustic pressure along all the eigenrays, we then know the spatial impulse response of the linear ocean-medium filter. By using the RRA Algorithm [Refs. 1, 2] together with the LSVOCN computer program [Refs. 3, 4, 5], we can predict the pulse shape at the receiver for a given transmitted signal and ocean medium model.

Chapter II is divided into two parts. Section A discusses the form of the coupling equations used in the computer program LSVOCN [Refs. 3, 4, 5] to model acoustic pulse propagation in a time-invariant, space-variant ocean medium. The derivation of the relationship between the source level (SL) in dB relative to the pressure P_{ref} and the amplitude scaling factor (A) used to model the transmitted pulse is provided in Section B.

Chapter III presents the computer simulation results of all the test cases. The first part of Chapter III presents the simulation results for an amplitude-modulated carrier propagating along a single eigenray in an unbounded (no boundaries), homogeneous (constant speed of sound) ocean medium with launch angles β_0 equal to 45, 90, and 135 degrees and path lengths equal to 1, 10, 100, and 1000 meters. Since the pulse is propagating in an unbounded, homogeneous ocean medium, we expect to see the following :

- The amplitude of the received pulse should fall off as 1/r, where r is the path length.
- The received pulse shape should not be distorted.

The second part of Chapter III presents the simulation results for an amplitude-modulated

carrier propagating along a single eigenray in a bounded homogeneous ocean medium with surface reflection coefficients equal to -0.5 and -1 (ideal pressure-release boundary), and bottom reflection coefficients equal to +0.5 and +1 (ideal rigid boundary). The launch angles β_0 are 30 and 150 degrees for the bottom and surface reflections, respectively. The path length is 1000 meters for all cases. The following phenomena are expected :

- The amplitude of the received pulse should fall off as 1/r times the magnitude of the reflecion coefficient of the boundary, where r is the total path length.
- The received pulse shape should not be distorted, except that there is a 180 degree phase shift of the received signal compared to the transmitted signal when the pulse hits the boundary with reflection coefficients equal to -1 and -0.5.

The third part of Chapter III presents the simulation results of the effects of different ocean medium environments on the received pulse shape. The ocean medium environments for these test cases are as follows :

- Homogeneous ocean waveguide (speed of sound is constant) with a flat bottom
- Homogeneous ocean waveguide with a randomly rough flat bottom
- Inhomogeneous ocean waveguide (speed of sound is an arbitrary function of depth) with a flat bottom
- Inhomogeneous ocean waveguide with a randomly rough flat bottom
- Homogeneous ocean waveguide with a 3 degree smooth up-slope bottom
- Homogeneous ocean waveguide with a 3 degree randomly rough up-slope bottom
- Inhomogeneous ocean waveguide with a 3 degree smooth up-slope bottom
- Inhomogeneous ocean waveguide with a 3 degree randomly rough up-slope bottom
- Homogeneous ocean waveguide with a 3 degree smooth down-slope bottom
- Homogeneous ocean waveguide with a 3 degree randomly rough down-slope bottom
- Inhomogeneous ocean waveguide with a 3 degree smooth down-slope bottom
- Inhomogeneous ocean waveguide with a 3 degree randomly rough down-slope bottom

Chapter IV summarizes the computer simulation test case results and the possible applications of using this simulation technique, and provides recommendations for future research.

II. THEORETICAL ANALYSIS

A. COUPLING EQUATIONS AND ACOUSTIC PULSE PROPAGATION IN A TIME-INVARIANT, SPACE-VARIANT OCEAN

In this thesis, we deal only with acoustic pulse propagation in a time-invariant, space-variant ocean medium. A time-invariant ocean implies that the transmit and receive apertures are motionless, and that no other motion is being modeled. A space-variant ocean implies that the speed of sound is a function of space and/or that the ocean medium is bounded. When the ocean medium is modeled as a linear, time-invariant, space-variant filter, the coupling relations are given by the set of equations [Ref. 6, pg. 665-666] specified below.

The time-domain output electrical signal (pulse) from the receive aperture at time t and spatial location $\boldsymbol{r} = (x, y, z)$ (see Figure 2.1) is

$$y(t, \boldsymbol{r}) = \int_{-\infty}^{\infty} X(f)\ H(f, \boldsymbol{r})\ A_R(f, \boldsymbol{r})\ \exp(+j2\pi ft)\ df\ , \tag{2.1}$$

where $X(f)$ is the frequency spectrum (Fourier transform) of the transmitted pulse, and

$$\begin{aligned} H(f, \boldsymbol{r}) &= H(f, x, y, z) \\ &= \int_{-\infty}^{\infty}\int_{-\infty}^{\infty}\int_{-\infty}^{\infty} D_T(f, f_X, f_Y, f_Z)\ H_M(f, x, y, z; f_X, f_Y, f_Z) \\ &\quad \times \exp[-j2\pi(f_X x + f_Y y + f_Z z)]\ df_X\ df_Y\ df_Z \end{aligned} \tag{2.2}$$

is the overall system complex frequency response. The function

$$D_T(f, f_X, f_Y, f_Z) = \sum_{m' = -MT'}^{MT'} \sum_{n' = -NT'}^{NT'} c_{m'n'}(f) \exp(+j2\pi f_X x_0) \times \exp(+j2\pi f_Y y_0) \exp(+j2\pi f_Z z_0) \quad (2.3)$$

is the far-field directivity function of a planar array of $MT \times NT$ (odd) complex-weighted point elements centered at ($x_T = 0, y_T, z_T = 0$) and lying in a plane parallel to the XY plane. In this equation MT' and NT' are given by

$$MT' = \frac{MT - 1}{2}, \quad (2.4)$$

$$NT' = \frac{NT - 1}{2}, \quad (2.5)$$

while $c_{m'n'}(f)$ is the frequency-dependent complex weight at element $m'n'$. The coordinates x_0 and y_0 are given by

$$x_0 = m\, d_{XT}, \quad (2.6)$$

$$y_0 = y_T + n\, d_{YT}, \quad (2.7)$$

when d_{XT} and d_{YT} are the inter-element spacings in the X and Y directions, respectively. Finally $H_M(f, x, y, z; f_X, f_Y, f_Z)$ is the time-invariant, space-variant transfer function of the ocean medium, and $A_R(f, \boldsymbol{r})$ is the complex receive aperture function.

Substituting Eq. (2.3) into Eq. (2.2) yields

$$H(f,\ x,\ y,\ z) = \int_{-\infty}^{\infty} \int_{-\infty}^{\infty} \sum_{m' = -MT'}^{MT'} \sum_{n' = -NT'}^{NT'} c_{m'n'}\ (f) \tag{2.8}$$

$$\times \int_{-\infty}^{\infty} H_M\ (f,\ x,\ y,\ z;\ f_X,\ f_Y,\ f_Z)\ \exp\left[-j2\pi f_Y(y-y_0)\right]\ df_Y$$

$$\times\ \exp\left[-j2\pi f_X(x-x_0)\right]\ \exp\left[-j2\pi f_Z(z-z_0)\right]\ df_X\ df_Z\ .$$

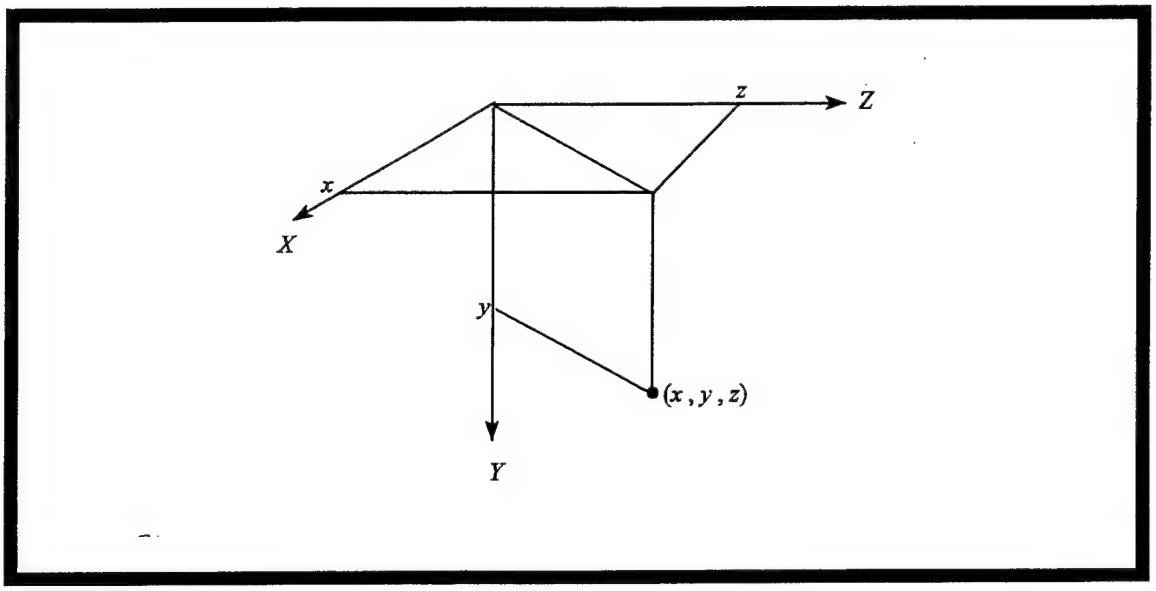

Figure 2.1 The Rectangular Coordinates (x , y , z).

By using the relationship [Ref. 6, pg. 654]

$$\int_{-\infty}^{\infty} H_M\,(f,\ x,\ y,\ z;\ f_X,\ f_Y,\ f_Z)\ \exp\left[-j2\pi f_Y(y-y_0)\right]\ df_Y \tag{2.9}$$

$$= H_M\,(f,\ x,\ y,\ z;\ f_X,\ y_0,\ f_Z)\ ,$$

Eq. (2.8) becomes

$$H(f,\ x,\ y,\ z) = \sum_{m'\,=\,-MT'}^{MT'}\ \sum_{n'\,=\,-NT'}^{NT'} c_{m'n'}\,(f)$$

$$\times \int_{-\infty}^{\infty}\int_{-\infty}^{\infty} H_M\,(f,\ x,\ y,\ z;\ f_X,\ y_0,\ f_Z) \tag{2.10}$$

$$\times\ \exp\left[-j2\pi\left[f_X(x-x_0)\ +\ f_Z(z-z_0)\right]\ \right]df_X\ df_Z\ .$$

Then using the relationship [Ref. 6, pg. 654]

$$\int_{-\infty}^{\infty} H_M\,(f,\ x,\ y,\ z;\ f_X,\ y_0,\ f_Z)\ \exp\left[-j2\pi f_X(x-x_0)\right]\ df_X \tag{2.11}$$

$$= H_M\,(f,\ x,\ y,\ z;\ x_0,\ y_0,\ f_Z)\ ,$$

Eq. (2.10) becomes

$$H(f,\ x,\ y,\ z) = \sum_{m'\,=\,-MT'}^{MT'}\ \sum_{n'\,=\,-NT'}^{NT'} c_{m'n'}\,(f)$$

$$\times \int_{-\infty}^{\infty} H_M\,(f,\ x,\ y,\ z;\ x_0,\ y_0,\ f_Z)\ \exp\left[-j2\pi f_Z(z-z_0)\right]\ df_Z\ . \tag{2.12}$$

Finally, by using the relationship [Ref. 6, pg. 654]

$$\int_{-\infty}^{\infty} H_M\,(f,\ x,\ y,\ z;\ x_0,\ y_0,\ f_Z)\ \exp\left[-j2\pi f_Z(z-z_0)\right]\ df_Z \qquad (2.13)$$

$$= H_M\,(f,\ x,\ y,\ z;\ x_0,\ y_0,\ z_0)\ ,$$

Eq. (2.12) becomes

$$H(f,\ x,\ y,\ z) = \sum_{m' = -MT'}^{MT'} \sum_{n' = -NT'}^{NT'} c_{m'n'}\,(f) \times H_M\,(f,\ x,\ y,\ z;\ x_0,\ y_0,\ z_0)\ . \qquad (2.14)$$

In this thesis, the transmit array is a single omnidirectional point source. Therefore, $MT = NT = 1$, and as a result, $MT' = NT' = 0$. Equation (2.14) then reduces to

$$H(f,\ x,\ y,\ z) = c_{00}\,(f) \times H_M\,(f,\ x,\ y,\ z;\ x_0,\ y_0,\ z_0)\ . \qquad (2.15)$$

The function $H_M(f, x, y, z; x_0, y_0, z_0)$ is the spatial impulse response (time-independent Green's function) of the time-invariant, space-variant ocean medium.

Note that the spatial impulse response $H_M(f, x, y, z; x_0, y_0, z_0)$ is obtained from the RRA Algorithm. In order to determine the output electrical signal $y(t, \mathbf{r})$ and its Fourier transform $Y(f, \mathbf{r})$, we need to know the complex frequency spectrum of the transmitted electrical signal $X(f)$, the frequency-dependent complex weight $c_{m'n'}(f)$ for each element $m'n'$ of the transmit aperture function, the transfer function of the linear, time-invariant, space-variant ocean-medium filter $H_M(f, x, y, z; x_0, y_0, z_0)$, and the complex receive aperture function $A_R(f, x, y, z)$. Note also that the

computer program LSVOCN is able to model the transmitted pulse and the transmit and receive apertures, and to couple these to the ocean medium via H_M. By using the LSVOCN computer program and the RRA Algorithm together, we can simulate underwater acoustic pulse propagation in a time-invariant, space-variant ocean medium and predict the received pulse shape at the receiver location for any given transmitted signal.

B. DERIVATION OF THE RELATIONSHIP BETWEEN SOURCE LEVEL (*SL*) AND THE AMPLITUDE SCALING FACTOR (*A*) USED TO MODEL THE TRANSMITTED ELECTRICAL SIGNAL

In order to provide consistency between the units of the transmitted electrical signal and the input acoustic signal to the ocean medium, a derivation of the relationship between source level (*SL*) and the amplitude scaling factor (*A*) used to model the transmitted electrical signal is presented in this section. The transmitter is an electroacoustic transducer which converts the transmitted electrical signal into an acoustic signal input to the ocean medium. The transmitted electrical signal has units of volts, while, the input acoustic pressure signal has units of Pascals (Pa). Source level (*SL*) is commonly used in acoustics in order to represent the strength of an acoustic signal transmitted by a sound source. The definition of *SL* in dB relative to (*re*) the reference pressure (P_{ref}) is

$$SL \triangleq 20\log_{10}\left(\frac{\frac{\sqrt{2}P_0}{2}}{P_{ref}}\right) \; dB \; re \; P_{ref}, \tag{2.16}$$

where P_0 is the peak acoustic pressure amplitude measured at a distance of one meter from the source along its acoustic axis, and P_{ref} is the reference pressure in Pa. For underwater acoustic problems it is conventional to take P_{ref} = 1 μPa (= 10^{-6} Pa).

The strength of the output acoustic signal from a transmitter, which is the input acoustic signal to the ocean medium, depends on both the level of the input electrical signal and the type of

transmitter used. The relationship between the input electrical signal to the transmitter and the output acoustic signal from the transmitter can be expressed in terms of the voltage sensitivity of the transmitter S_v. The voltage sensitivity of the transmitter S_v, with units of Pa/V, is defined as [Ref. 7, pg. 353]

$$S_v \triangleq \frac{P_{1m_{rms}}}{V_{rms}}, \tag{2.17}$$

where $P_{1m_{rms}}$ is the rms pressure in Pascals measured at a distance of 1 meter from the source along its acoustic axis, and V_{rms} is the rms value of the driving voltage in volts. Note that the value of the transmitting sensitivity S_v depends on the type of transmitter used.

In this thesis , the input electrical signal to the transmitter, $x(t)$, is an amplitude and angle modulated carrier signal given by

$$x(t) = Aa(t)\cos[2\pi f_c t + \theta(t)], \tag{2.18}$$

where $a(t)$ and $\theta(t)$ are real amplitude- and angle-modulating signals, respectively, $\cos[2\pi f_c t]$ is the carrier waveform, f_c is the carrier frequency in hertz, and A is the amplitude scaling factor that scales the input electrical signal so that it corresponds to the source level of the output acoustic signal. The amplitude modulation $a(t)$ satisfies the condition $-1 \le a(t) \le 1$. The complex envelope of $x(t)$ is denoted by $\tilde{x}(t)$ and is given by [see Ref. 6, pg. 607]

$$\tilde{x}(t) = Aa(t)\ \exp[+j\theta(t)]\ . \tag{2.19}$$

The rms value of the input electrical signal $x(t)$ in the time interval T_0 seconds is given by

$$x_{rms} = \sqrt{\frac{1}{T_0}\int_{T_0} x^2(t)\ dt}\ . \tag{2.20}$$

where the integral in Eq. (2.20) is over a single period of length T_0 . Since the energy E_x of the signal $x(t)$ in the time interval T_0 is

$$E_x = \int_{T_0} x^2(t)\ dt\ , \tag{2.21}$$

and since [see Ref. 6, pg. 612]

$$E_x = \frac{E_{\tilde{x}}}{2}\ , \tag{2.22}$$

the rms value of the signal x_{rms} can be expressed as

$$x_{rms} = \sqrt{\frac{E_x}{T_0}} = \sqrt{\frac{E_{\tilde{x}}}{2T_0}}\ . \tag{2.23}$$

By using the definition of the time-average power of the complex envelope $\tilde{x}(t)$ and Parseval's theorem, we find that

$$\frac{E_{\tilde{x}}}{T_0} = \frac{1}{T_0}\int_{T_0} |\tilde{x}(t)|^2\ dt = \sum_{n\,=\,-\infty}^{\infty} |c_n|^2 = P_{avg\tilde{x}} \tag{2.24}$$

where $\{c_n\}$ are the Fourier series coefficients of the complex envelope $\tilde{x}(t)$ and $P_{avg\tilde{x}}$ is the time-average power of the complex envelope in the time interval T_0. Substituting Eq. (2.24) into Eq. (2.23) yields

$$x_{rms} = \sqrt{\frac{P_{avg\tilde{x}}}{2}} \,. \tag{2.25}$$

Then, upon substituting Eq.(2.19) into Eq. (2.25), we obtain

$$P_{avg\tilde{x}} = \frac{A^2}{T_0} \int_{T_0} a^2(t)\, dt = A^2 P_{avga} \,, \tag{2.26}$$

where P_{avga} is the time-average power of the normalized amplitude modulating signal $a(t)$ in the time interval T_0. Finally, by substituting Eq. (2.26) into Eq. (2.25), we can express x_{rms} as

$$x_{rms} = \sqrt{\frac{P_{avg\tilde{x}}}{2}} = A\sqrt{\frac{P_{avga}}{2}} \,. \tag{2.27}$$

The last step in the analysis is to rewrite Eq. (2.16) and Eq. (2.17) as

$$P_{1m_{rms}} = P_{ref}\, 10^{\frac{SL}{20}} \tag{2.28}$$

and

$$P_{1m_{rms}} = S_v\, x_{rms} \tag{2.29}$$

where

$$P_{1m_{rms}} = \frac{\sqrt{2}P_0}{2} \tag{2.30}$$

is used to obtain Eq. (2.28) and V_{rms} is replaced by x_{rms} to obtain Eq. (2.29). By substituting Eq. (2.27) and Eq. (2.28) into Eq. (2.29), the amplitude scaling factor A can be expressed as

$$A = \frac{P_{ref}\, 10^{\frac{SL}{20}}}{S_v \sqrt{\frac{P_{avga}}{2}}} \tag{2.31}$$

where P_{ref} = 1 μPa (rms). In order to correctly model the transmitted electrical signal for a given source level of the output acoustic signal from the transmitter, the amplitude modulating signal $a(t)$ has to be multiplied by the amplitude scaling factor A.

III. COMPUTER SIMULATION RESULTS

This chapter presents the computer simulation results of all the test cases. Section A examines the test cases for an amplitude-modulated carrier propagating along a single eigenray in an unbounded (no boundaries) homogeneous (constant speed of sound) ocean medium. Section B examines the test cases for an amplitude-modulated carrier propagating along a single eigenray in a bounded and homogeneous ocean medium. The computer simulation results for an amplitude-modulated carrier propagating in an ocean waveguide with different ocean medium environments are presented in Section C.

The acronyms used to describe the various test cases (CASE) in this chapter can be decoded as follows:

U :	Unbounded
B :	Bounded
HMG :	Homogeneous
INHMG :	Inhomogeneous
D :	Degrees (the number before D is the launch angle β_0)
M :	Meters (the number before M is the path length)
R :	Reflection coefficient (the number after R : is the value of the reflection coefficient)
WVGD :	Waveguide
F:	Flat bottom
US3D :	3 degree up-slope bottom
DS3D :	3 degree down-slope bottom

For example, case UHMG45D1M stands for an amplitude-modulated carrier propagating along a single eigenray in an unbounded, homogeneous ocean medium with launch angle β_0 equal to 45 degrees and path length equal to 1 meter. Additional acronyms that appear as labels in the figures in this chapter are as follows : YT is the y coordinate (depth) of the tra-

nsmitter, and XR, YR, and ZR are the coordinates of the cross-range, depth, and horizontal range of the receiver, respectively.

A. TEST CASES FOR AN AMPLITUDE-MODULATED CARRIER PROPAGATING ALONG A SINGLE EIGENRAY IN AN UNBOUNDED, HOMOGENEOUS OCEAN MEDIUM

The amplitude-modulated carrier used for all the test cases in this section is a rectangular-envelope continuous-wave (CW) pulse with Lanczos smoothing as illustrated in Figure 3.1-1. The pulse is represented by 13 frequency components (NFREQ); it has an amplitude (A) of 2054.3, a pulse length (TP) of 12.5 msec, a pulse-repetition frequency (PRF) (fundamental frequency) of 40 Hz, and a carrier frequency (FC) of 400 Hz. The transmitter's voltage sensitivity S_v was chosen to be equal to 1 Pa/V. The amplitude (A) of 2054.3 corresponds to the transmitted acoustic signal having a source level of 180 dB *re* 1μPa. The transmitter is modeled as a single omnidirectional point source. For a pulse propagating in an unbounded homogeneous ocean medium, the amplitude of the pulse should decrease as 1/r where r is the path length, and the shape of the pulse should not distort as it propagates.

In order to demonstrate the expected results, four path lengths of 1, 10, 100, and 1000 meters were simulated for each of three different launch angles β_0. The three launch angles were chosen as 45, 90, and 135 degrees, respectively corresponding to transmission of rays downward, horizontally, and upward. The speed of sound was taken to be 1500 m/s while the geometry of the relationship between the launch angle β_0, the path length, the depth YT of the transmitter, and the depth YR of the receiver is illustrated in Figure 3.1-2. Since the speed of sound is constant, a single eigenray propagates as a straight line from the transmitter to the receiver.

Figures 3.1-3 through 3.1-6 show the received pulse shapes corresponding to the transmitted amplitude-modulated carrier shown in Figure 3.1-1 propagating along a single eigenray in an unbounded, homogeneous ocean medium, with a launch angle of 45 degrees and with path lengths of 1, 10, 100, and 1000 meters. From the shapes and the amplitudes

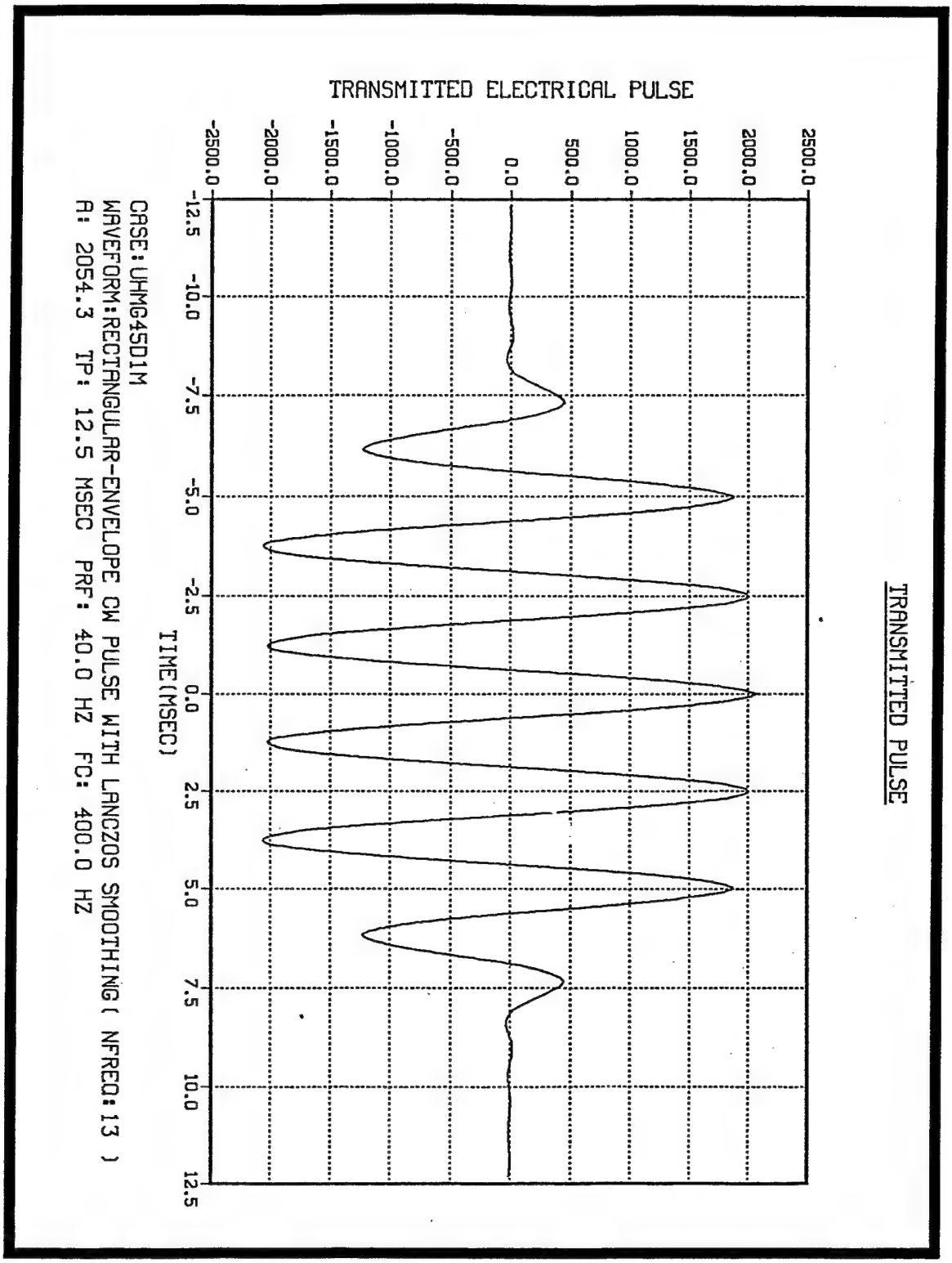

Figure 3.1-1 Transmitted Rectangular-envelope Continuous-wave Pulse with Lanczos Smoothing.

of the received pulses in these figures, it can be seen that there is no distortion in the received pulse shapes and that the amplitudes of the received pulses fall off as 1/r, where r is the path length, compared to the amplitude of the pulse at 1 meter from the transmitter.

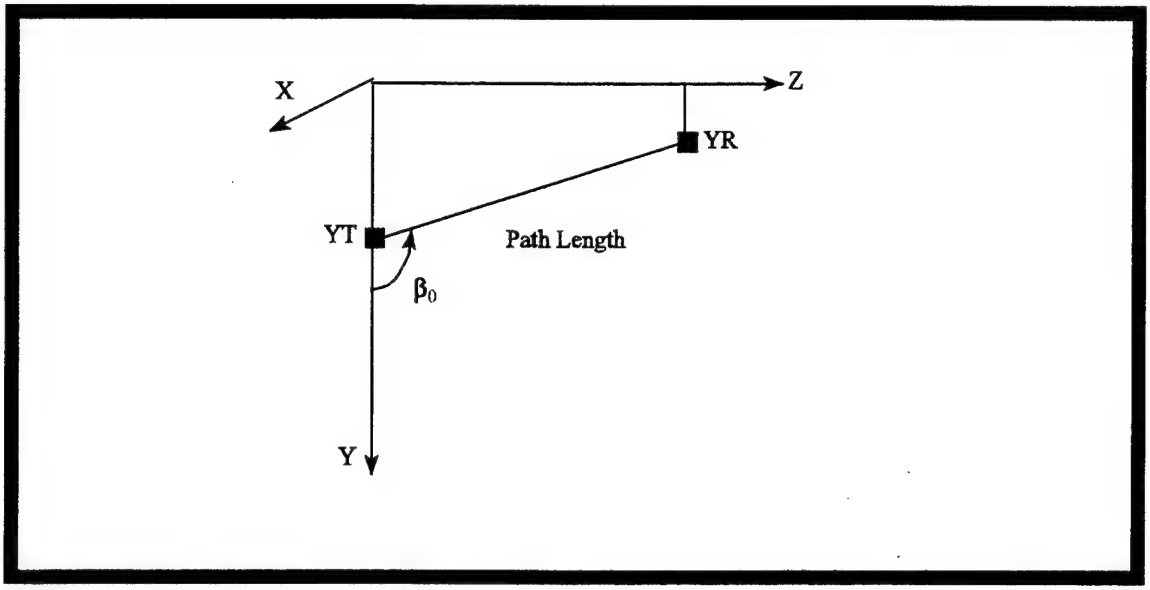

Figure 3.1-2 The Geometry of The Relationship between β_0, YT, and YR.

Figures 3.1-7, 3.1-8, 3.1-9, and 3.1-10 show the received pulses corresponding to cases UHMG90D1M, UHMG90D10M, UHMG90D100M, and UHMG90D1000M, respectively. These figures clearly illustrate that the received pulse shapes are not distorted and that the amplitudes of the received pulses fall off as 1/r compared to the amplitude of the pulse at 1 meter from the transmitter.

Figures 3.1-11 through 3.1-14, show the received pulses corresponding to cases UHMG135D1M, UHMG135D10M, UHMG135D100M, and UHMG135D1000M, respectively. There is no distortion of the received pulse shapes and the amplitudes of the received pulses fall off as 1/r, compared to the amplitude of the pulse at 1 meter from the transmitter. The computer simulation results of all the test cases presented in this section are thus seen to match theory exactly.

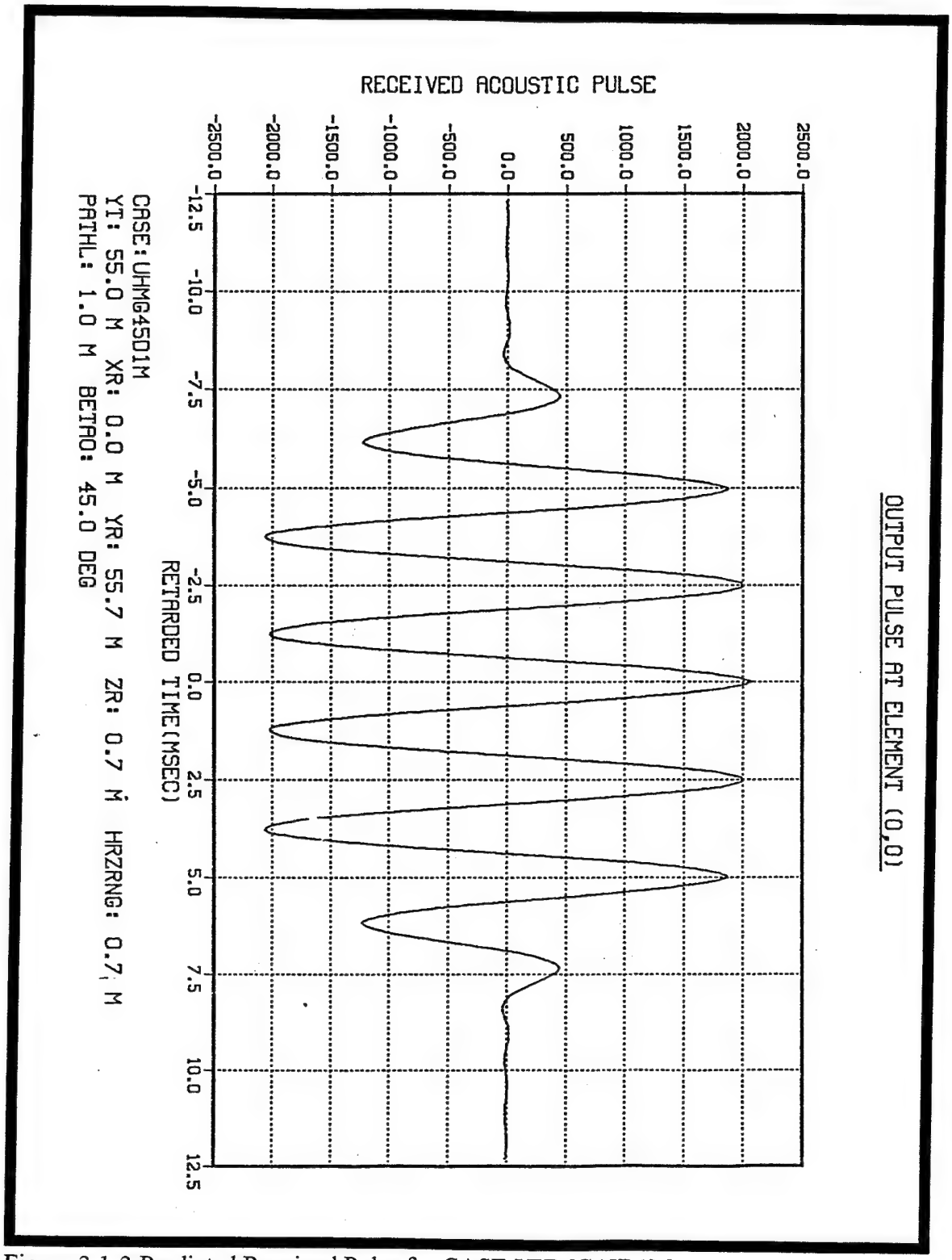

Figure 3.1-3 Predicted Received Pulse for CASE:UHMG45D1M.

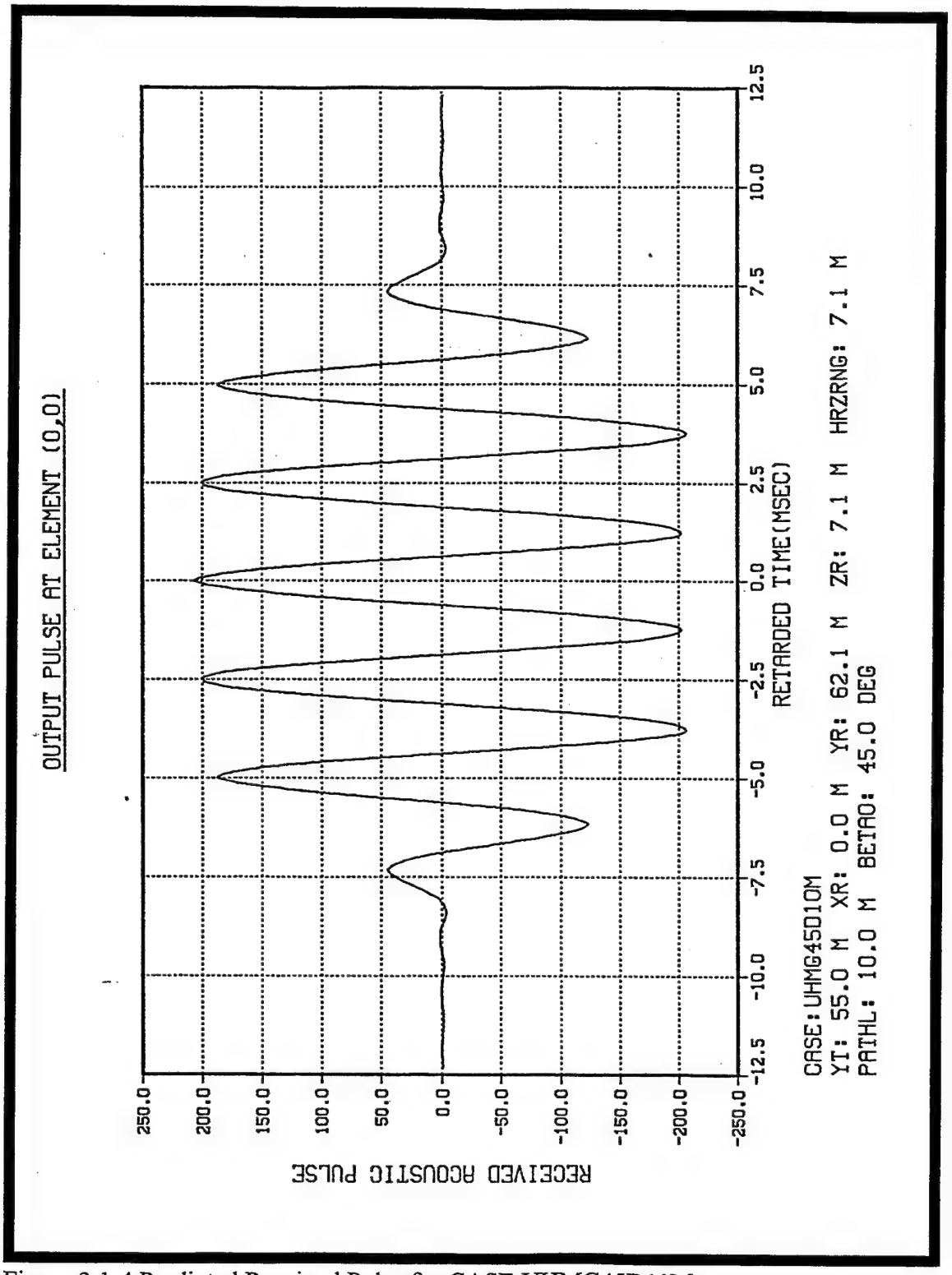

Figure 3.1-4 Predicted Received Pulse for CASE:UHMG45D10M.

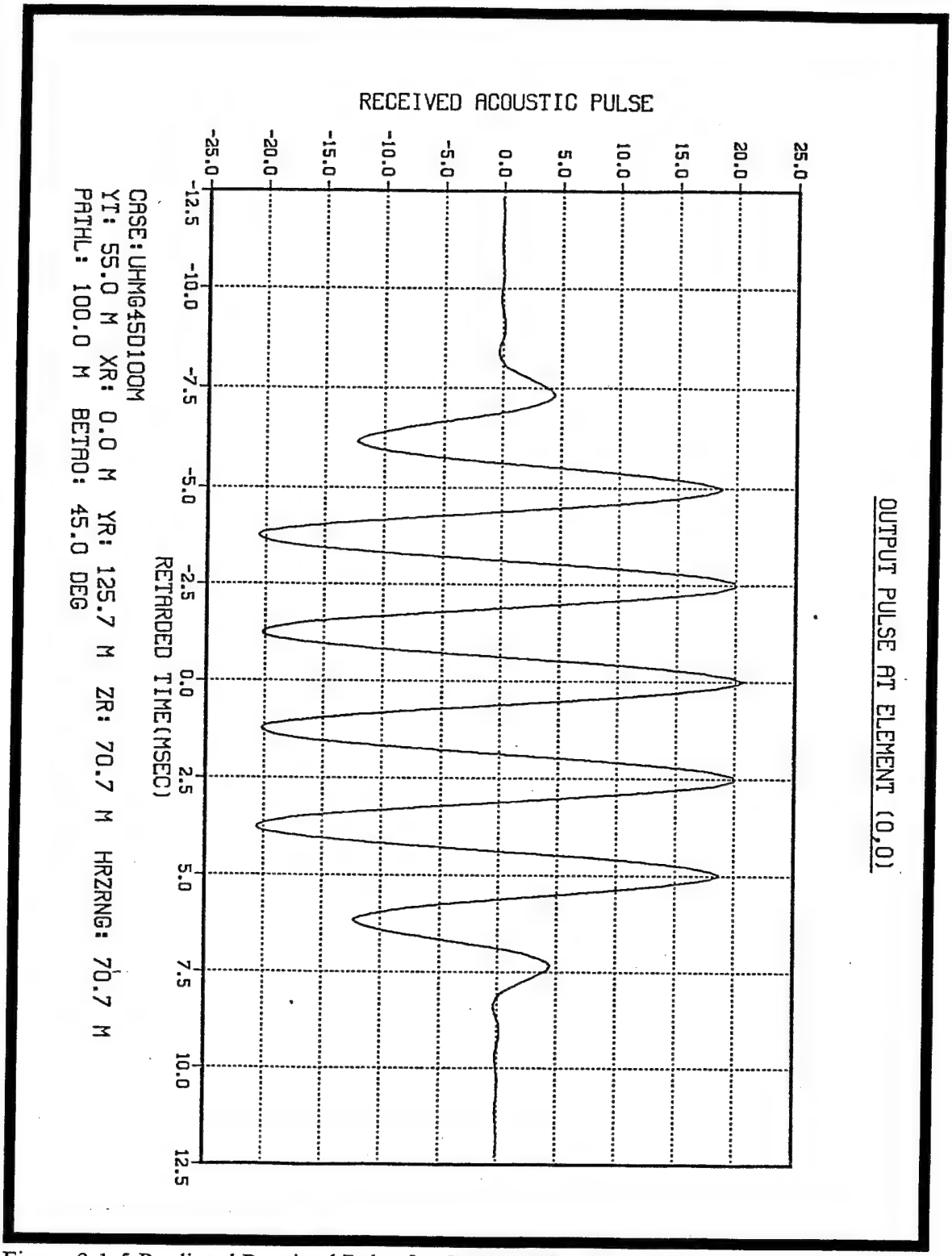

Figure 3.1-5 Predicted Received Pulse for CASE:UHMG45D100M.

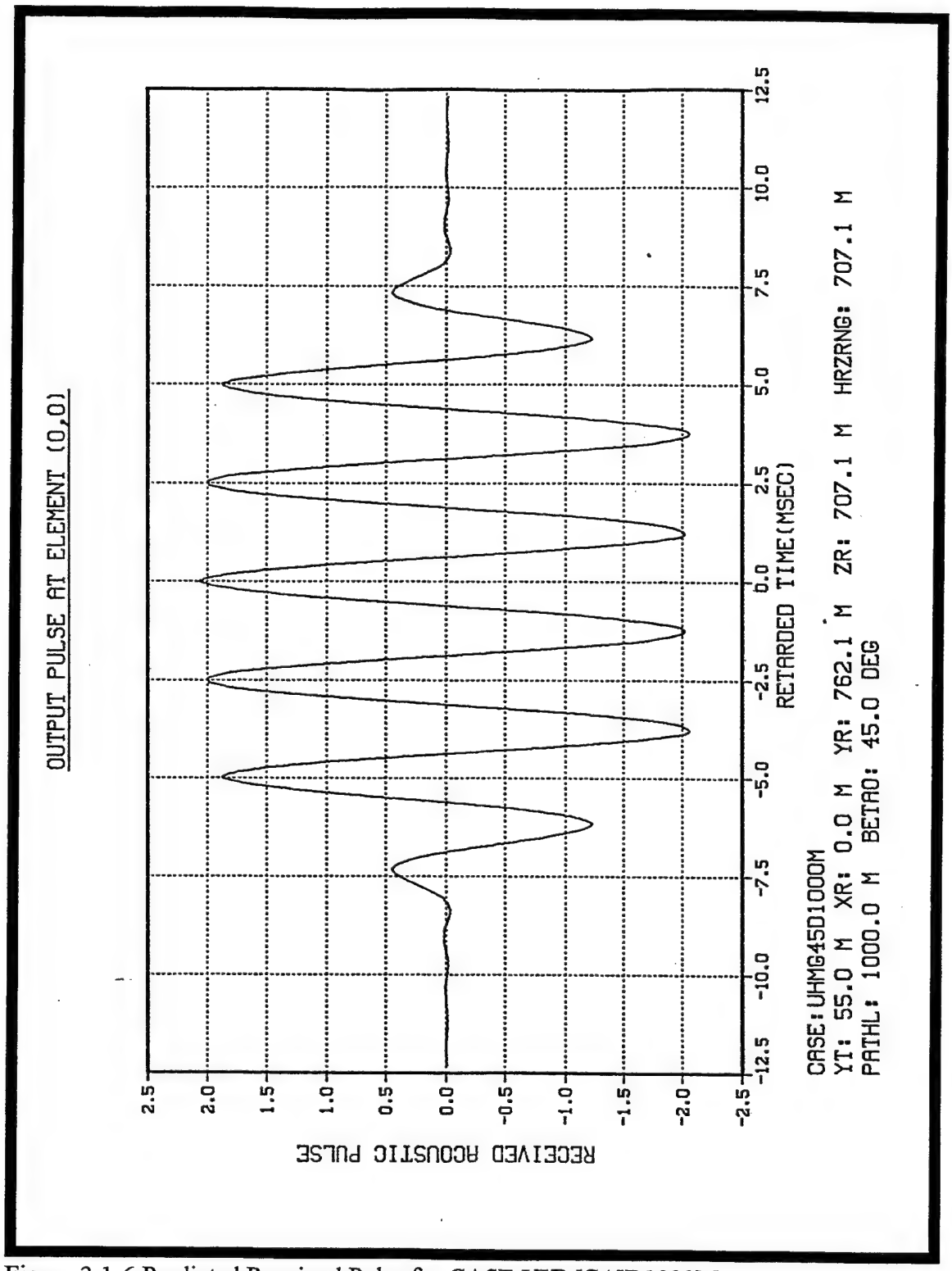

Figure 3.1-6 Predicted Received Pulse for CASE:UHMG45D1000M.

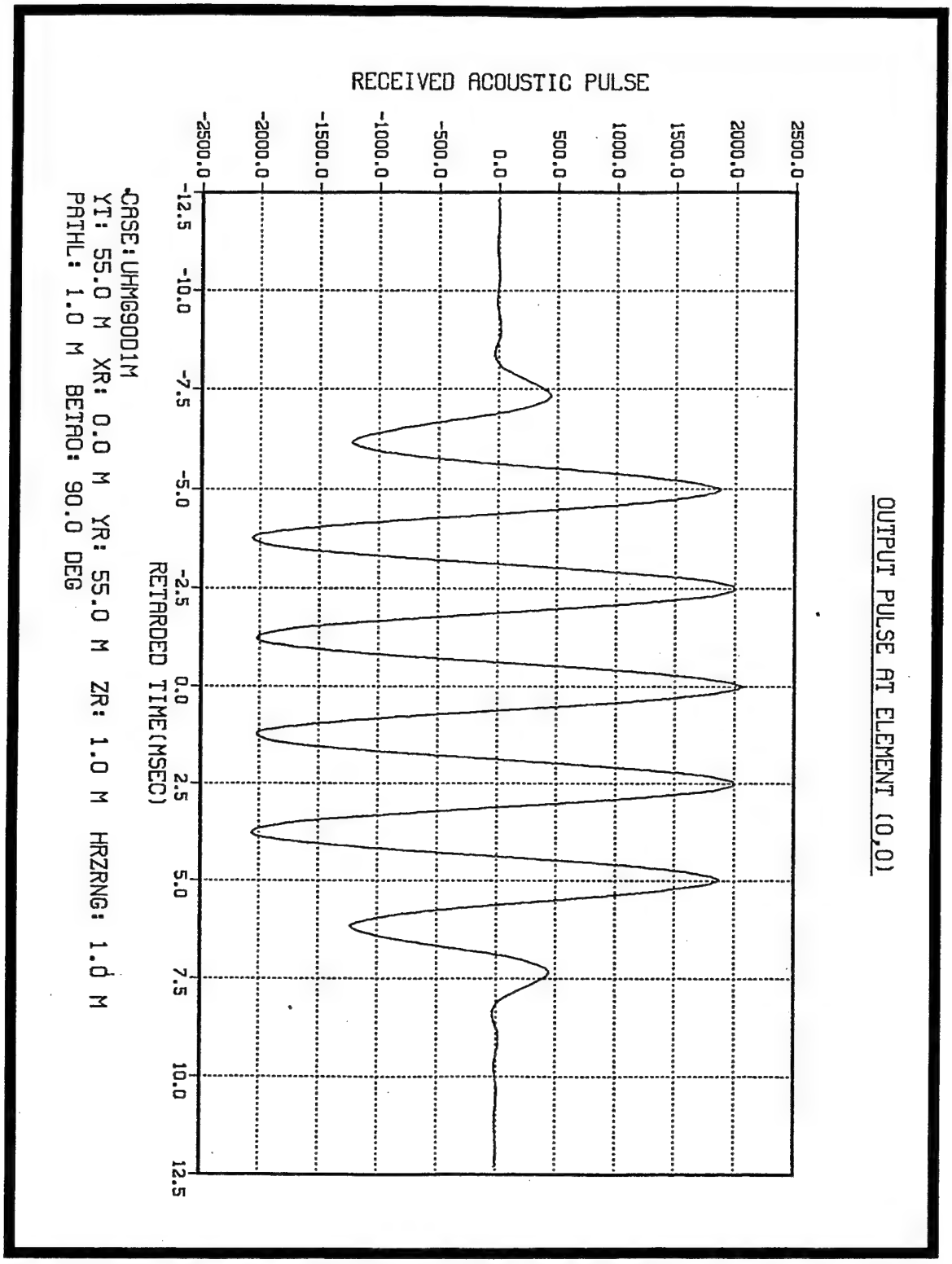

Figure 3.1-7 Predicted Received Pulse for CASE:UHMG90D1M.

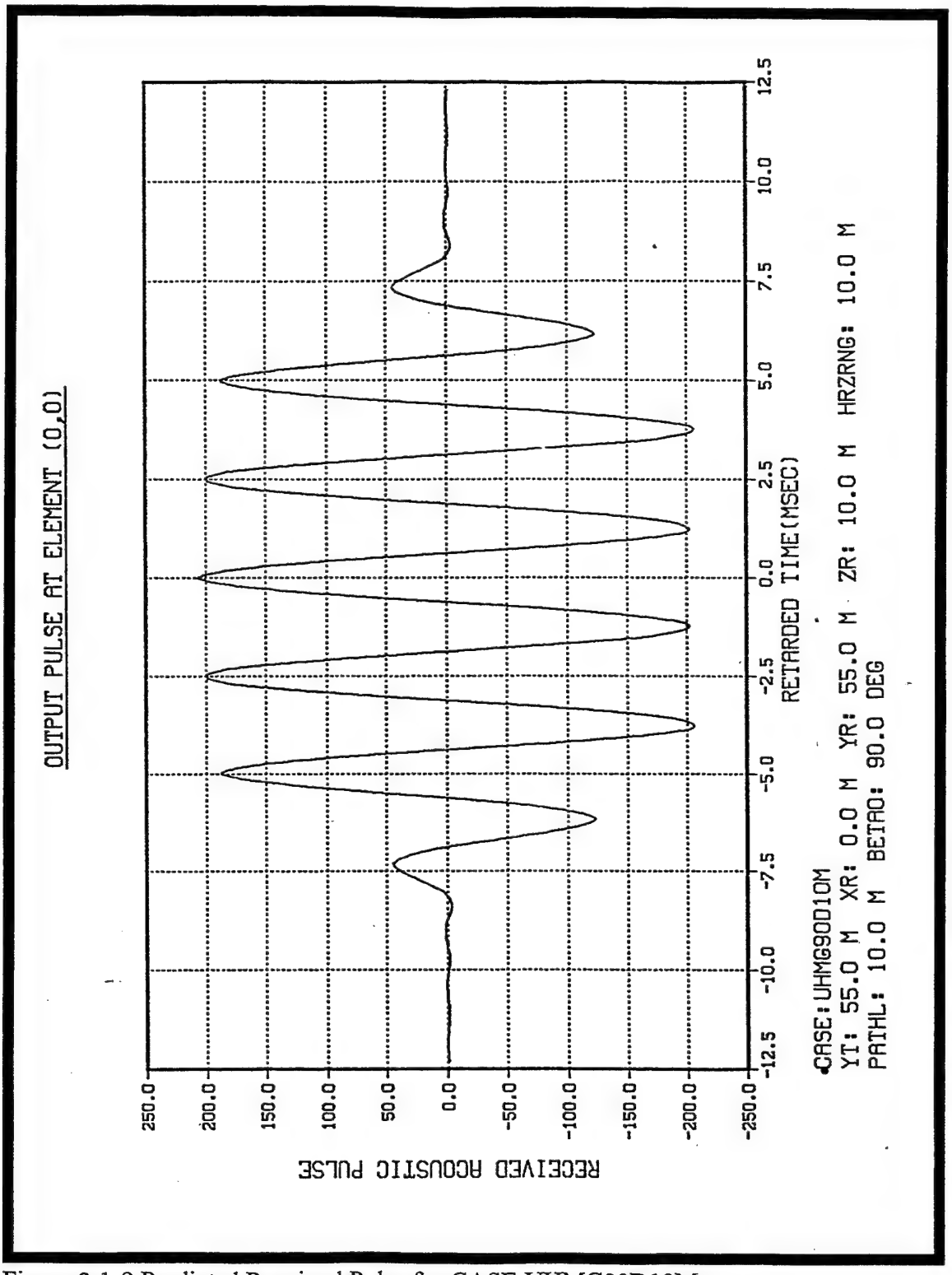

Figure 3.1-8 Predicted Received Pulse for CASE:UHMG90D10M.

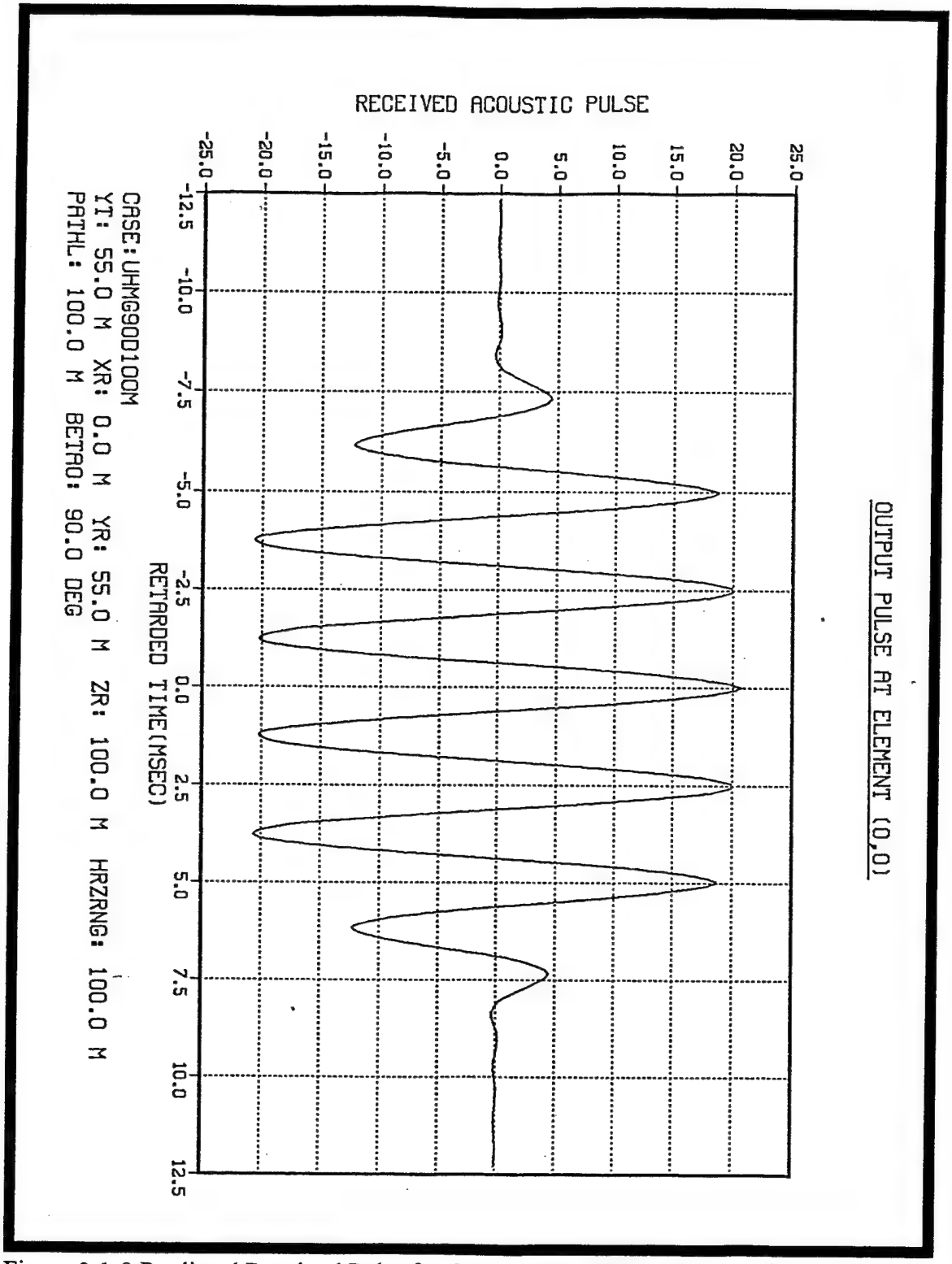

Figure 3.1-9 Predicted Received Pulse for CASE:UHMG90D100M.

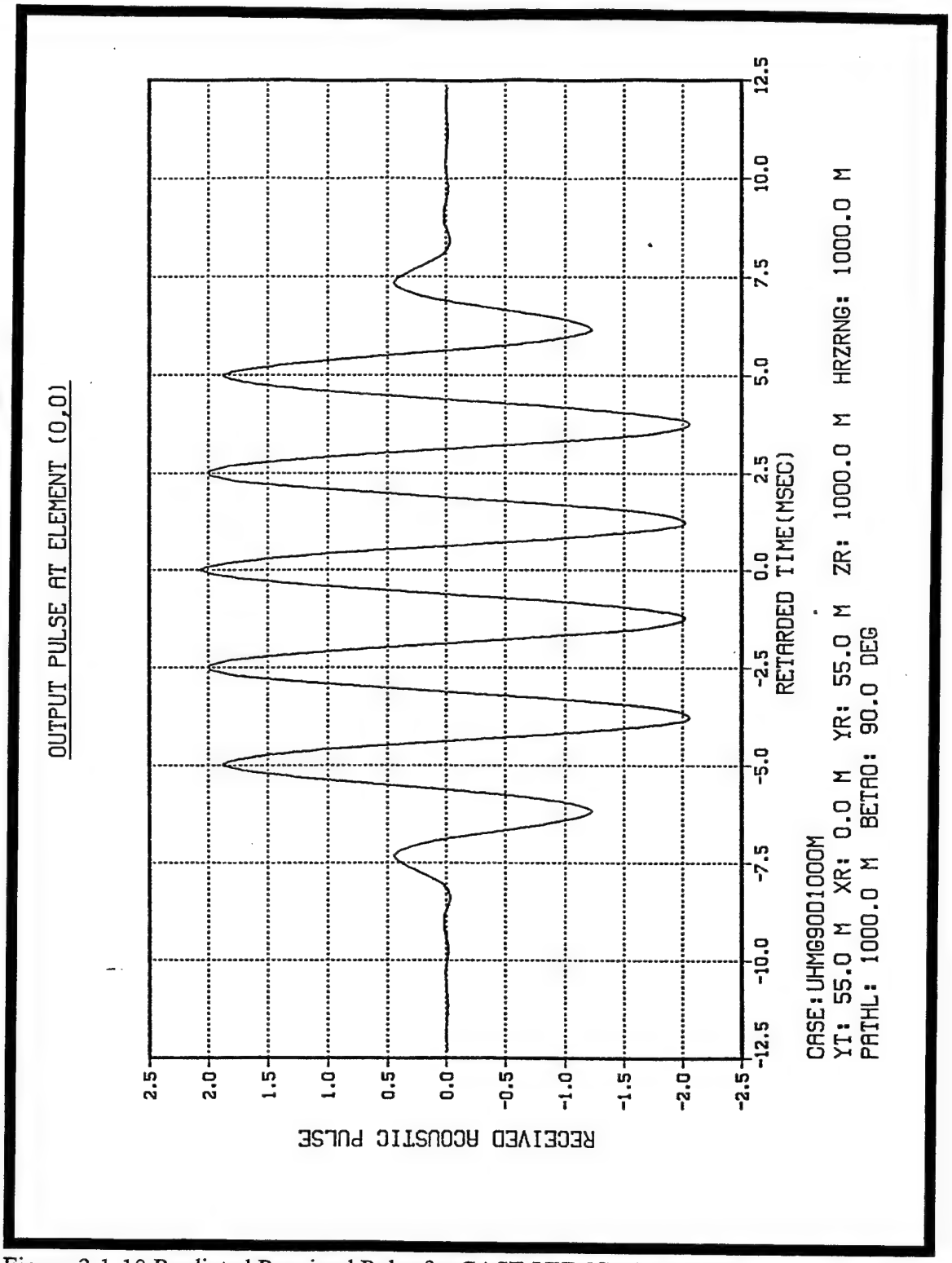

Figure 3.1-10 Predicted Received Pulse for CASE:UHMG90D1000M.

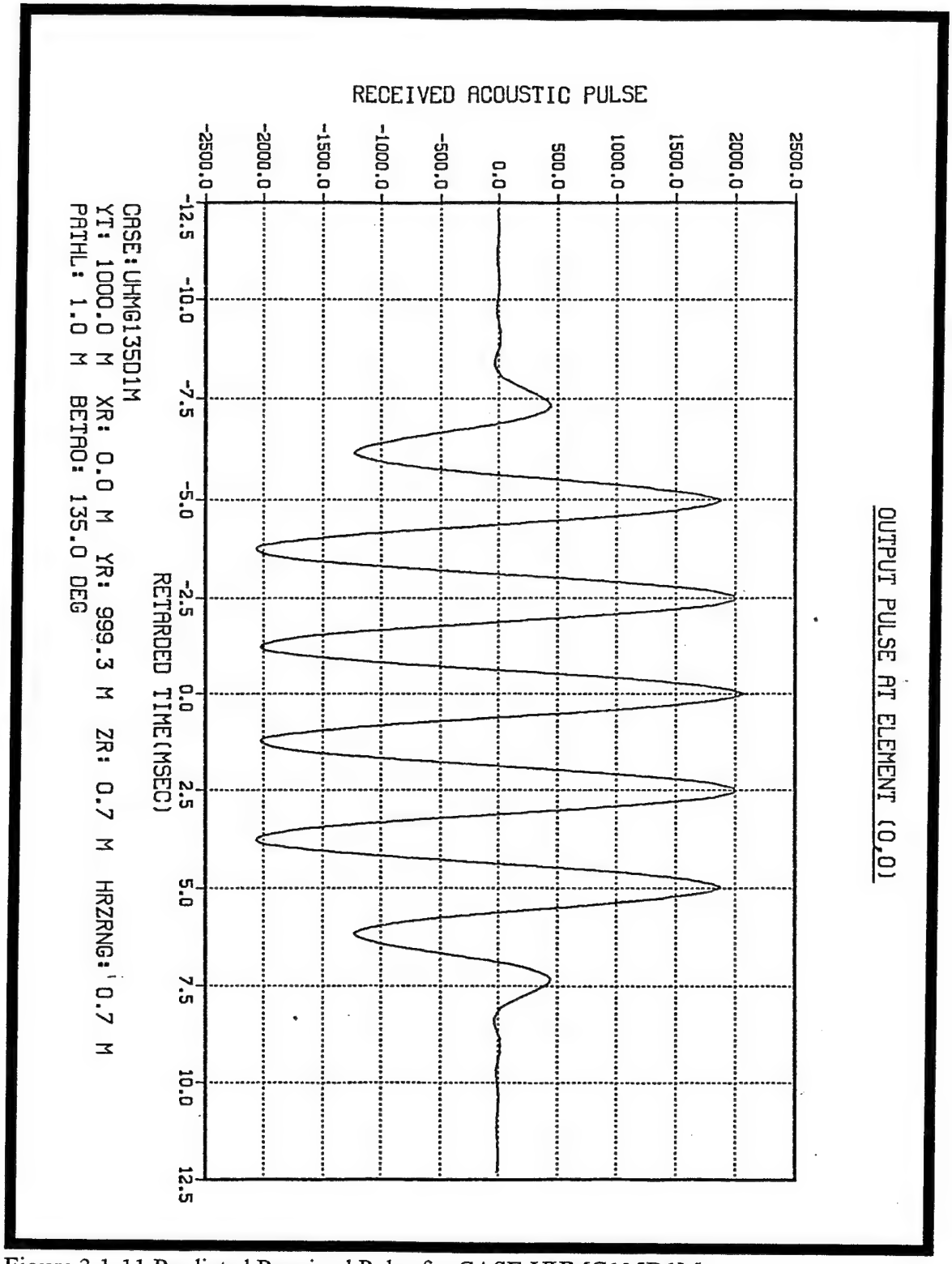

Figure 3.1-11 Predicted Received Pulse for CASE:UHMG135D1M.

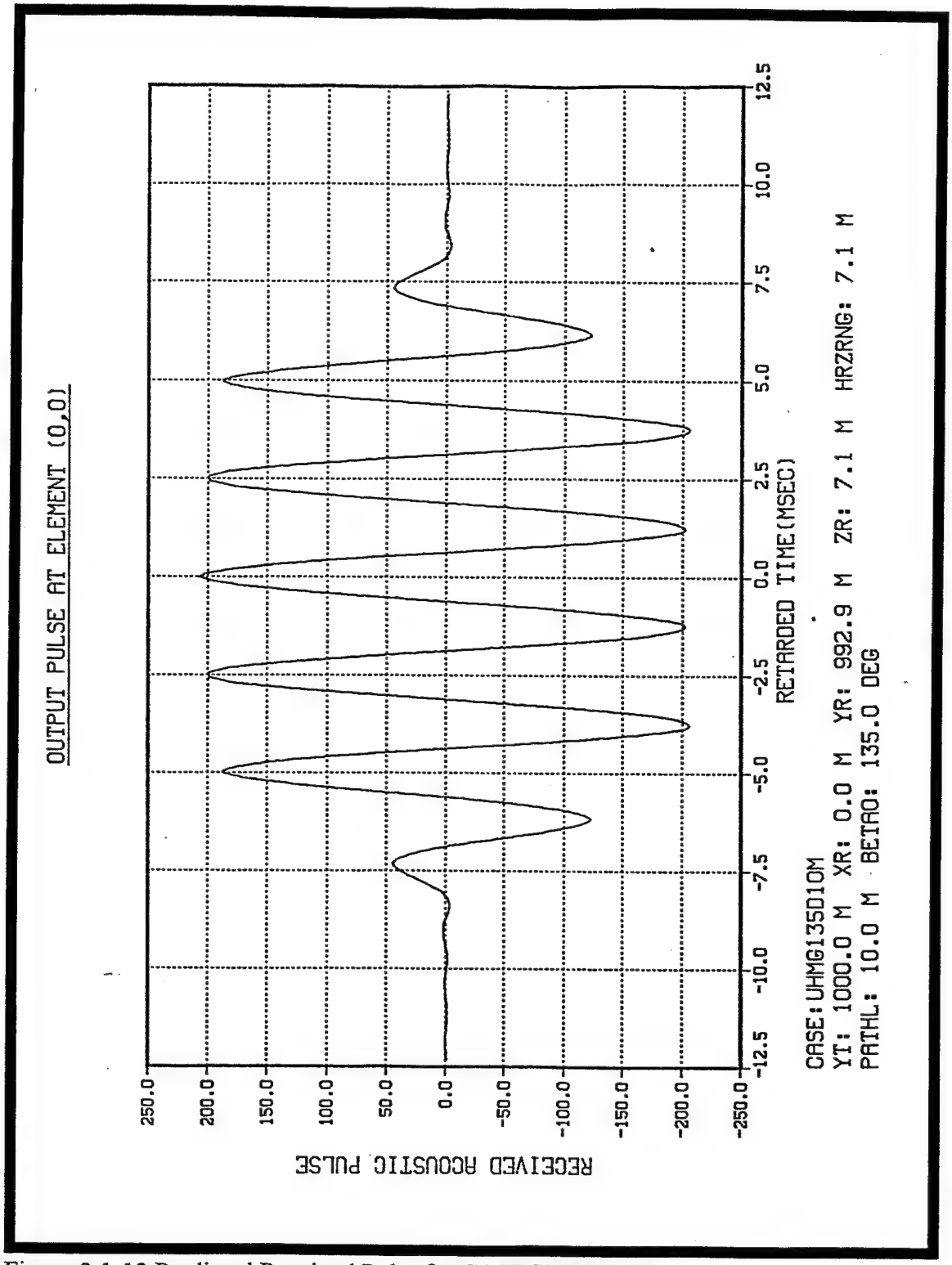

Figure 3.1-12 Predicted Received Pulse for CASE:UHMG135D10M.

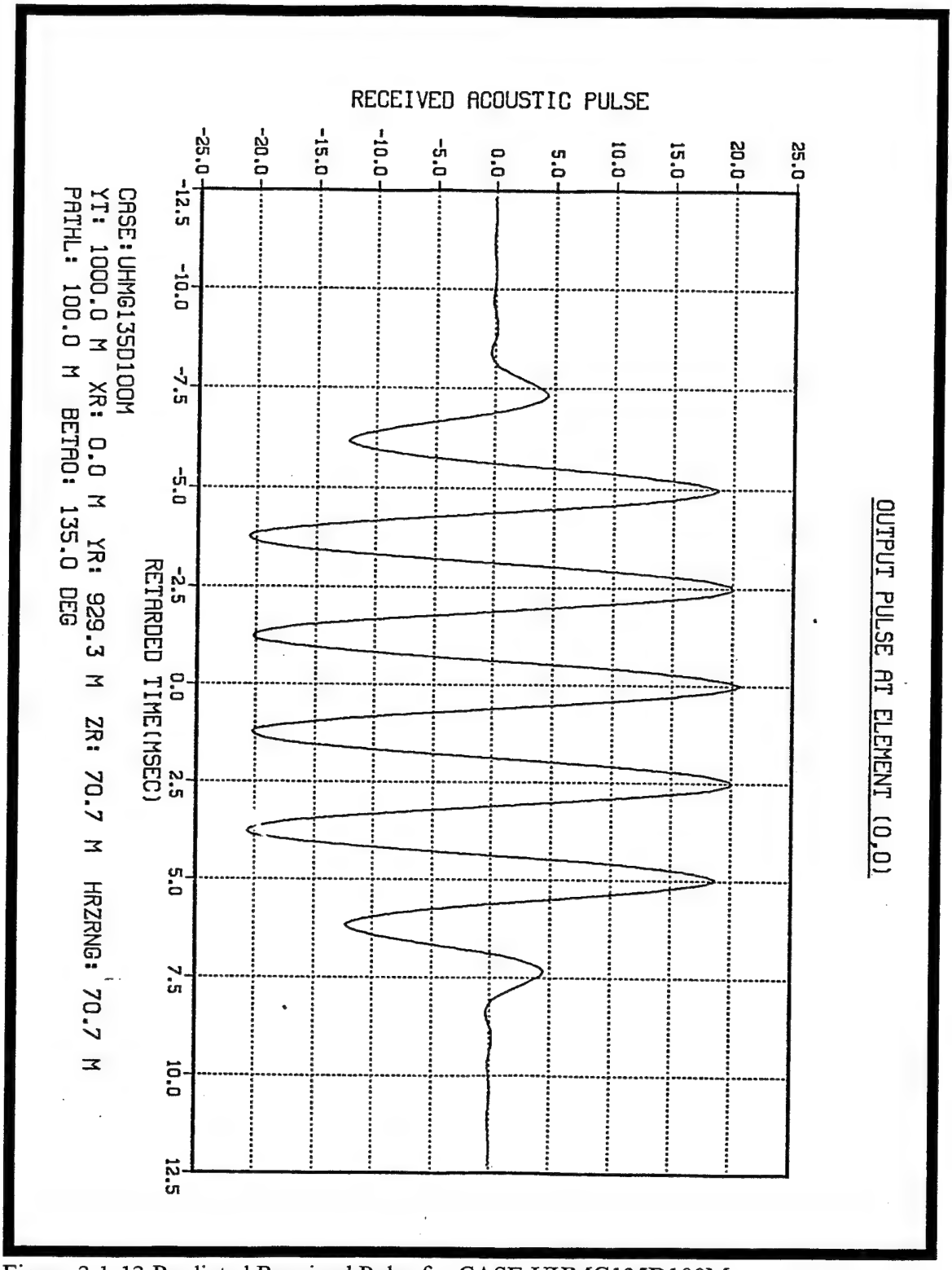

Figure 3.1-13 Predicted Received Pulse for CASE:UHMG135D100M.

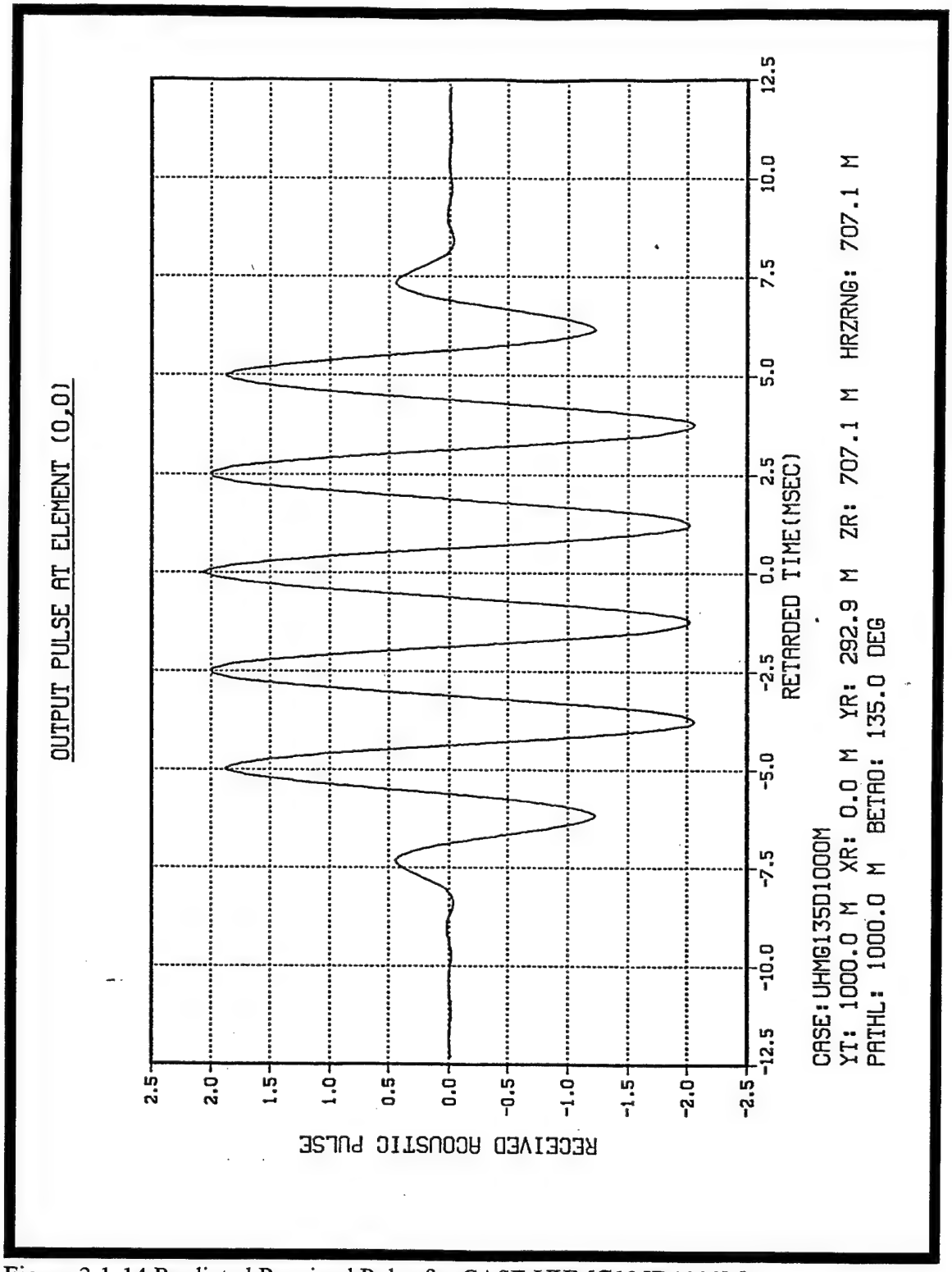

Figure 3.1-14 Predicted Received Pulse for CASE:UHMG135D1000M.

B. TEST CASES FOR AN AMPLITUDE-MODULATED CARRIER PROPAGATING ALONG A SINGLE EIGENRAY IN A BOUNDED, HOMOGENEOUS OCEAN MEDIUM

This section examines the received pulse shapes and amplitudes for an amplitude-modulated carrier that has been reflected from either the ocean bottom or surface. In order to clearly see the effects of a reflection coefficient on the phase of the received pulse, only one surface or bottom bounce was used for each test case. The reflection coefficients used for the test cases in this section were -0.5 and -1.0 (ideal pressure-release boundary) for surface reflections, and +0.5 and +1.0 (ideal rigid boundary) for bottom bounces. The transmitted pulse is the same as that shown in Figure 3.1-1. The launch angles used were 30 and 150 degrees for the bottom and surface reflections, respectively. The total path length was 1000 meters and the speed of sound was taken to be 1500 m/s for all the test cases in this section. The geometries of the transmission path along a single eigenray between the transmitter and receiver with a surface or bottom reflection are illustrated in Figures 3.2-1 and 3.2-2, respectively.

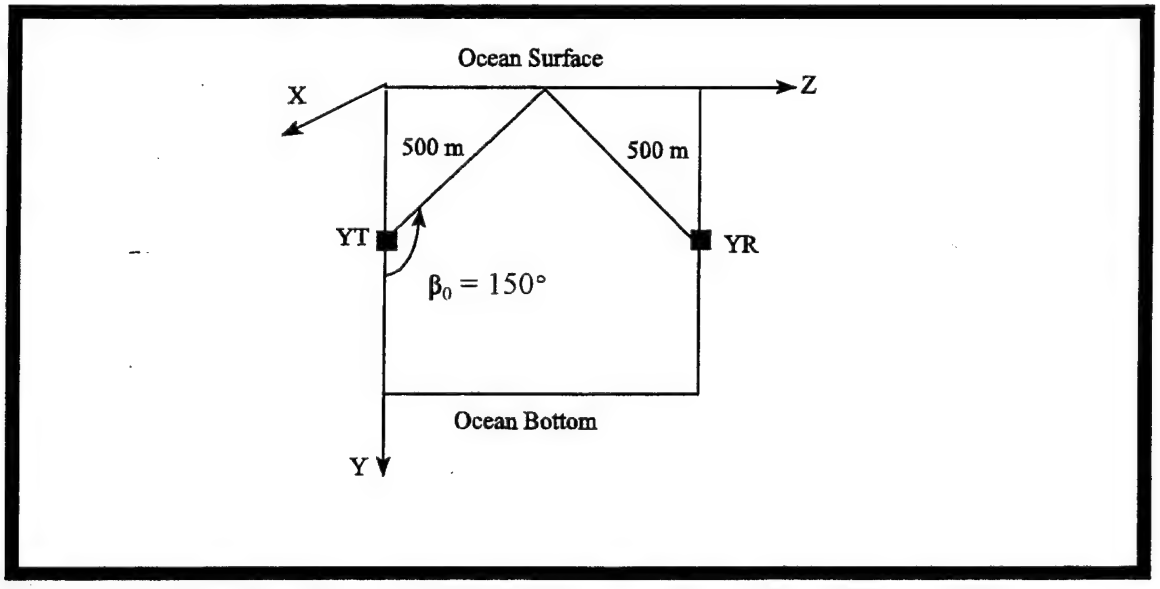

Figure 3.2-1 The Geometry of a Pulse Propagating along a Single Eigenray between a Transmitter and a Receiver with One Surface Reflection.

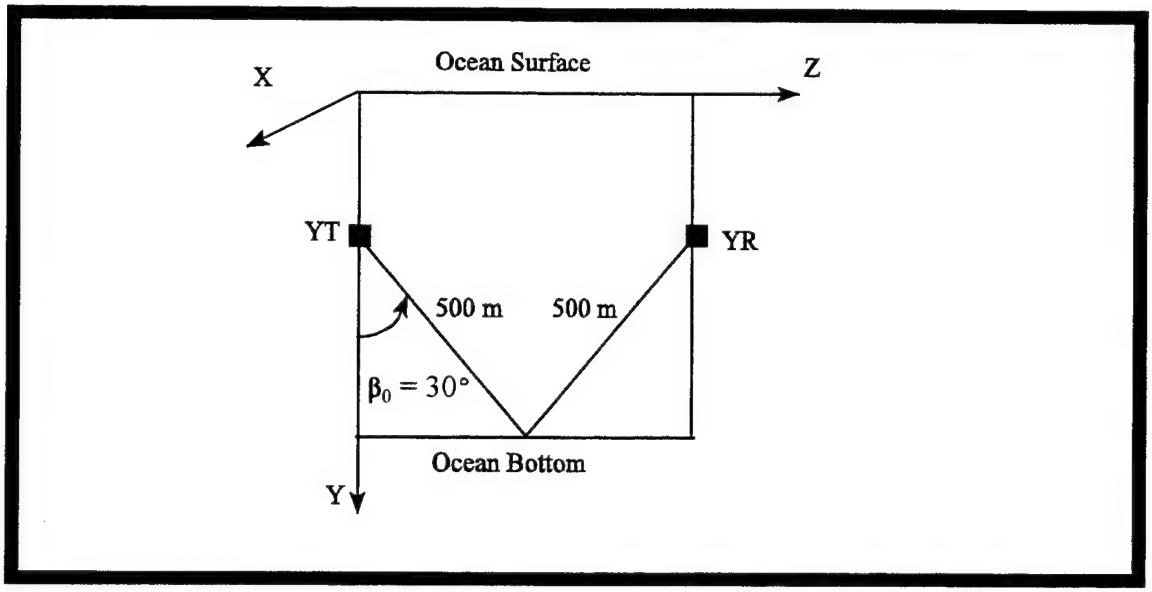

Figure 3.2-2 The Geometry of a Pulse Propagating along a Single Eigenray between a Transmitter and a Receiver with One Bottom Reflection.

There is no phase shift as the pulse hits the bottom with reflection coefficients equal to +1 and +0.5. However, the amplitude of the pulse reduces to one-half the amplitude of the incident pulse as it hits the ocean bottom with reflection coefficient equal to +0.5. Similarly, for surface reflection coefficients of -1 and -0.5, there is a 180-degree phase shift in the received pulse compared to the transmitted pulse for both surface reflection coefficients, and the amplitude of the received pulse reduces to one-half the amplitude of the incident pulse for a reflection coefficient equal to -0.5. In addition to the effects of the surface and bottom reflection coefficients, the amplitude of the received pulse should be 1/1000 of the amplitude of the pulse at 1 meter from the transmitter for the total path length of 1000 meters.

Figures 3.2-3 through 3.2-6 show the received pulses corresponding to cases BHMGR:-1.0150D1000M, BHMGR:-0.5150D1000M, BHMGR:+1.030D1000M, and BHMGR:+0.530D1000M, respectively. Notice that in Figures 3.2-3 and 3.2-4, there is a 180-degree phase shift in the received pulses compared to the transmitted pulse, and that the amplitudes fall off as 1/1000 and 1/2000 for the reflection coefficients of -1.0 and -0.5, respectively. The results illustrated in Figures 3.2-5 and 3.2-6 show that there is no phase shift in the received pulses; however, the amplitudes fall off as 1/1000 and 1/2000 for the

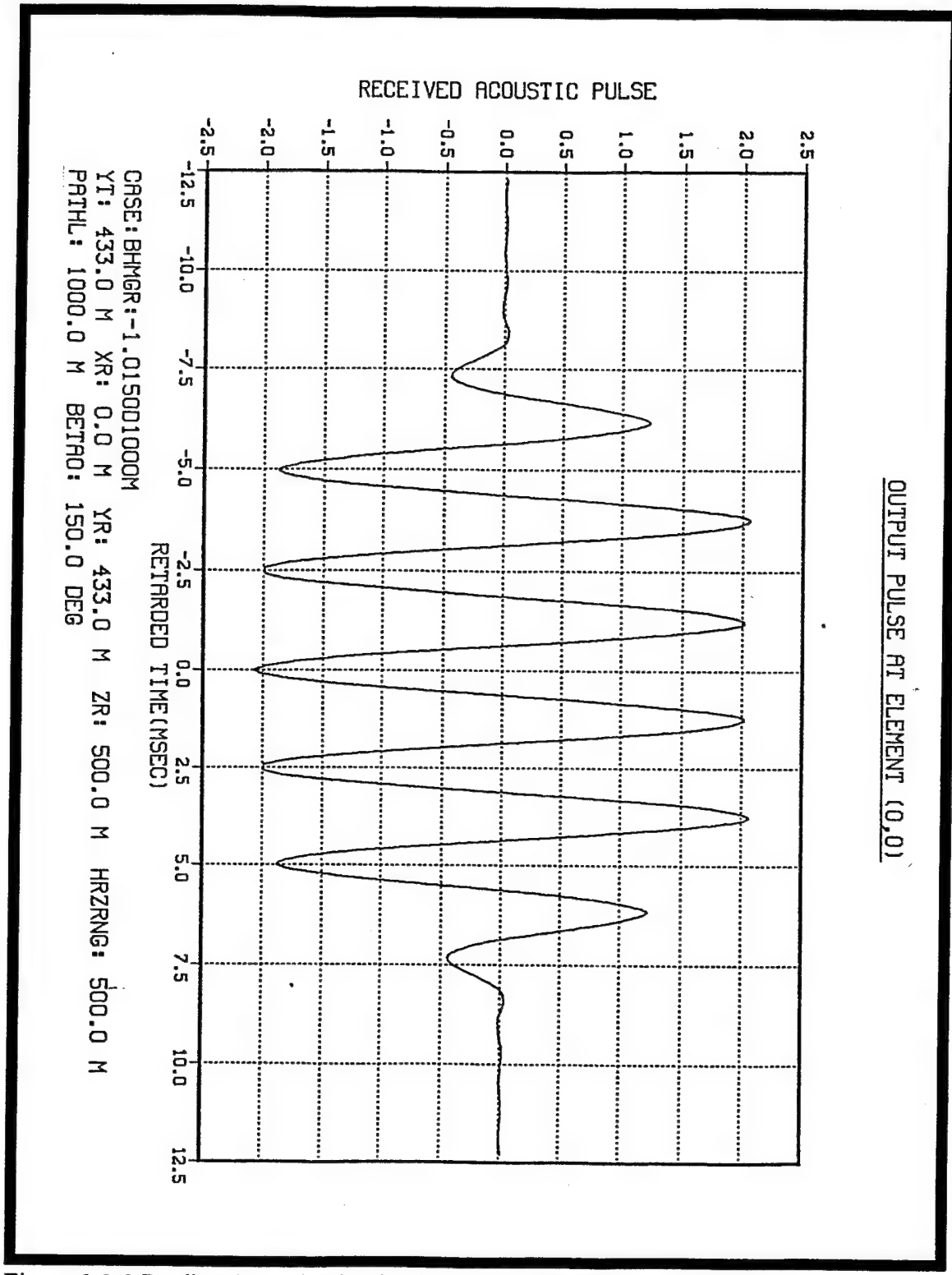

Figure 3.2-3 Predicted Received Pulse for CASE:BHMGR:-1.0150D1000M.

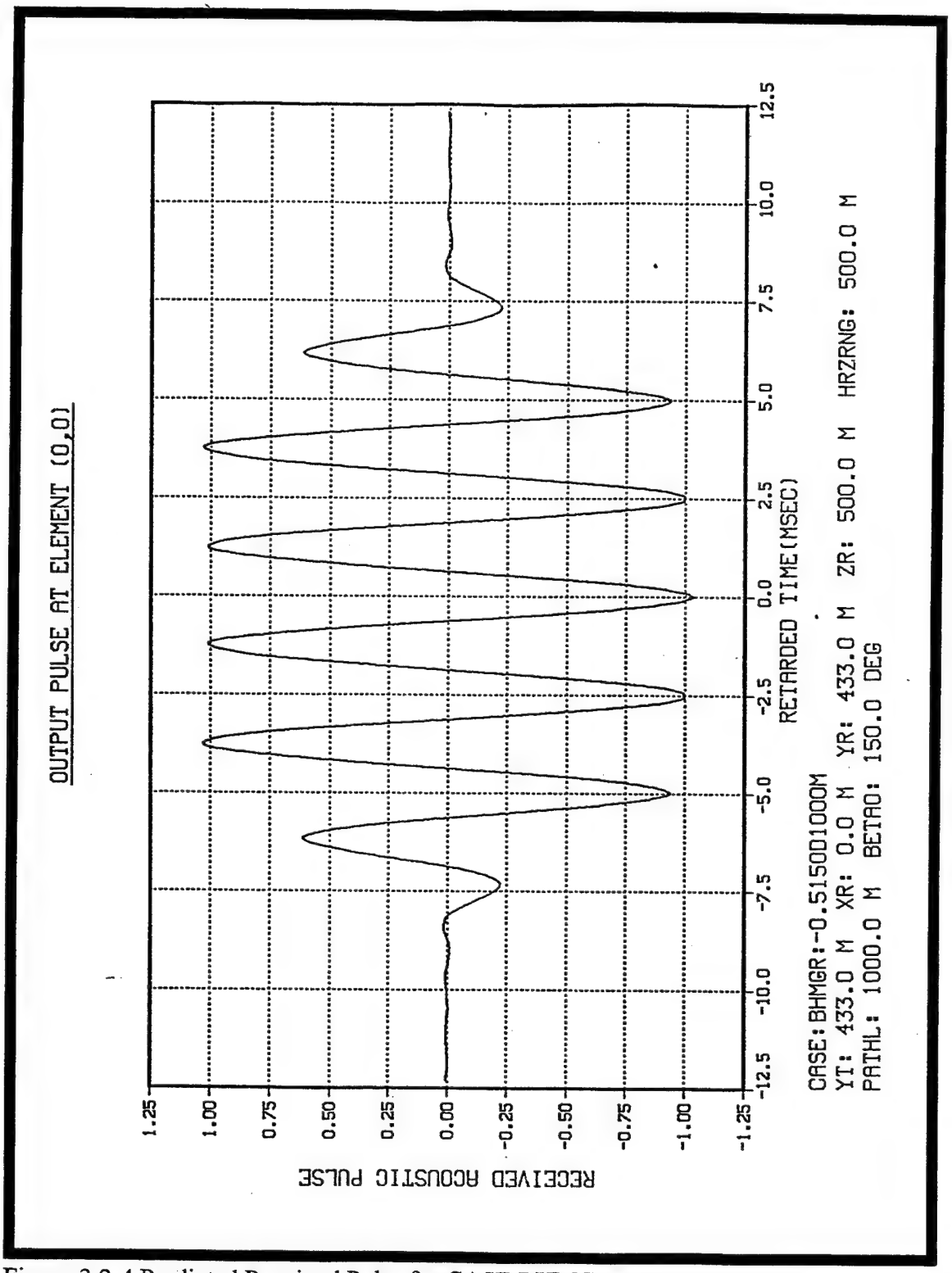

Figure 3.2-4 Predicted Received Pulse for CASE:BHMGR:-0.5150D1000M.

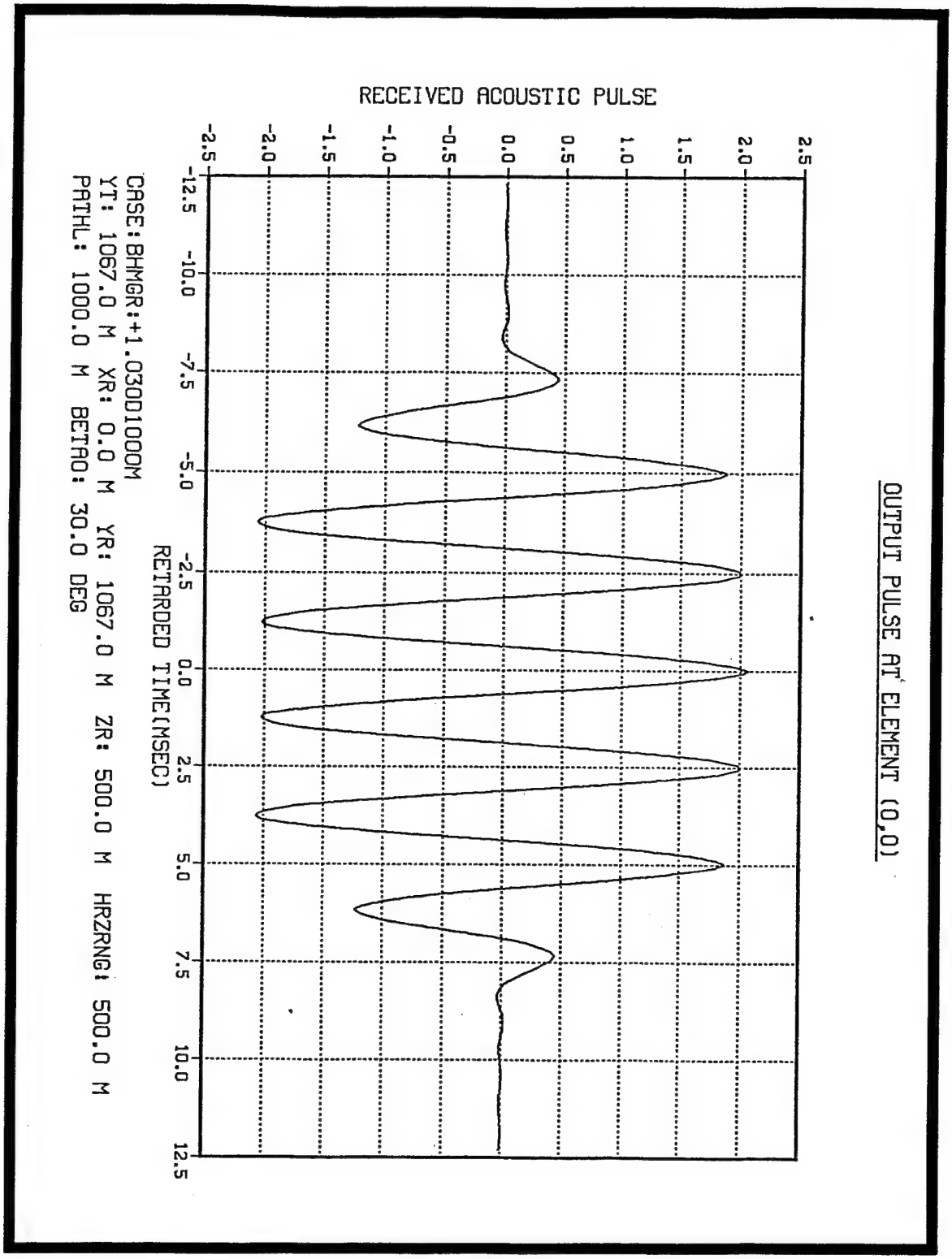

Figure 3.2-5 Predicted Received Pulse for CASE:BHMGR:+1.030D1000M.

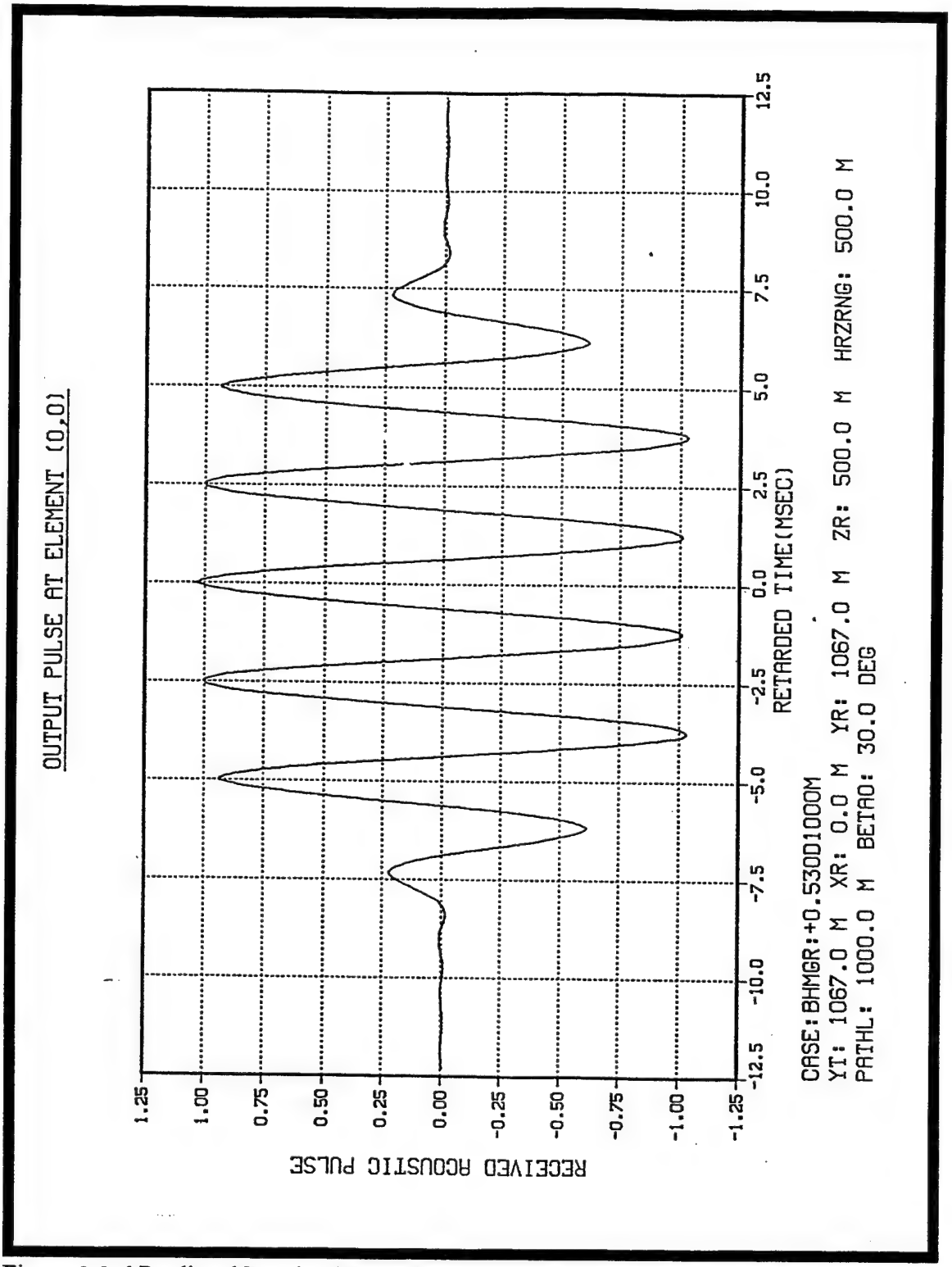

Figure 3.2-6 Predicted Received Pulse for CASE:BHMGR:+0.530D1000M.

reflection coefficients of +1.0 and +0.5, respectively. These simulation results correspond exactly to results predicted by theory.

C. TEST CASES FOR PULSE PROPAGATION IN AN OCEAN WAVEGUIDE WITH DIFFERENT OCEAN MEDIUM ENVIRONMENTS

This section presents the computer simulation results for an amplitude-modulated carrier propagating in an ocean waveguide with different ocean medium environments. The ocean medium is modeled with a speed of sound that is either constant or an arbitrary function of depth. The ocean surface is exposed to air with density $\rho_1 = 1.21$ kg/m^3 and speed of sound $c_1 = 343$ m/s. The ocean bottom is a fluidlike quartz sand with density $\rho_3 = 2070$ kg/m^3 and speed of sound $c_3 = 1730$ m/s. The transmitted signal is a continuous-wave (CW) pulse with Hamming envelope, as illustrated in Figure 3.3-1. The transmitted pulse is represented by 77 frequency components (NFREQ), it has an amplitude (A) of 7928.8, a pulse length (TP) of 100 msec, a pulse-repetition frequency (PRF) of 0.8 Hz, and a carrier frequency (FC) of 250 Hz. The amplitude (A) of 7928.8 corresponds to the transmitted acoustic signal having a source level of 180 dB *re* 1 μPa. For all the test cases discussed in this section, the transmitter is located at YT = 30 m below the ocean surface, and X = 0 m, and Z = 0 m; the receiver is located above the transmitter at YR = 20 m below the ocean surface, and XR = 0 m, and ZR = 4 km. The relative geometry of the transmitter, the receiver, the ocean surface, and the ocean bottom is depicted in Figure 3.3-2.

In order to predict the received pulse corresponding to the transmitted electrical signal illustrated in Figure 3.3-1, we need to find all the eigenrays arriving at the receiver and calculate the overall system complex frequency response at the receiver. The RRA Algorithm is able to search for all the eigenrays and calculate the overall system complex frequency response at the receiver. The parameters used to search for the eigenrays are YERROR = 0.1 m, DLTS = 0.5 m, and ANGSTP = 0.01 degree. This means that the RRA Algorithm will search for eigenrays by launching rays using an angle step size of 0.01 degrees and an arc length step size of 0.5 meters. If the rays reach the horizonal range where

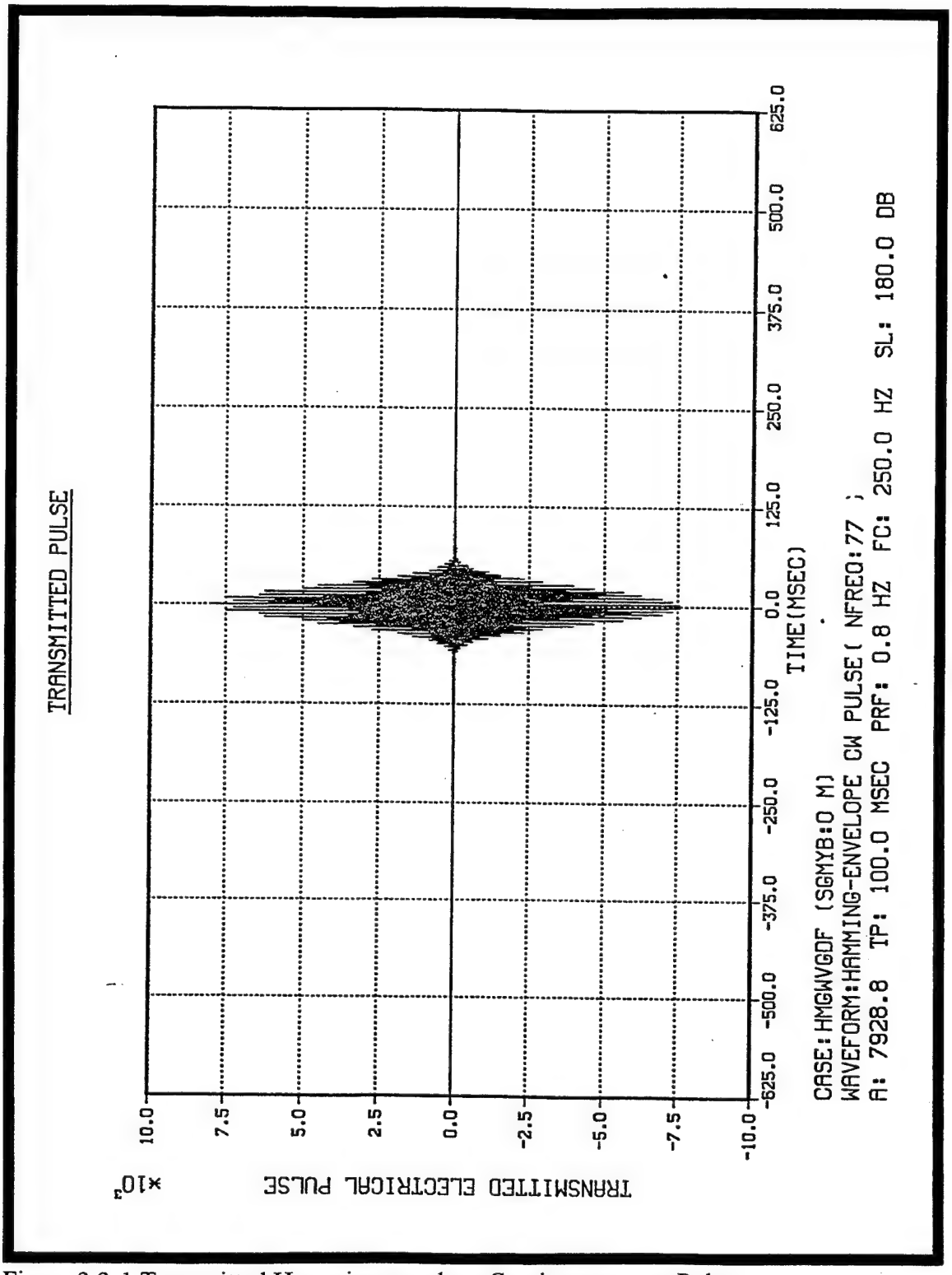

Figure 3.3-1 Transmitted Hamming-envelope Continuous-wave Pulse.

the receiver is located and are within ±0.1 meters of the depth of the receiver, then they will be considered as eigenrays. By using the RRA Algorithm and the LSVOCN computer program together, the received pulse corresponding to a given transmitted electrical signal can be predicted at the receiver.

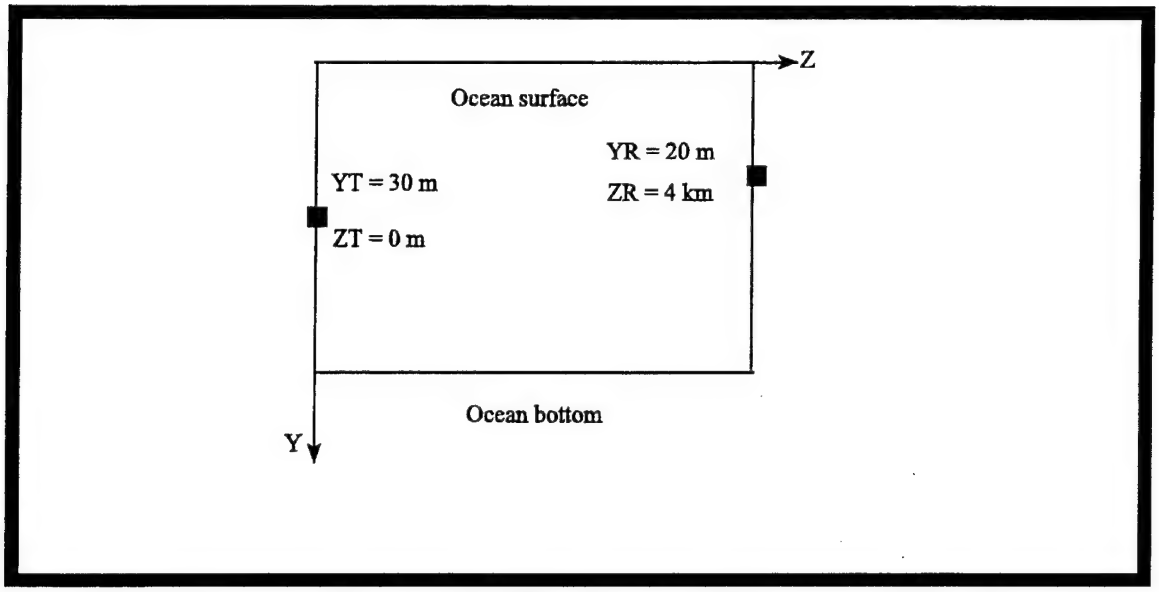

Figure 3.3-2 The Relative Geometry of The Transmitter, The Receiver, The Ocean Surface, and The Ocean Bottom.

In order to see the effects of the ocean medium environment on the received pulse shape, computer simulation results were produced based on cases of a homogeneous and inhomogeneous ocean medium, and for ocean bottom cases where the bottom is flat, flat but randomly rough, has a 3 degree smooth up-slope, a 3 degree randomly rough up-slope, a 3 degree smooth down-slope, and a 3 degree randomly rough down-slope. The parameter SGMYB (in meters) is used to model the randomly rough ocean bottom. It is the standard deviation of a zero-mean gaussian random variable that is added to the original ocean bottom depth data.

Figures 3.3-3 and 3.3-4 are the received pulse and the eigenrays plot, respectively, corresponding to case HMGWVGDF(SGMYB:0M), where SGMYB = 0M indicates that the ocean bottom is smooth. In the eigenrays plot, Y0 and YRCVR are the depths of the transm-

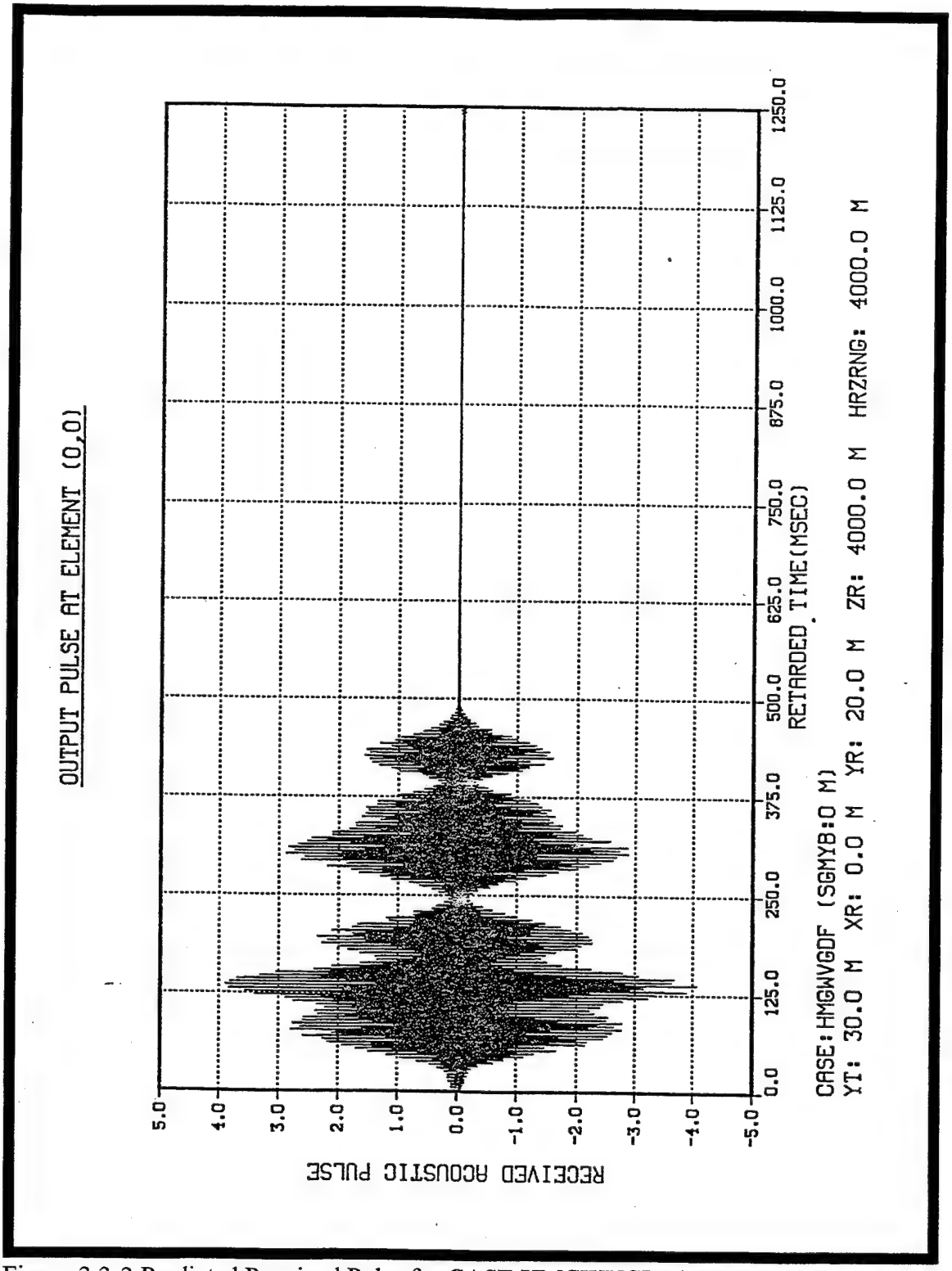

Figure 3.3-3 Predicted Received Pulse for CASE:HMGWVGDF(SGMYB:0M).

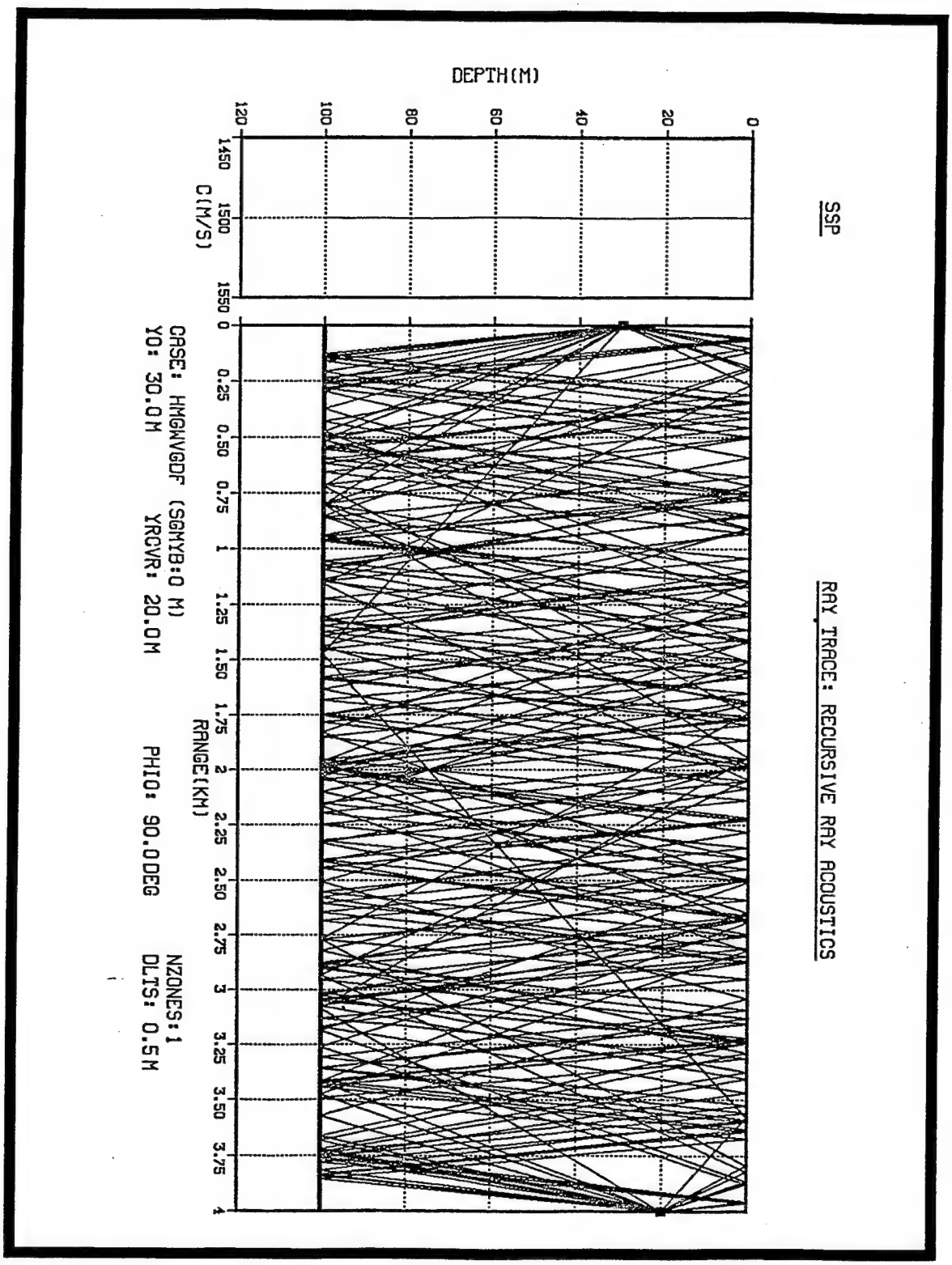

Figure 3.3-4 Eigenrays Plot Corresponding to CASE:HMGWVGDF(SGMYB:0M).

itter and receiver, respectively, and PHI0 is the azimuthal launch angle measuredfrom the cross-range axis (X) to the projection of the initial ray path in the XZ plane.

The speed of sound data and the ocean bottom data are listed in Tables 1 and 2, respectively. In Table 1, XDATA,YDATA, ZDATA, and CDATA are the cross-range, depth, horizontal range and speed of sound data, respectively. In Table 2, XBDATA, ZBDATA, and YBDATA are the ocean bottom cross-range, ocean bottom horizontal range, and ocean bottom depth data, respectively.

XDATA(M)	YDATA(M)	ZDATA(M)	CDATA(M/S)
0.00	0.00	0.00	1500.00
0.00	8.75	0.00	1500.00
0.00	17.50	0.00	1500.00
0.00	26.25	0.00	1500.00
0.00	35.00	0.00	1500.00
0.00	43.75	0.00	1500.00
0.00	52.50	0.00	1500.00
0.00	61.25	0.00	1500.00
0.00	100.00	0.00	1500.00

Table 1. Speed of sound data used in case HMGWVGDF(SGMYB:0M)

XBDATA(M)	ZBDATA(M)	YBDATA(M)
0.00	0.00	100.00
0.00	1000.00	100.00
0.00	3000.00	100.00
0.00	5000.00	100.00
0.00	7000.00	100.00
0.00	8000.00	100.00
0.00	9000.00	100.00
0.00	10000.00	100.00

Table 2. Ocean bottom data used in case HMGWVGDF(SGMYB:0M

Since the speed of sound $_c$ in the ocean medium is less than the speed of sound c_3 in the ocean bottom, the critical angle of incidence for bottom reflections is given by

$$\theta_c = \sin^{-1}\left(\frac{c_2}{c_3}\right) \quad for \quad c_2 < c_3 \ . \tag{3.1}$$

For all angles of incidence less than the critical angle of incidence, the magnitude of the reflection coefficient is very small. The critical angle of incidence θ_c is calculated to be 60.1 degrees by using Eq. (3.1) with $_c$ = 1500 m/s and c_3 = 1730 m/s. Therefore, we searched for eigenrays by using launch angles β_0 from 60 degrees to 120 degrees. The ocean surface is an ideal pressure-release boundary with reflection coefficient equal to -1. The relationship between the launch angle β_0 and the angle of incidence θ_i for surface and bottom reflections in a homogeneous ocean medium with a flat surface and bottom are illustrated in Figures 3.3-5 and 3.3-6, respectively.

The distortion and dispersion of the received pulse compared to the transmitted pulse is due to the different travel times of each eigenray, and the effects of constructive and destructive interference. Figures 3.3-7 and 3.3-8 are the received pulse and eigenrays plot, respectively, corresponding to case HMGWVGDF(SGMYB:1M), where SGMYB = 1M indicates that the ocean bottom is basically flat , but now randomly rough. The speed of sound data and ocean bottom data are the same as those used in the previous case, with the exception that the bottom data has been randomized. We see that the received pulse is totally different from that in the previous case (see Figure 3.3-3). The launch angles used for finding the eigenrays were from 50 to 130 degrees. However, launch angles between 40 and 140 degrees were also used in order to insure that no eigenrays would be missed.

Figures 3.3-9 and 3.3-10 are the received pulse and eigenrays plot, respectively, for the case INHMGWVGDF(SGMYB: 0M). The launch angles used for finding the eigenrays were from 60 to 120 degrees. Once again, a wider angular sector was used to insure that there were no eigenrays to be found outside of the sector. The ocean bottom data used in

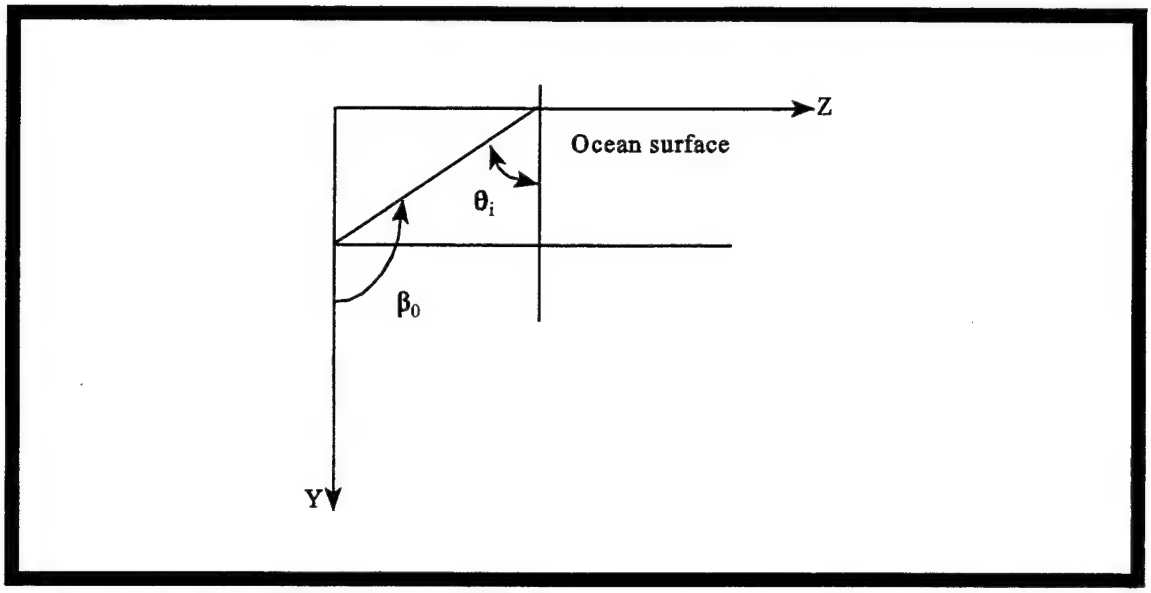

Figure 3.3-5 The Relationship between The Launch Angle β_0 and The Angle of Incidence θ_i for a Surface Reflection in a Homogeneous Ocean Medium with a Flat Surface.

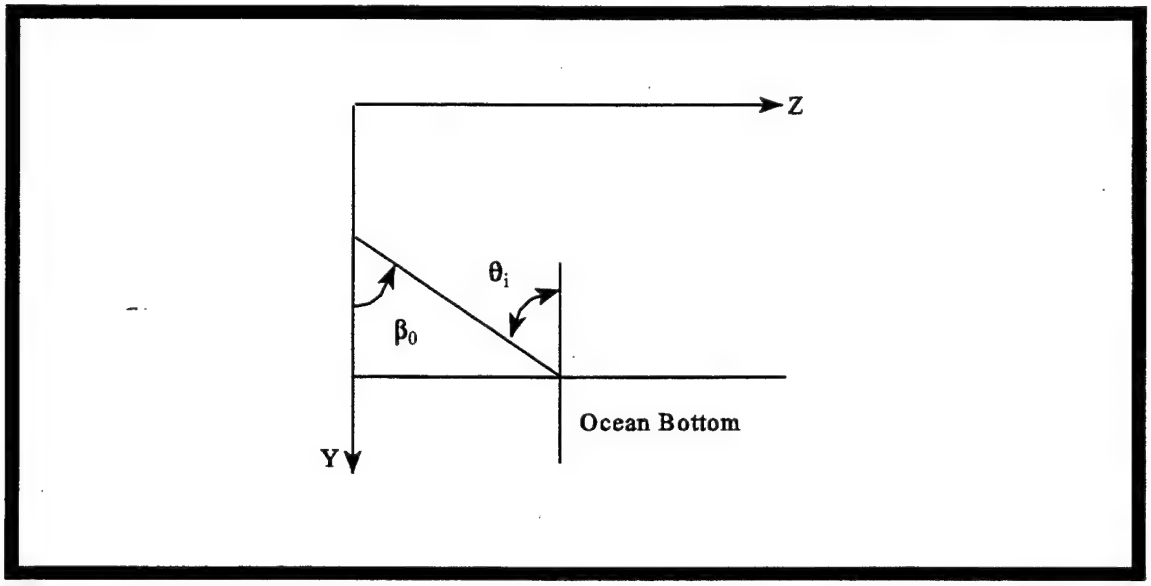

Figure 3.3-6 The Relationship between The Launch Angle β_0 and The Angle of Incidence θ_i for a Bottom Reflection in a Homogeneous Ocean Medium With a Flat Bottom.

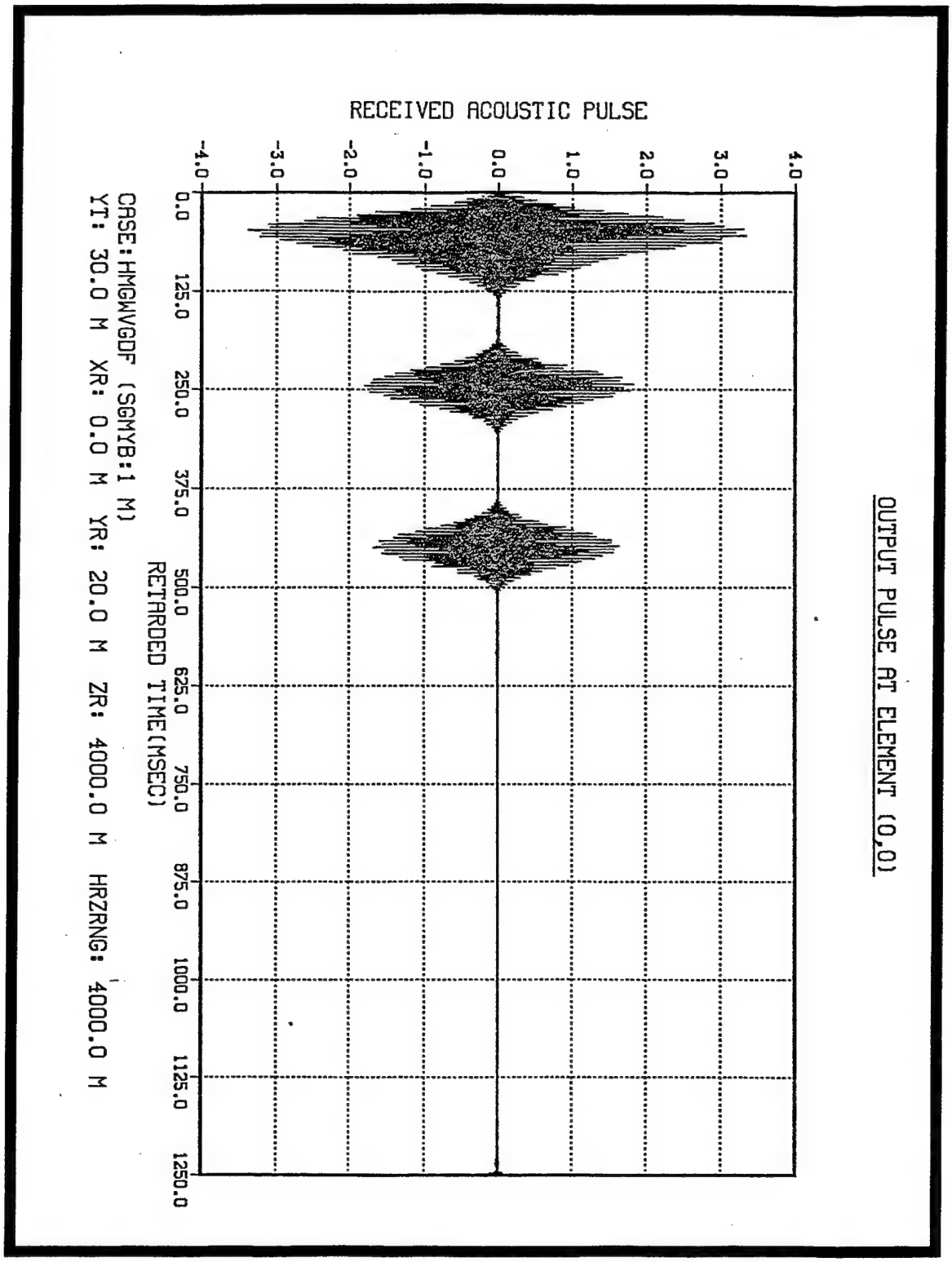

Figure 3.3-7 Predicted Received Pulse for CASE:HMGWVGDF(SGMYB:1M).

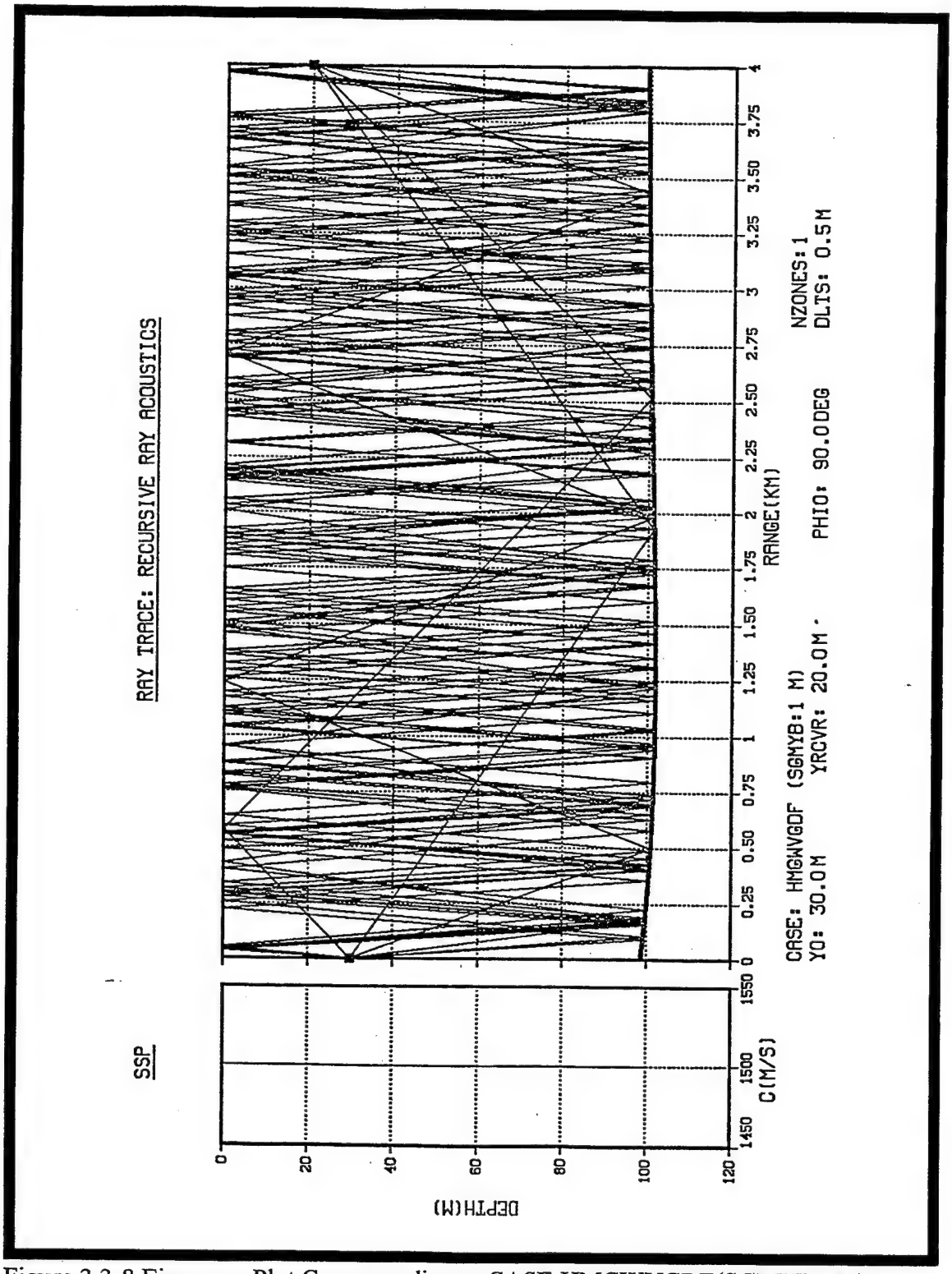

Figure 3.3-8 Eigenrays Plot Corresponding to CASE:HMGWVGDF(SGMYB:1M).

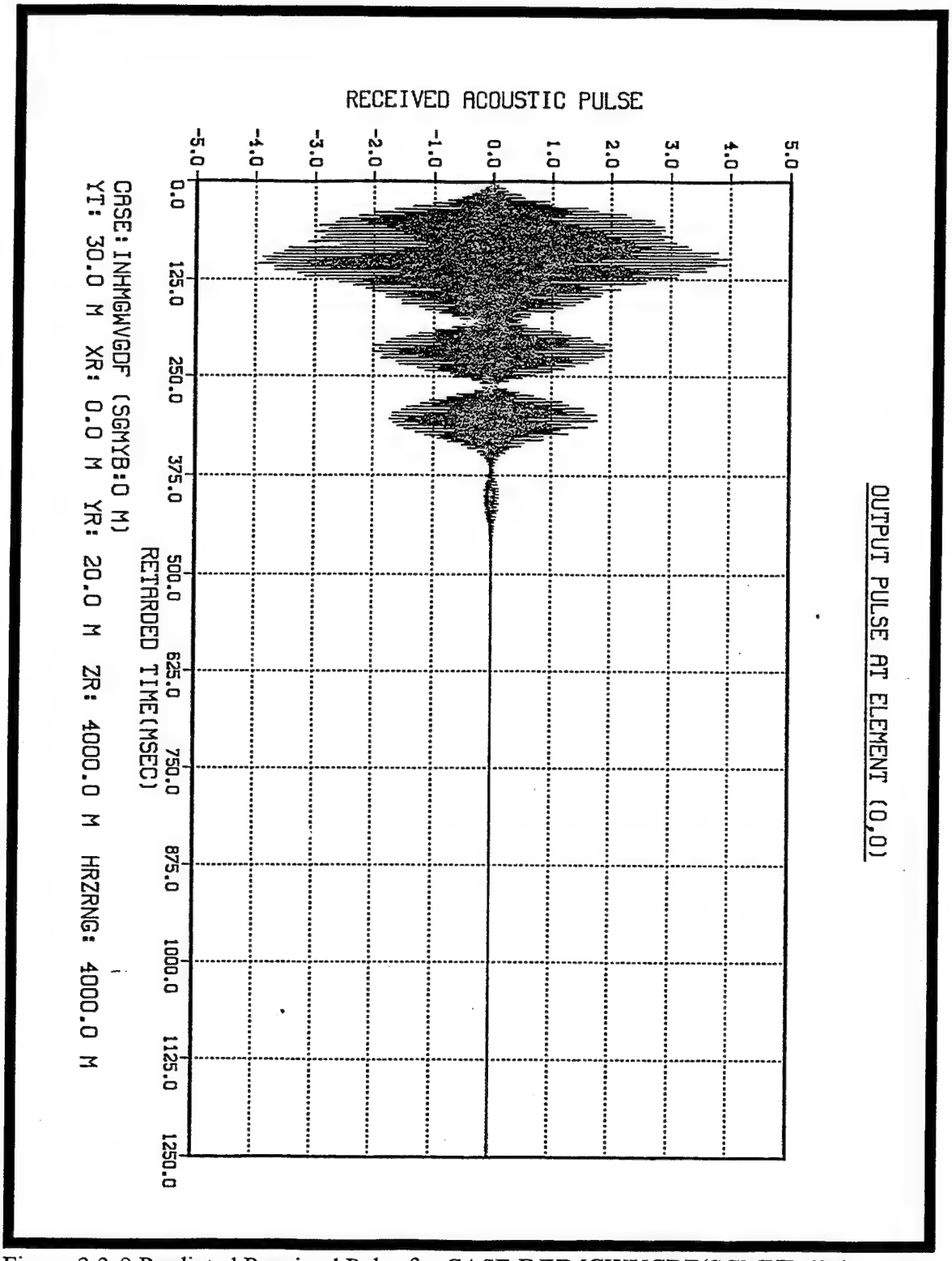

Figure 3.3-9 Predicted Received Pulse for CASE:INHMGWVGDF(SGMYB:0M).

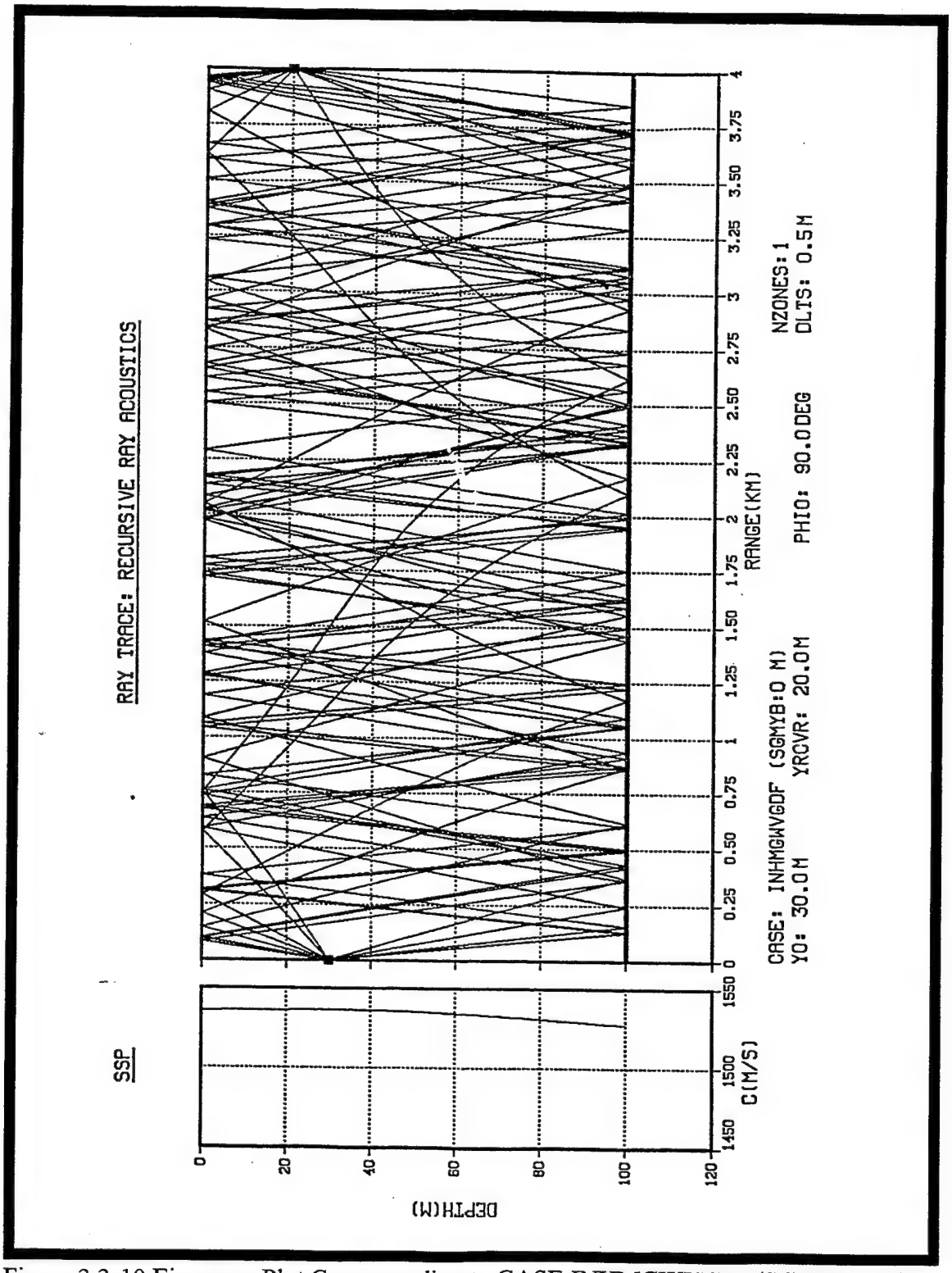

Figure 3.3-10 Eigenrays Plot Corresponding to CASE:INHMGWVGDF(SGMYB:0M).

this case are the same as those in Table 2. However, for this test case, the ocean medium is taken to be inhomogeneous with speed of sound data listed in Table 3.

XDATA(M)	YDATA(M)	ZDATA(M)	CDATA(M/S)
0.00	0.00	0.00	1535.94
0.00	10.00	0.00	1536.19
0.00	20.00	0.00	1536.33
0.00	30.00	0.00	1536.40
0.00	50.00	0.00	1535.52
0.00	75.00	0.00	1531.93
0.00	100.00	0.00	1527.22
0.00	125.00	0.00	1523.75
0.00	150.00	0.00	1522.20

Table 3. Speed of sound data used in case INHMGWVGDF(SGMYB:0M)

Figures 3.3-11 and 3.3-12 are the received pulse and eigenrays plot, respectively, corresponding to case INHMGWVGDF(SGMYB:1M). The launch angles used for finding the eigenrays were from 50 to 130 degrees. The ocean bottom data and the speed of sound data are the same as those in the previous case, with the exception that the bottom data has been randomized. Note the difference between the received pulses shown in Figures 3.3-9 and 3.3-11, due to the randomly rough ocean bottom.

Figures 3.3-13 and 3.3-14 are the received pulse and eigenrays plot, respectively, corresponding to case HMGWVGDUS3D(SGMYB:0M). The launch angles used for finding the eigenrays were from 60 to 120 degrees. The speed of sound data and the 3 degree up-slope ocean bottom data are listed in Table 4 and Table 5, respectively.

Figures 3.3-15 and 3.3-16 are the received pulse and eigenrays plot, respectively, corresponding to case HMGWVGDUS3D(SGMYB:1M). The launch angles used for finding the eigenrays were from 60 to 120 degrees. The speed of sound data and the ocean bottom data are the same as listed in Table 4 and Table 5, respectively, with the exception that the

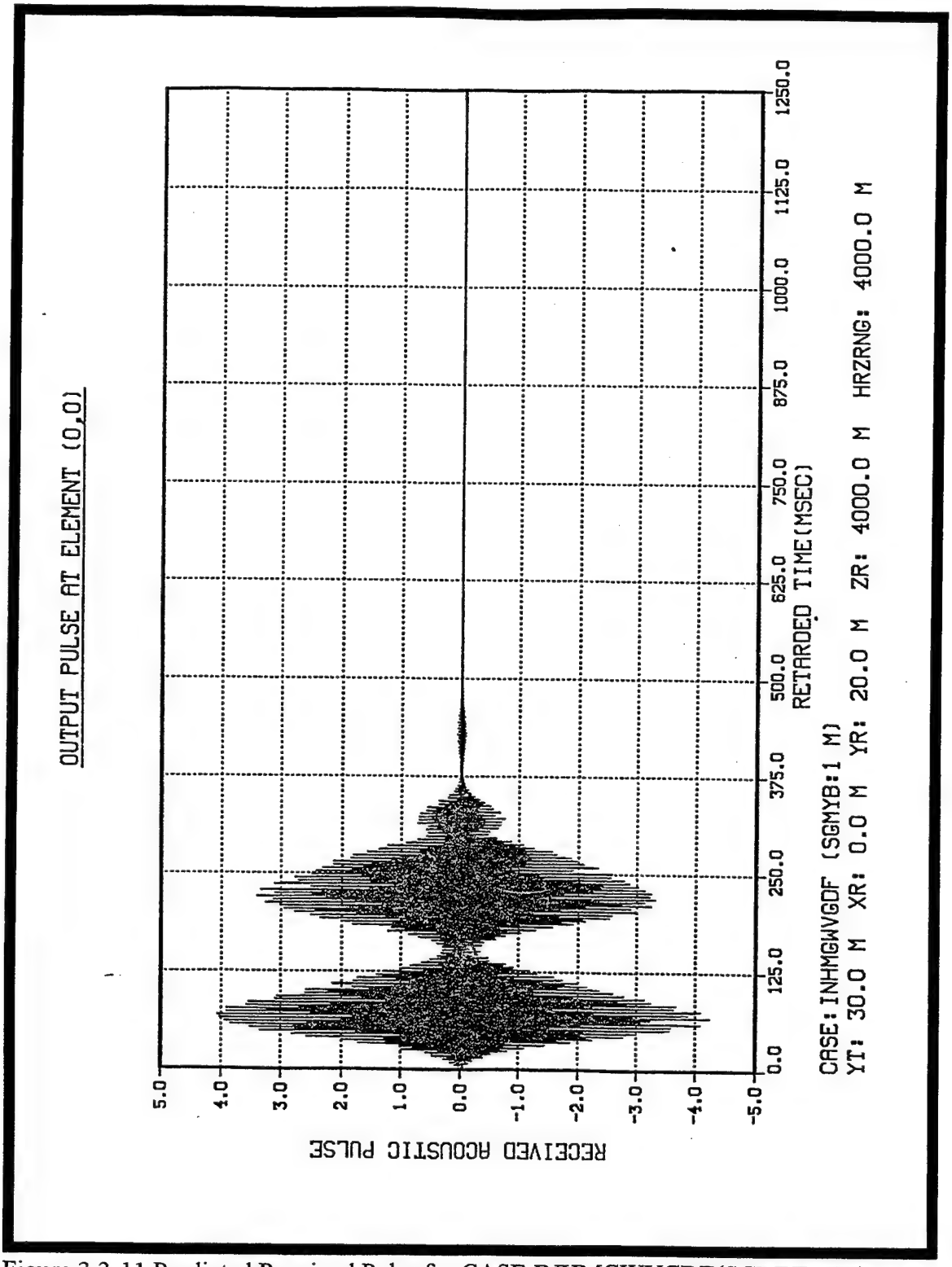

Figure 3.3-11 Predicted Received Pulse for CASE:INHMGWVGDF(SGMYB:1M).

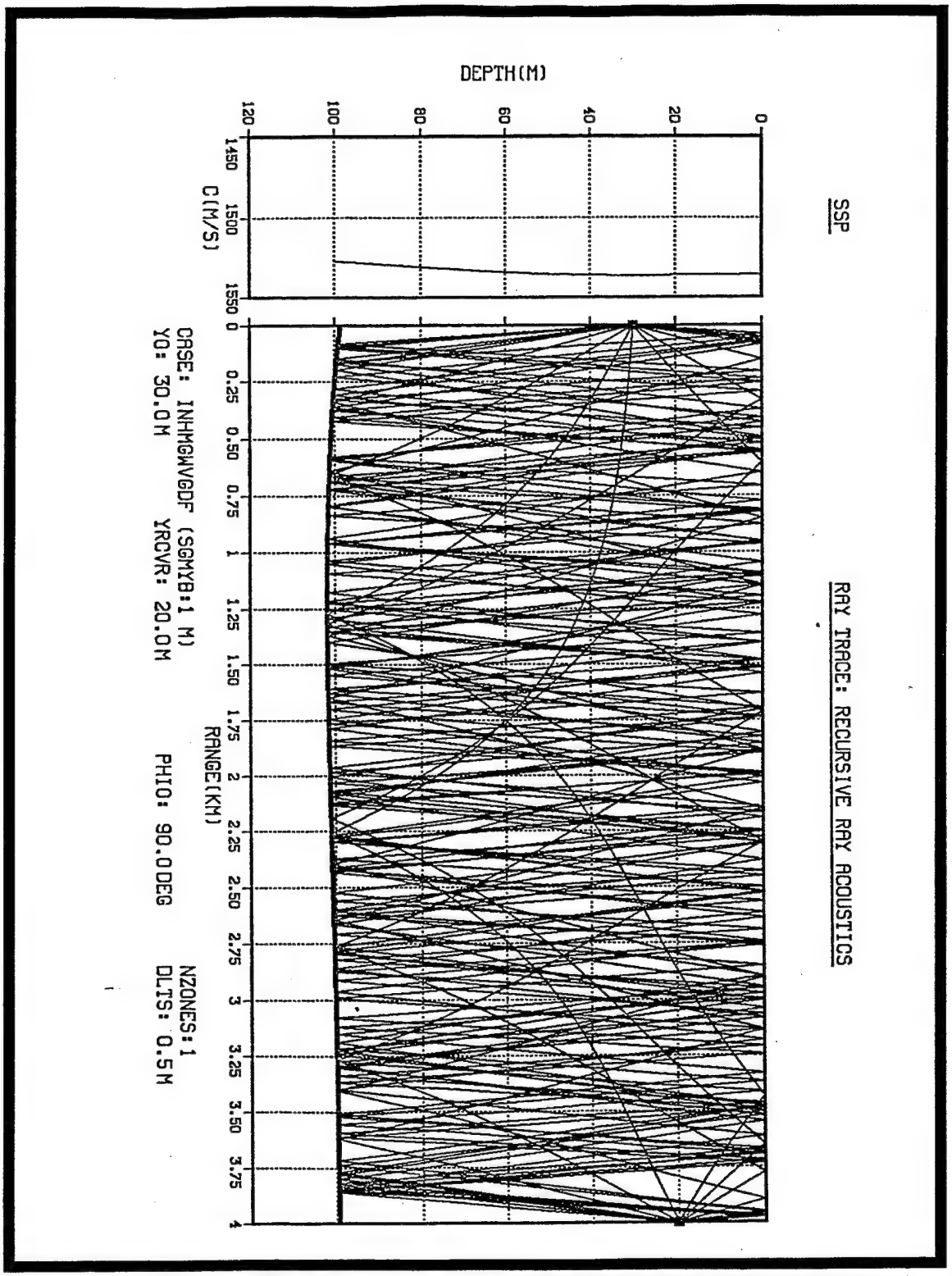

Figure 3.3-12 Eigenrays Plot Corresponding to CASE:INHMGWVGDF(SGMYB:1M).

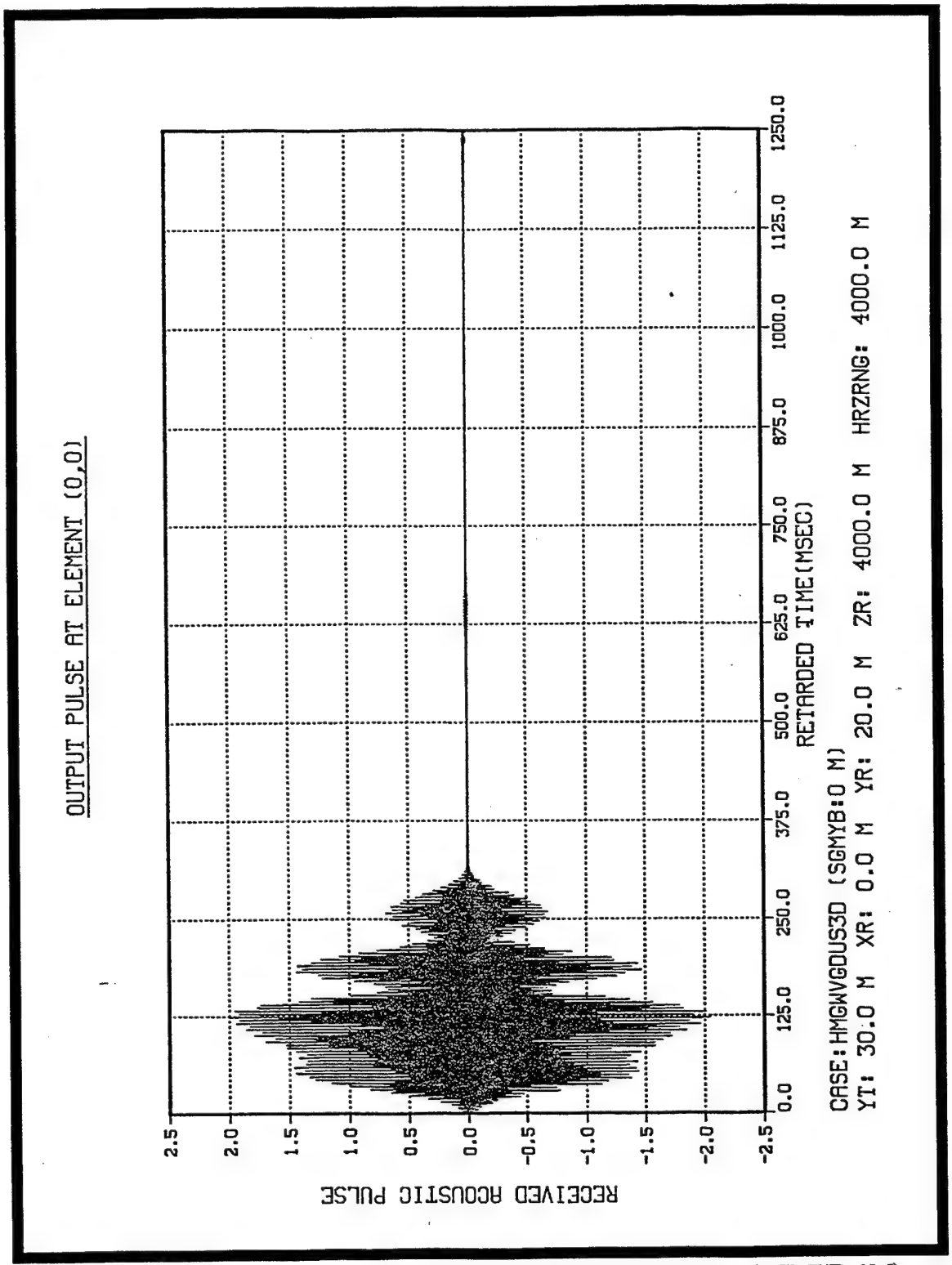

Figure 3.3-13 Predicted Received Pulse for CASE:HMGWVGDUS3D(SGMYB:0M).

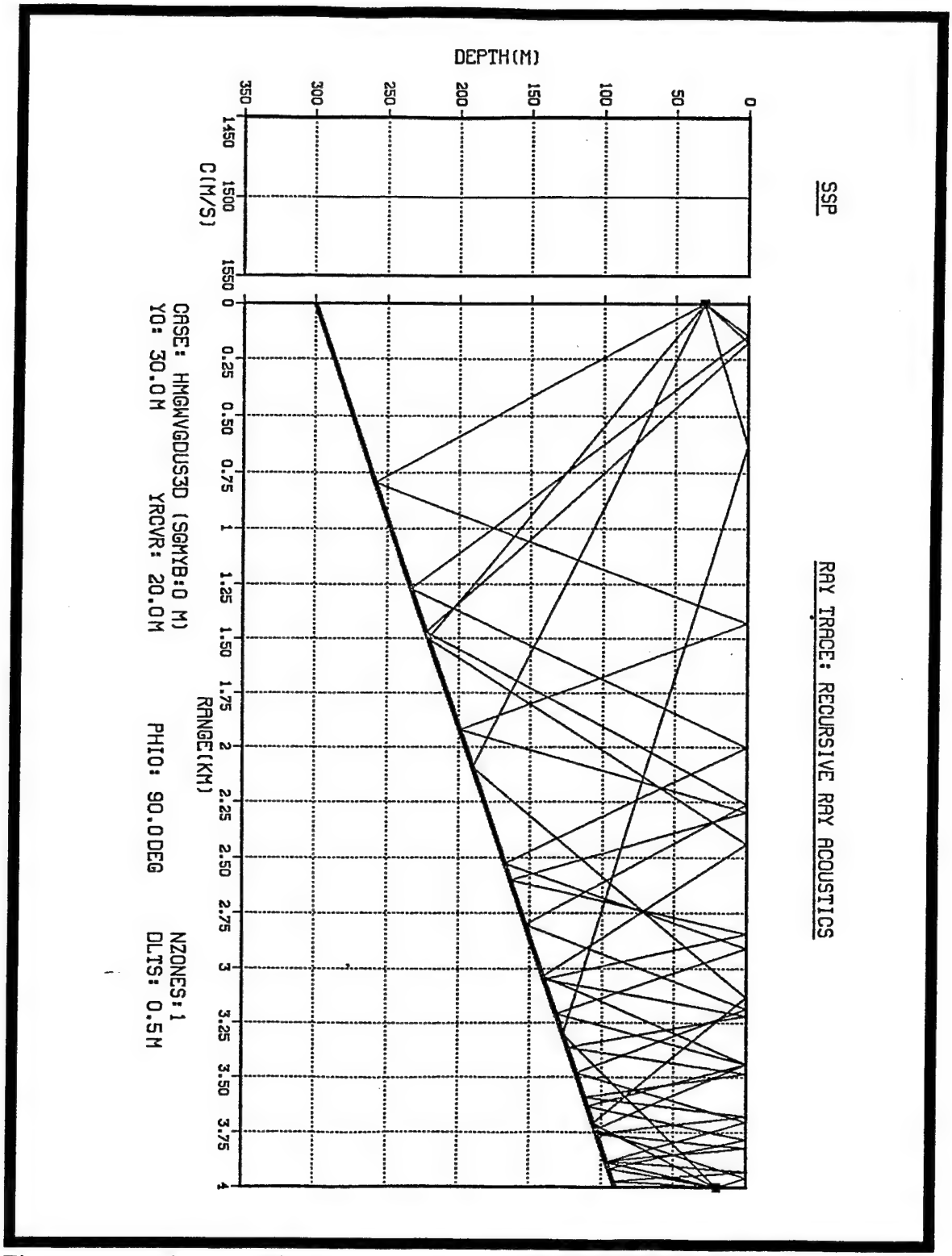

Figure 3.3-14 Eigenrays Plot Corresponding to CASE: HMGWVGDUS3D (SGMYB:0M).

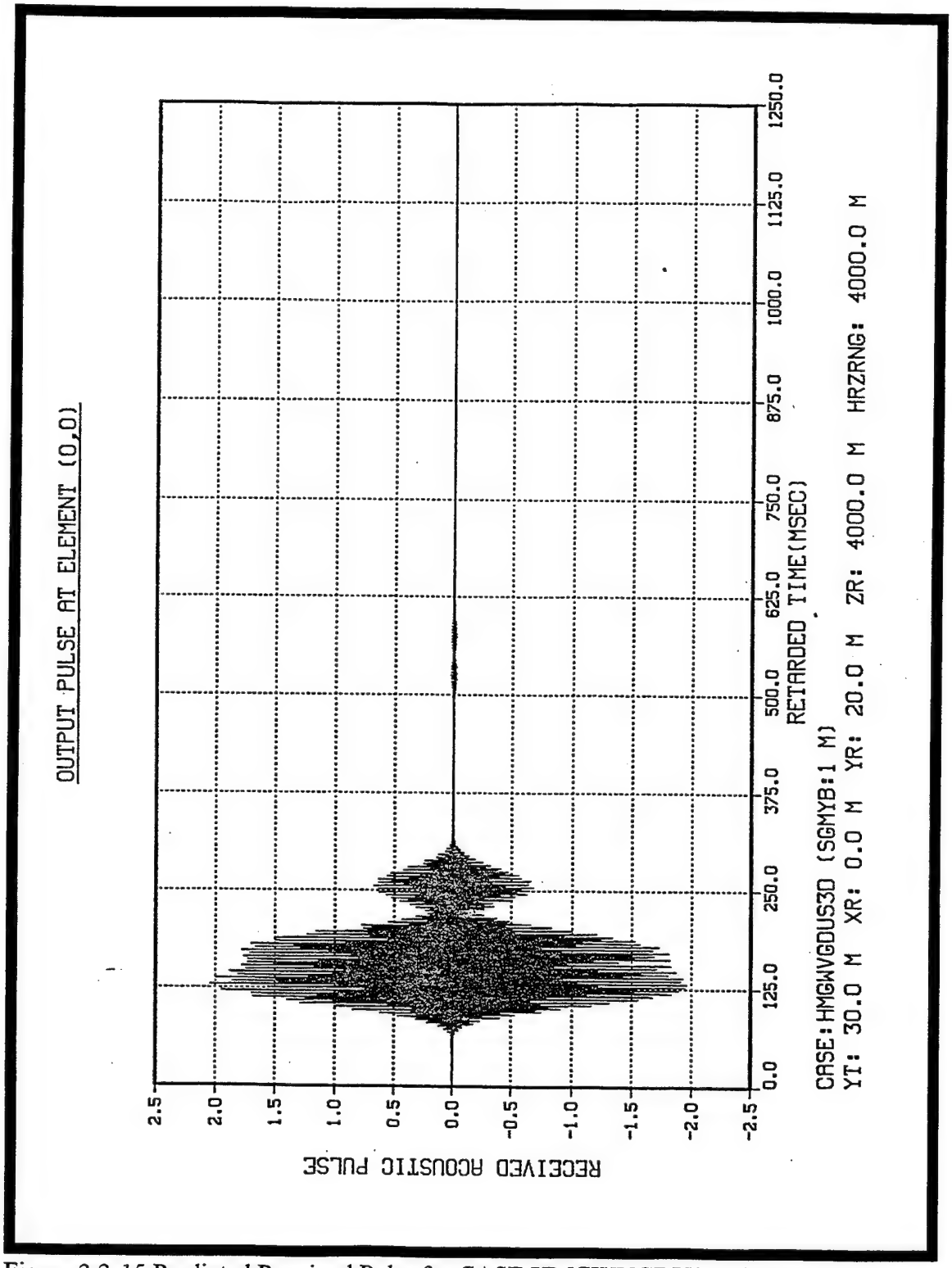

Figure 3.3-15 Predicted Received Pulse for CASE:HMGWVGDUS3D(SGMYB:1M).

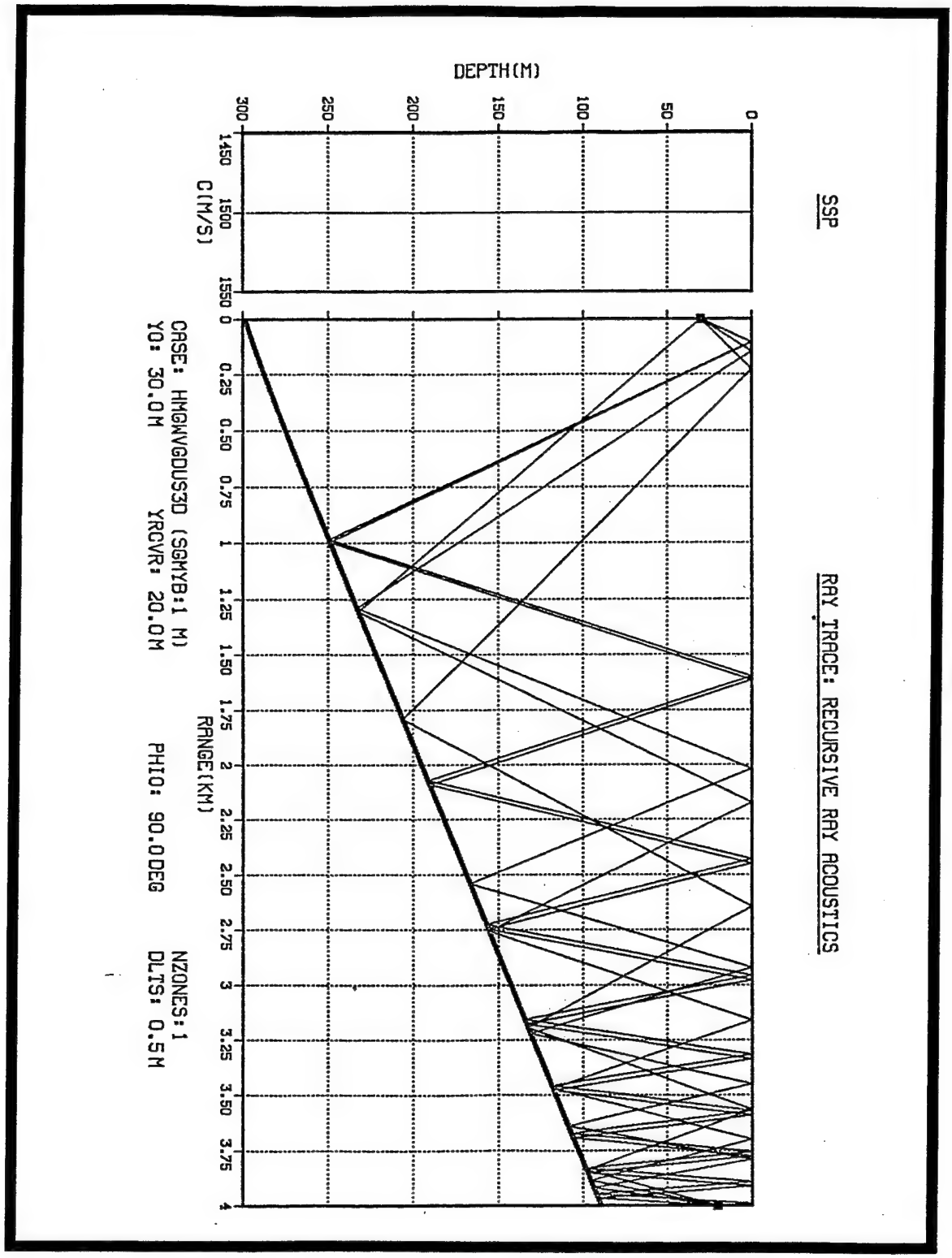

Figure 3.3-16 Eigenrays Plot Corresponding to CASE:HMGWVGDUS3D (SGMYB:1M).

bottom data has been randomized. Again, note the difference between the received pulses shown in Figures 3.3-13 and 3.3-15, due to the randomly rough ocean bottom.

XDATA(M)	YDATA(M)	ZDATA(M)	CDATA(M/S)
0.00	0.00	0.00	1500.00
0.00	10.00	0.00	1500.00
0.00	20.00	0.00	1500.00
0.00	30.00	0.00	1500.00
0.00	50.00	0.00	1500.00
0.00	75.00	0.00	1500.00
0.00	100.00	0.00	1500.00
0.00	125.00	0.00	1500.00
0.00	150.00	0.00	1500.00
0.00	200.00	0.00	1500.00
0.00	250.00	0.00	1500.00
0.00	300.00	0.00	1500.00
0.00	400.00	0.00	1500.00

Table 4. Speed of sound data used in case HMGWVGDUS3D(SGMYB:0M)

Figures 3.3-17 and 3.3-18 are the received pulse and eigenrays plot, respectively, corresponding to case INHMGWVGDUS3D(SGMYB:0M). The launch angles used for finding the eigenrays were from 60 to 120 degrees. The ocean bottom data are the same as listed in Table 5. The speed of sound data are listed in Table 6.

Figures 3.3-19 and 3.3-20 are the received pulse and eigenrays plot, respectively, corresponding to case INHMGWVGDUS3D(SGMYB:1M). The launch angles used for finding the eigenrays were from 60 to 120 degrees. The ocean bottom data are the same as listed in Table 5, with the exception that the bottom data has been randomized. The speed of sound data are the same as listed in Table 6. Note the difference between the received pulses shown in Figures 3.3-17 and 3.3-19, again due to the randomly rough ocean bottom.

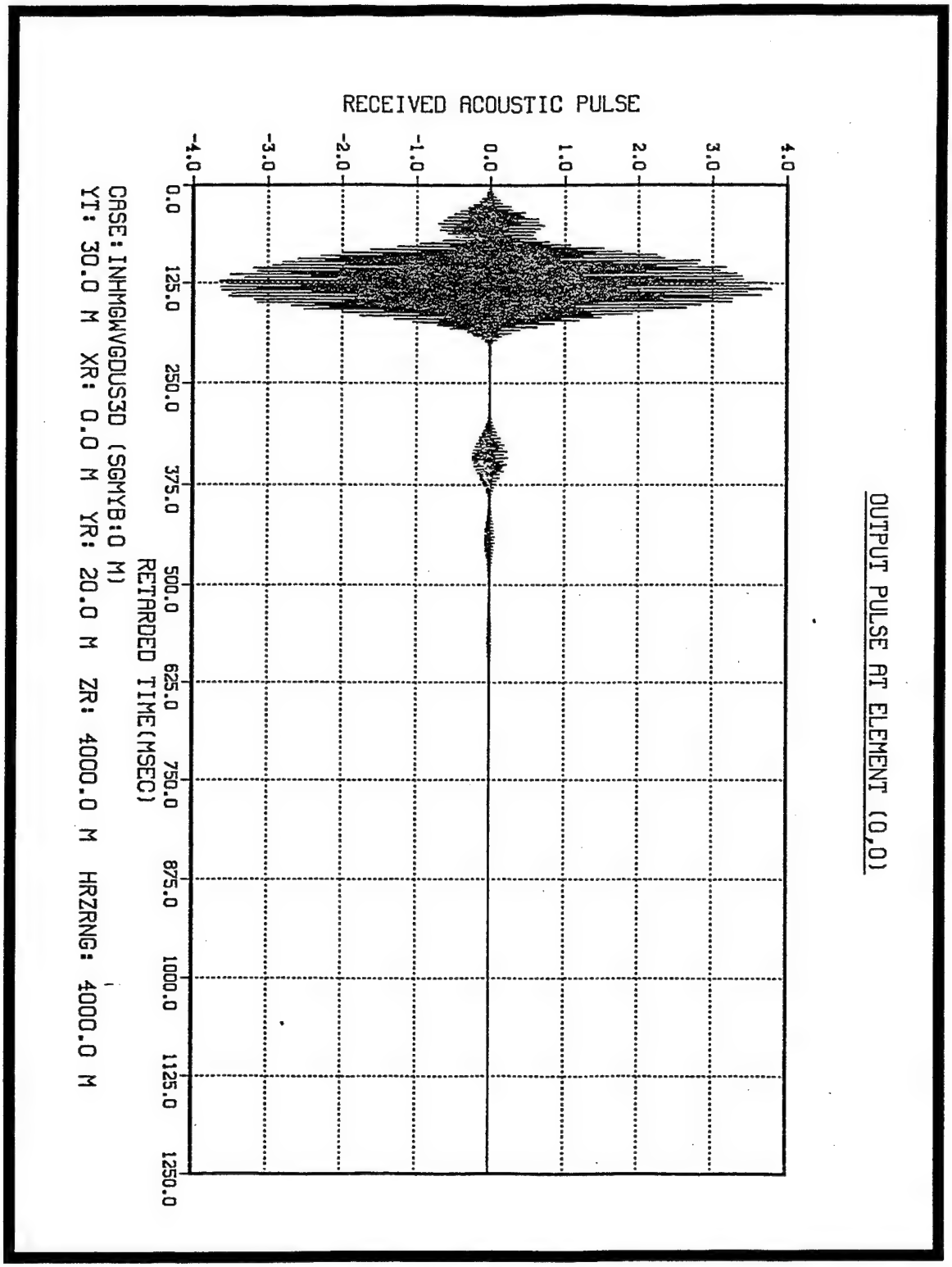

Figure 3.3-17 Predicted Received Pulse for CASE:INHMGWVGDUS3D(SGMYB:0M).

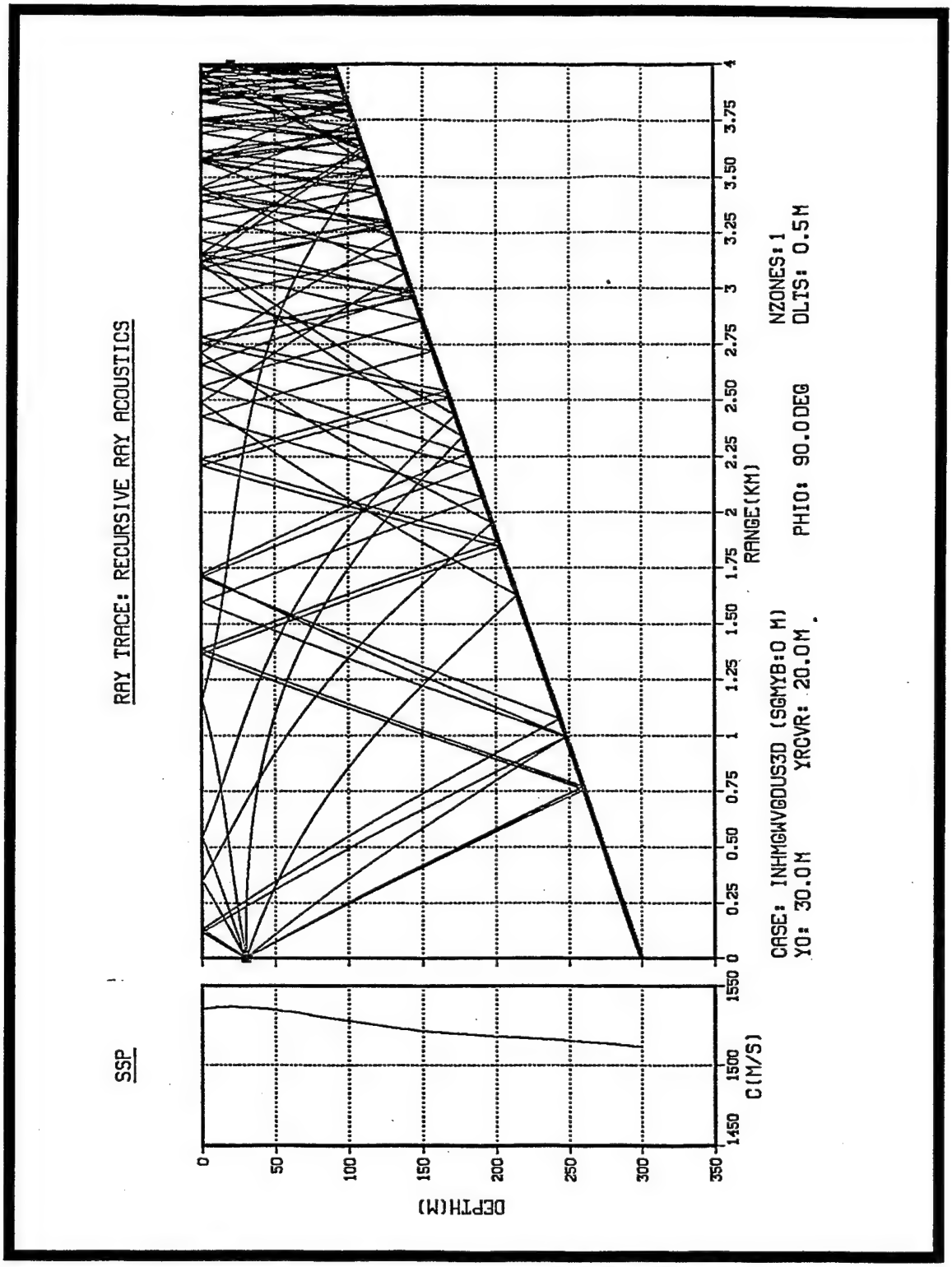

Figure 3.3-18 Eigenrays Plot Corresponding to CASE:INHMGWVGDUS3D (SGMYB:0M).

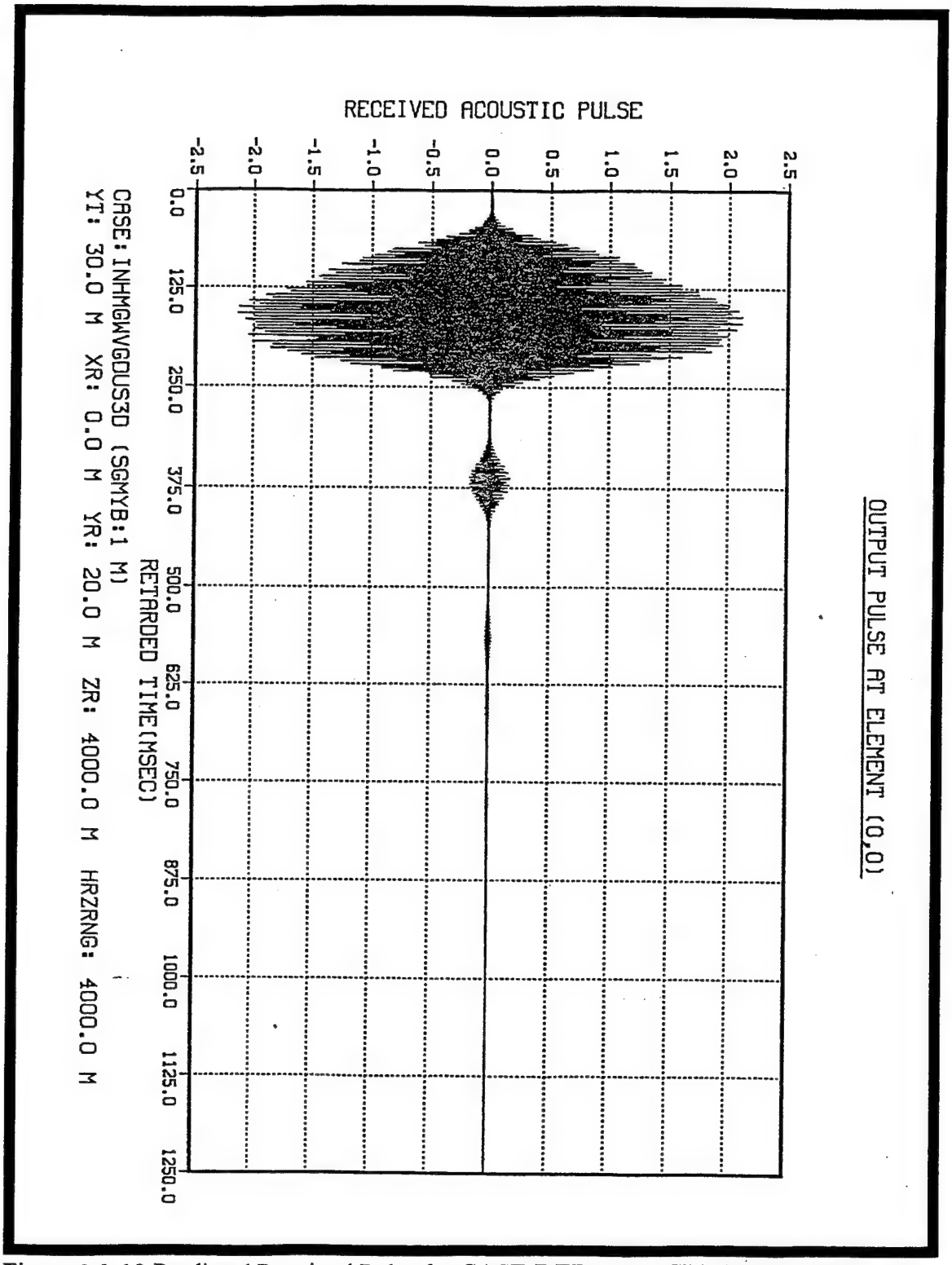

Figure 3.3-19 Predicted Received Pulse for CASE:INHMGWVGDUS3D(SGMYB:1M).

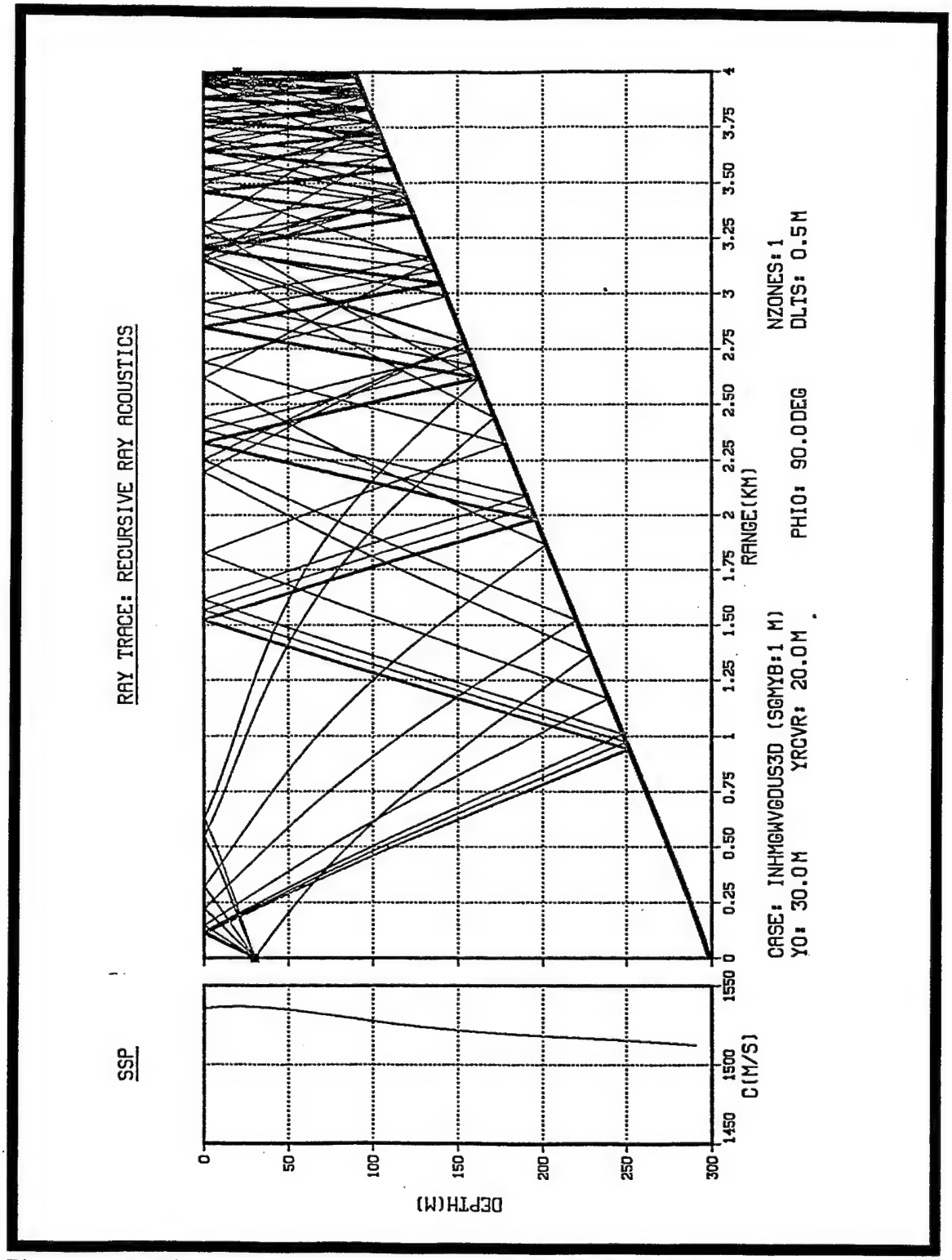

Figure 3.3-20 Eigenrays Plot Corresponding to CASE:INHMGWVGDUS3D (SGMYB:1M).

XBDATA(M)	ZBDATA(M)	YBDATA(M)
0.000	0.000	300.000
0.000	600.597	268.524
0.000	1012.024	246.962
0.000	1508.798	220.927
0.000	1969.944	196.760
0.000	2435.185	172.377
0.000	2975.981	144.035
0.000	3573.274	112.733
0.000	3976.196	91.616
0.000	4441.562	67.228
0.000	5000.000	37.961

Table 5. Ocean bottom data used in case HMGWVGDUS3D(SGMYB:0M)

XDATA(M)	YDATA(M)	ZDATA(M)	CDATA(M/S)
0.00	0.00	0.00	1535.94
0.00	10.00	0.00	1536.19
0.00	20.00	0.00	1536.33
0.00	30.00	0.00	1536.40
0.00	50.00	0.00	1535.52
0.00	75.00	0.00	1531.93
0.00	100.00	0.00	1527.22
0.00	125.00	0.00	1523.75
0.00	150.00	0.00	1522.20
0.00	200.00	0.00	1518.70
0.00	250.00	0.00	1515.16
0.00	300.00	0.00	1511.81
0.00	400.00	0.00	1507.41

Table 6. Speed of sound data used in case INHMGWVGDUS3D(SGMYB:0M)

Figures 3.3-21 and 3.3-22 are the received pulse and eigenrays plot, respectively, corresponding to case HMGWVGDDS3D(SGMYB:0M). The launch angles used for finding the eigenrays were from 0 to 180 degrees. The speed of sound data are the same as listed in Table 4. The 3 degree down-slope ocean bottom data are listed in Table 7.

Figures 3.3-23 and 3.3-24 are the received pulse and eigenrays plot, respectively, corresponding to case HMGWVGDDS3D(SGMYB:1M). The launch angles used for finding the eigenrays were from 0 to 180 degrees. The speed of sound data and the 3 degree down-slope ocean bottom data are listed in Table 4 and Table 7, respectively, with the exception that the bottom data has been randomized. Once again, note the difference between the received pulses shown in Figures 3.3-21 and 3.3-23, respectively, due to making the ocean bottom randomly rough.

Figures 3.3-25 and 3.3-26 are the received pulse and eigenrays plot, respectively, corresponding to case INHMGWVGDDS3D(SGMYB:0M). The launch angles used for finding the eigenrays were from 0 to 180 degrees. The speed of sound data and the 3 degree down-slope ocean bottom data are listed in Table 6 and Table 7, respectively.

Figures 3.3-27 and 3.3-28 are the received pulse and eigenrays plot corresponding to case INHMGWVGDDS3D(SGMYB:1M). The launch angles used for finding the eigenrays were from 0 to 180 degrees. The speed of sound data and the 3 degree down-slope ocean bottom data are listed in Table 6 and Table 7, respectively, with the exception that the bottom data has been randomized. The difference between the received pulses shown in Figures 3.3-25 and 3.3-27, as before is due to making the ocean bottom randomly rough.

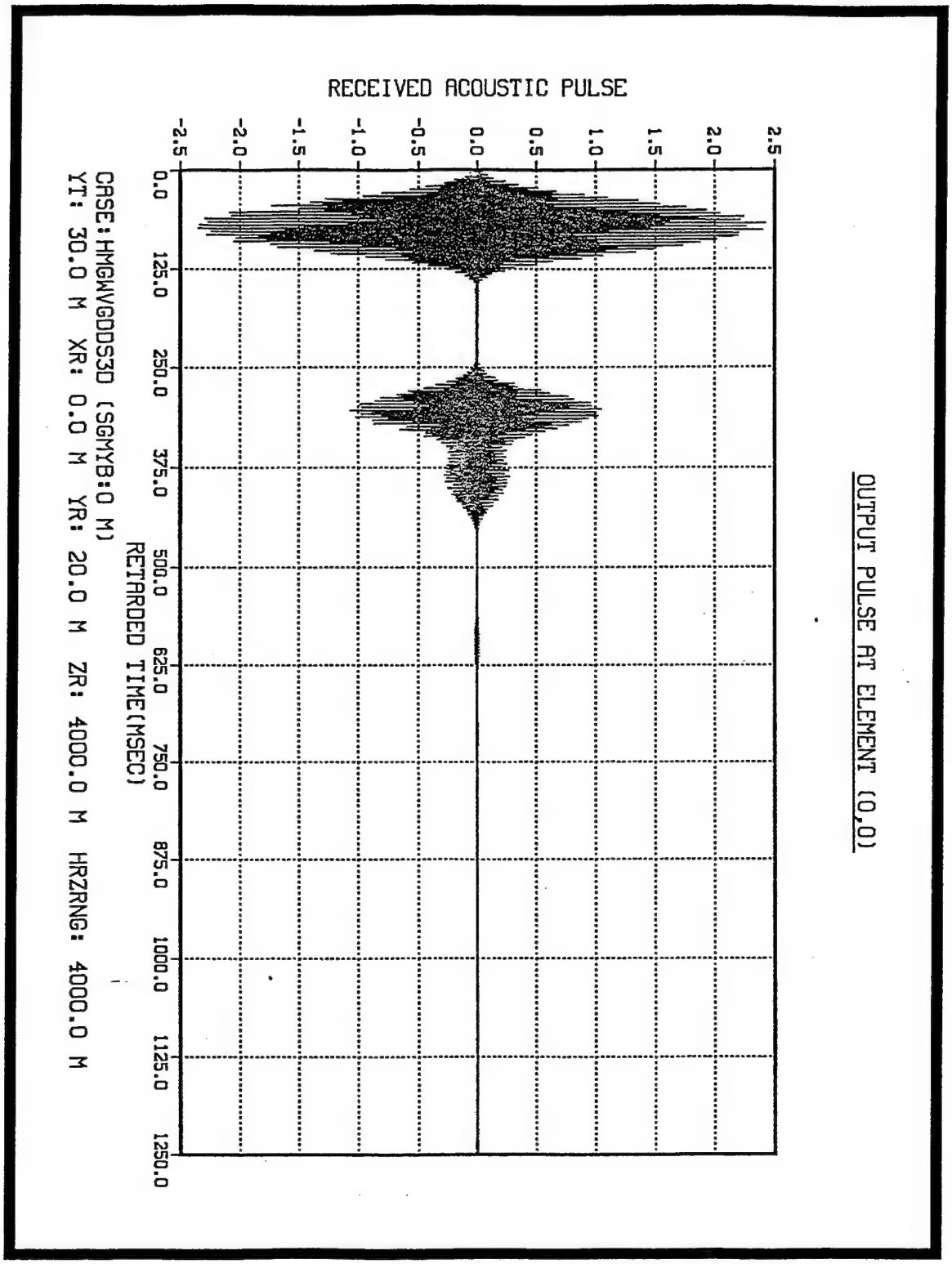

Figure 3.3-21 Predicted Received Pulse for CASE:HMGWVGDDS3D(SGMYB:0M).

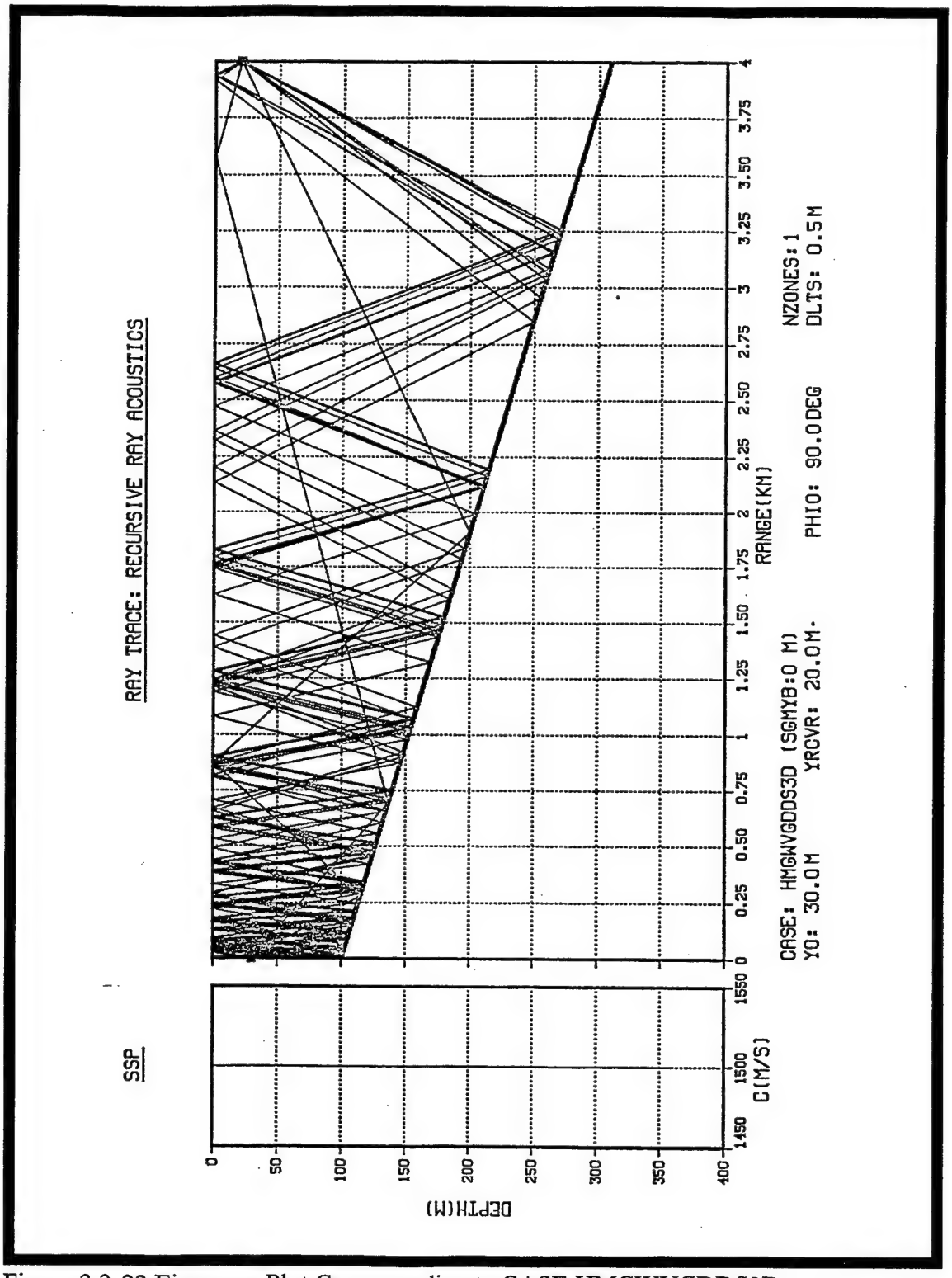

Figure 3.3-22 Eigenrays Plot Corresponding to CASE:HMGWVGDDS3D (SGMYB:0M).

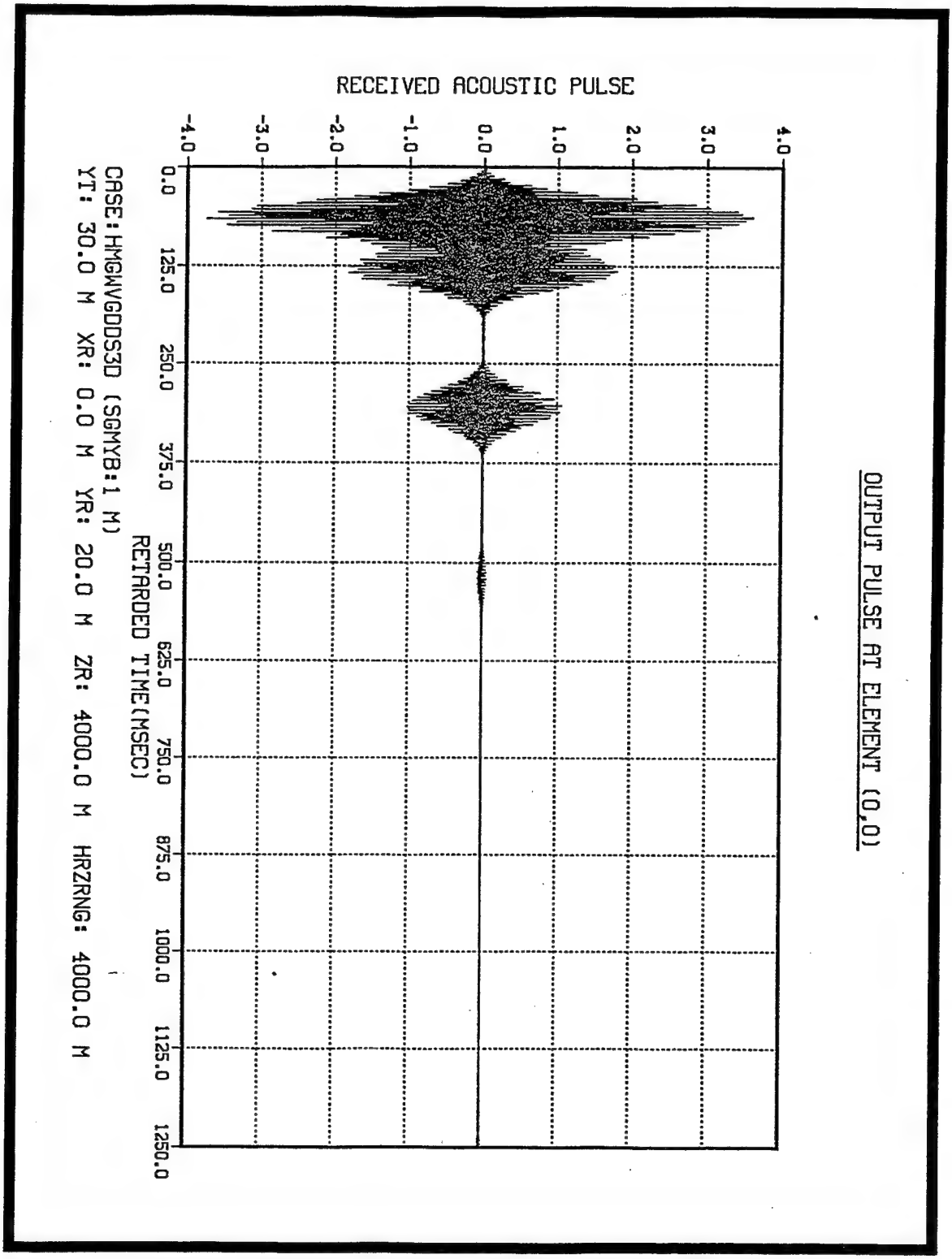

Figure 3.3-23 Predicted Received Pulse for CASE:HMGWVGDDS3D(SGMYB:1M).

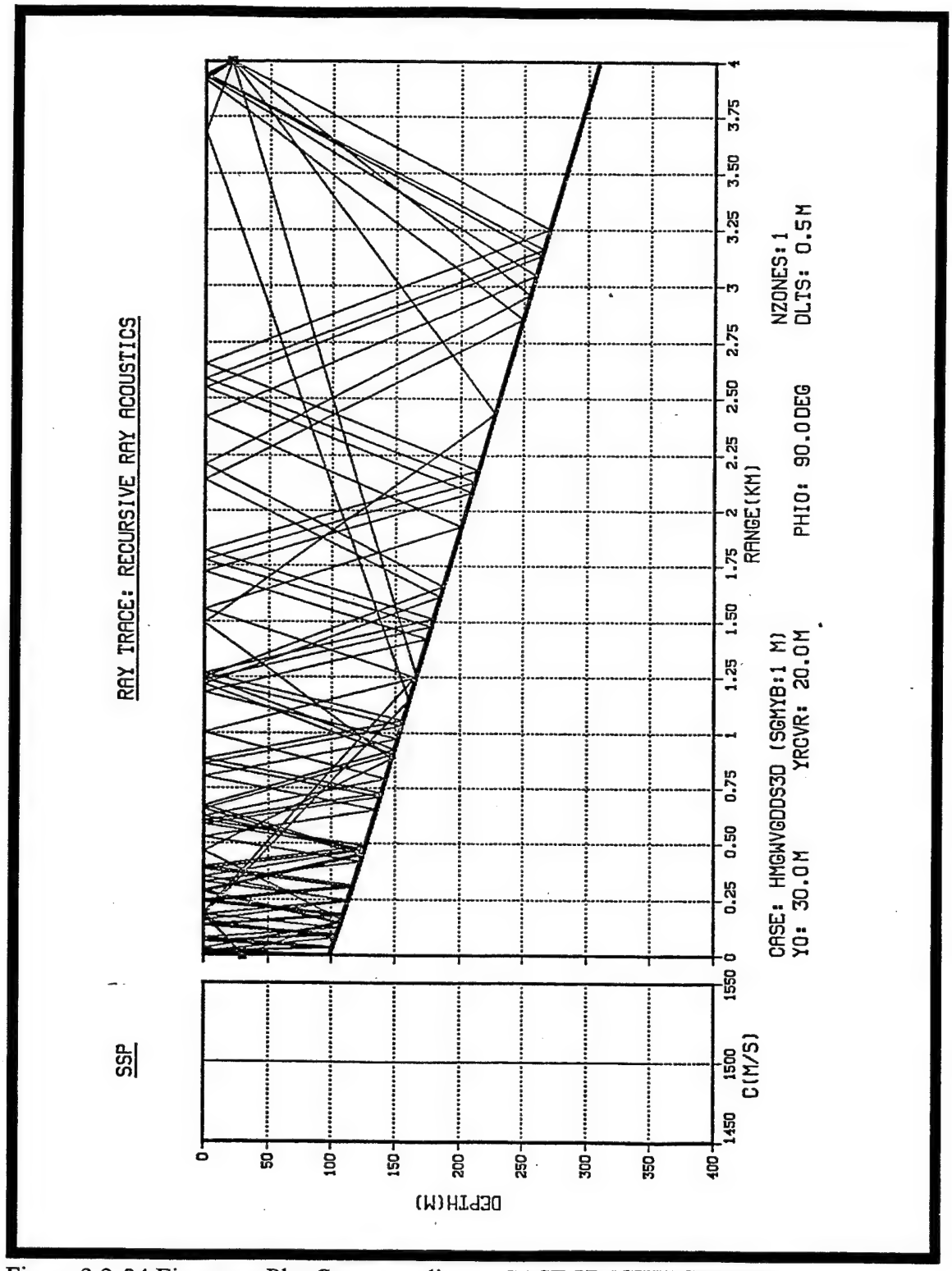

Figure 3.3-24 Eigenrays Plot Corresponding to CASE:HMGWVGDDS3D (SGMYB:1M).

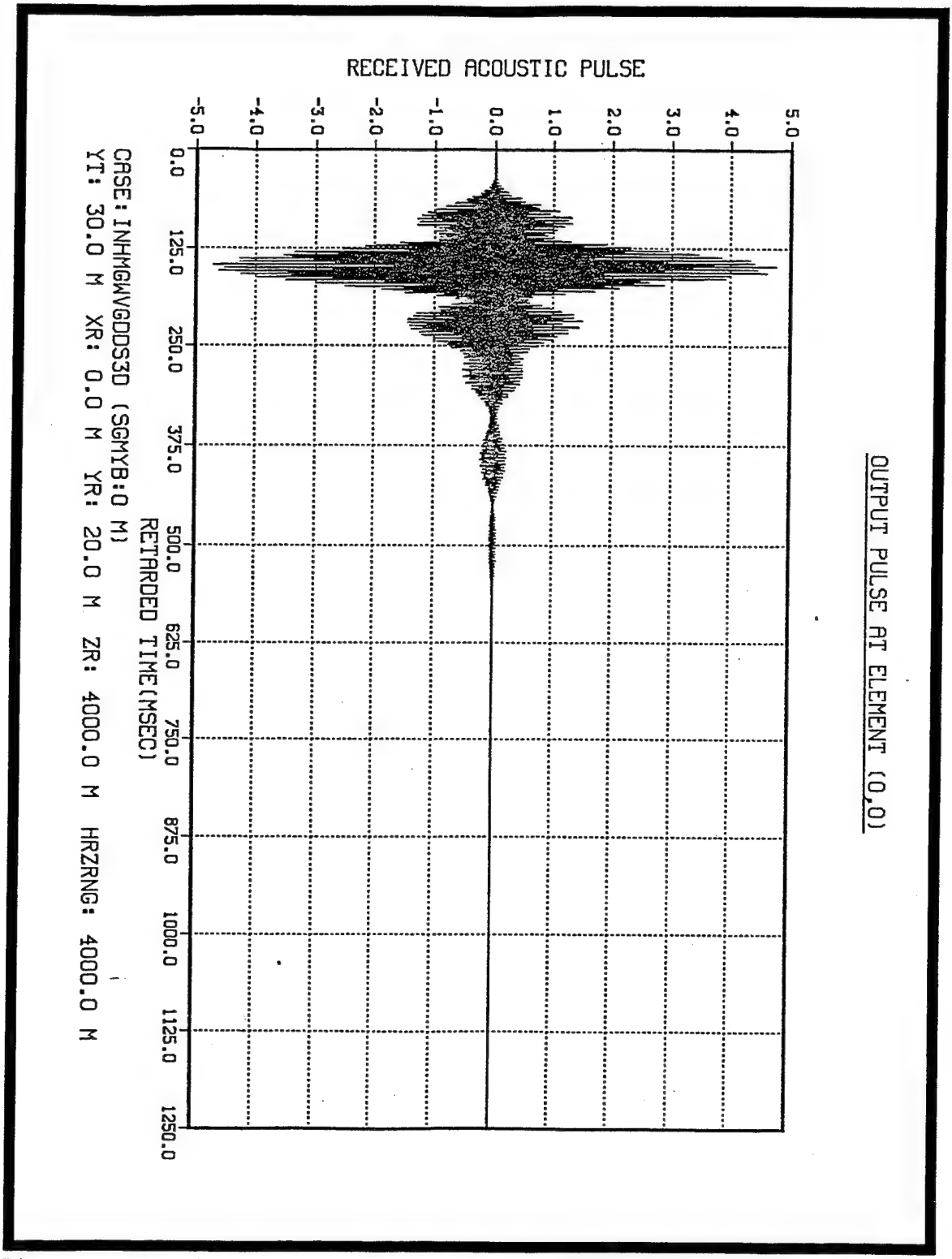

Figure 3.3-25 Predicted Received Pulse for CASE:INHMGWVGDDS3D(SGMYB:0M).

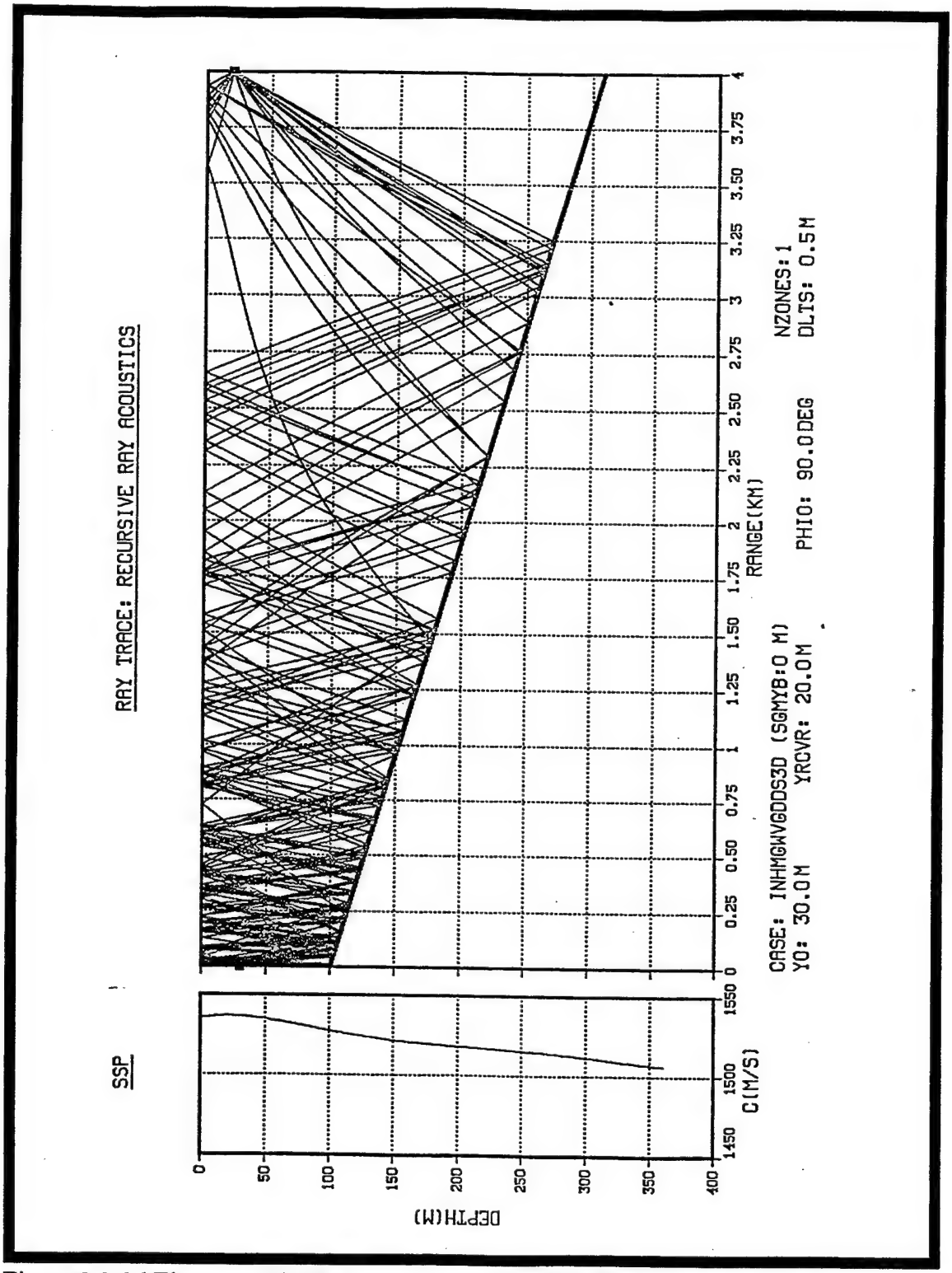

Figure 3.3-26 Eigenrays Plot Corresponding to CASE:INHMGWVGDDS3D (SGMYB:0M).

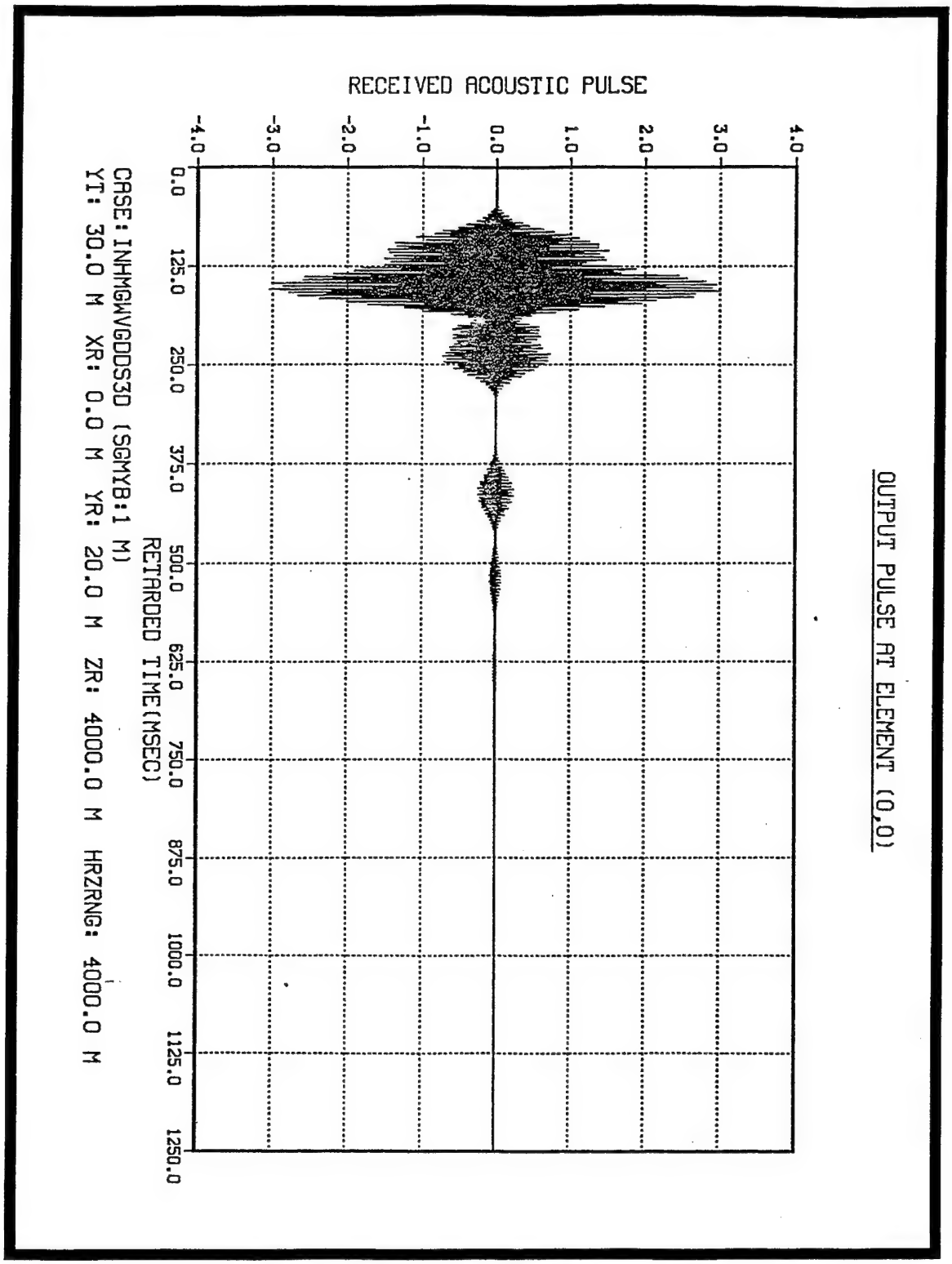

Figure 3.3-27 Predicted Received Pulse for CASE:INHMGWVGDDS3D(SGMYB:1M).

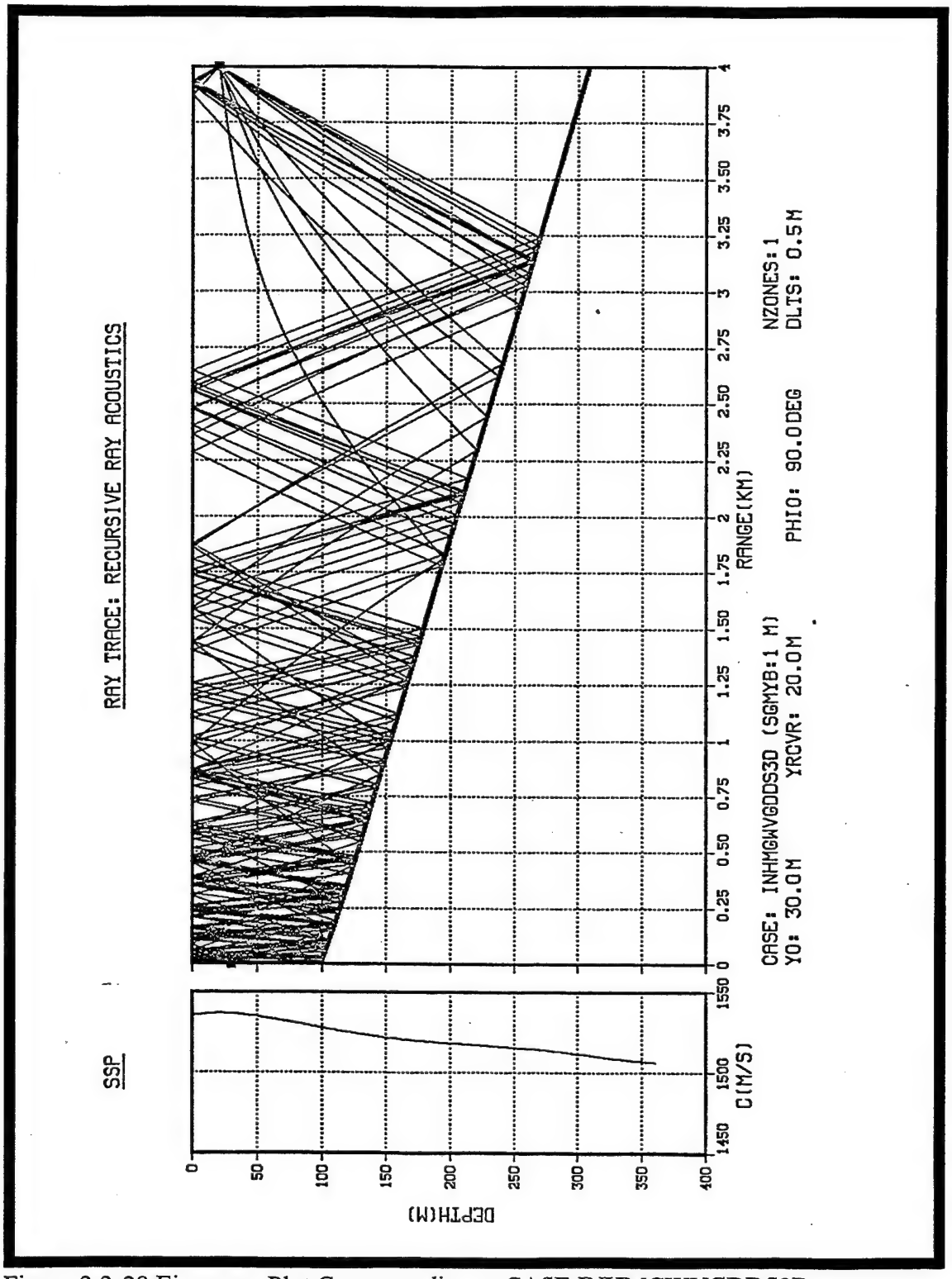

Figure 3.3-28 Eigenrays Plot Corresponding to CASE:INHMGWVGDDS3D (SGMYB:1M).

XBDATA(M)	ZBDATA(M)	YBDATA(M)
0.000	0.000	100.000
0.000	600.597	131.476
0.000	1012.024	153.038
0.000	1508.798	179.073
0.000	1969.944	203.240
0.000	2435.185	227.623
0.000	2975.981	255.965
0.000	3573.274	287.267
0.000	3976.196	308.384
0.000	4441.562	332.772
0.000	5000.000	362.039

Table 7. Ocean bottom data used in case HMGWVGDDS3D(SGMYB:0M)

All of the computer simulation test case results presented in this section show that the shape of the received pulse at the receiver is strongly affected by the ocean medium environment, that is, the speed of sound and type of ocean bottom. It can be seen that the eigenrays found for the same ocean bottom but with different speed of sound profiles are different. It can also be seen that the eigenrays found for the same speed of sound profile but with different ocean bottoms are different as well. Therefore, the received pulse is different from case to case.

IV. CONCLUSIONS AND RECOMMENDATIONS

This thesis demonstrates that the Recursive Ray Acoustics (RRA) Algorithm [Refs. 1, 2] and the Linear Space-Variant Ocean (LSVOCN) computer program [Refs. 3, 4, 5] can be joined together to successfully predict the received pulse for a given transmitted signal and ocean-medium environment. The RRA Algorithm was used as a subroutine to calculate the spatial impulse response or complex frequency response of the ocean-medium filter. The LSVOCN computer program, which incorporates the coupling equations, successfully couples the transmitted electrical signal, and the transmit and receive apertures to the ocean-medium filter to predict the received pulse.

The computer simulation test case results presented in Chapter III show the effects of different ocean-medium environments on the shape of the received pulse. The propagation of an amplitude-modulated carrier along a single eigenray in an unbounded and bounded homogeneous ocean medium is discussed in Sections A and B, respectively. The shape of the received pulse is not distorted and the amplitude of the received pulse decreases as 1/r, where r is the total path length, for the test cases in Sections A and B. In Section B, the received pulse shows a 180-degree phase shift, compared to the transmitted signal, for those cases when the reflection coefficient has values of -1 and -0.5. These results match theory exactly and were used to validate the pulse-propagation computer code.

Section C demonstrates the effects of different ocean-medium environments on the shape of the received pulse. The ocean bottom was modeled as either flat, randomly-rough flat, or having a 3 degree smooth up-slope, a 3 degree randomly-rough up-slope, a 3 degree smooth down-slope, or a 3 degree randomly-rough down-slope for the different test cases. The speed of sound profile was modeled as being a constant (homogeneous) medium or an arbitrary function of depth (inhomogeneous) medium for each type of ocean bottom. The computer simulation results show that the shape of the received pulse is strongly affected by the different ocean-medium environments. The ability to predict the received pulse can be very useful in underwater communication applications and in target localization

problems.

In this thesis, the speed of sound was treated as a function of depth and the ocean bottom was treated as a function of horizontal-range. Since the RRA Algorithm is able to handle a three-dimensional speed of sound, it is recommended to further conduct pulse-propagation studies for a speed of sound that is a function of one, two, and three spatial coordinates and to use an ocean bottom that is a function of both horizontal-range and cross-range. Another recommendation for future research is to decrease the angle step size, the arc length step size, and the YERROR parameter to obtain more precise results, subject to reasonable computation time.

LIST OF REFERENCES

1. L. J. Ziomek and F. Wynn Polnicky, "The RRA Algorithm: Recursive Ray Acoustics For Three-Dimensional Speeds of Sound," *IEEE J. Oceanic Engineering*, Vol. 18, 25-30 (1993).

2. L. J. Ziomek, "Sound-Pressure Level Calculations Using the RRA Algorithm for Depth-Dependent Speeds of Sound Valid at Turning Points and Focal Points," *IEEE J. Oceanic Engineering*, Vol. 19, 242-248 (1994).

3. L. J. Ziomek, L. A. Souza, and P. R. Campbell, "Pulse Propagation In A Random Ocean-A Linear Systems Theory Approach," *OCEANS* '89, 1211-1216, September 18-21, 1989, Seattle, Washington.

4. L. J. Ziomek, "LSVOCN: A Pulse-Propagation Model for a Linear, Space-Variant Ocean," *119th Meeting of the Acoustical Society of America*, May 21-25, 1990, The Pennsylvania State University, University Park, Pennsylvania, *J. Acoust. Soc. Am. Suppl.* 1, Vol. 87, S130-S131.

5. L. J. Ziomek, "Linear Systems Theory and its Relationship to Ocean Acoustics," *120th Meeting of the Acoustical Society of America*, November 26-30, 1990, San Diego, California, *J. Acoust. Soc. Am. Suppl.* 1, Vol. 88, S37 (Invited Paper).

6. L. J. Ziomek, *Fundamentals of Acoustic Field Theory and Space-Time Signal Processing*, CRC Press, Inc., Boca Raton, Florida, 1995.

7. L. E. Kinsler, A. R. Frey, A. B. Coppens, and J. V. Sanders, *Fundamentals of Acoustics*, pp. 353, John Wiley & Sons, Inc., New York, NY, 1982.

INITIAL DISTRIBUTION LIST

	No. Copies
1. Defense Technical Information Center Cameron Station Alexandria, Virginia 22304-6145	2
2. Library, Code 52 Naval Postgraduate School Monterey, California 93943-5101	2
3. Professor Lawrence J. Ziomek, Code EC/Zm Electrical and Computer Engineering Department Naval Postgraduate School Monterey, California 93943-5121	3
4. Professor Charles W. Therrien, Code EC/Ti Electrical and Computer Engineering Department Naval Postgraduate School Monterey, California 93943-5121	1
5. LT Mei-chun Yuan SGC # 1627 Naval Postgraduate School Monterey CA 93943-5000	1
6. LT Ding-chen Chang 13th Floor, 27, Lane 21, Nan Chang Street, Feng Shan, Kaohsiung, Taiwan R. O. C	2